INFORMATION TO USERS

This material was produced from a microfilm copy of the original document. While the most advanced technological means to photograph and reproduce this document have been used, the quality is heavily dependent upon the quality of the original submitted.

The following explanation of techniques is provided to help you understand markings or patterns which may appear on this reproduction.

1. The sign or "target" for pages apparently lacking from the document photographed is "Missing Page(s)". If it was possible to obtain the missing page(s) or section, they are spliced into the film along with adjacent pages. This may have necessitated cutting thru an image and duplicating adjacent pages to insure you complete continuity.

2. When an image on the film is obliterated with a large round black mark, it is an indication that the photographer suspected that the copy may have moved during exposure and thus cause a blurred image. You will find a good image of the page in the adjacent frame.

3. When a map, drawing or chart, etc., was part of the material being photographed the photographer followed a definite method in "sectioning" the material. It is customary to begin photoing at the upper left hand corner of a large sheet and to continue photoing from left to right in equal sections with a small overlap. If necessary, sectioning is continued again — beginning below the first row and continuing on until complete.

4. The majority of users indicate that the textual content is of greatest value, however, a somewhat higher quality reproduction could be made from "photographs" if essential to the understanding of the dissertation. Silver prints of "photographs" may be ordered at additional charge by writing the Order Department, giving the catalog number, title, author and specific pages you wish reproduced.

5. PLEASE NOTE: Some pages may have indistinct print. Filmed as received.

Xerox University Microfilms

300 North Zeeb Road
Ann Arbor, Michigan 48106

75-10,189

HYER, Michael William, 1942-
NONLINEAR VIBRATION OF THREE-LAYER BEAMS.

The University of Michigan, Ph.D., 1974
Engineering Mechanics

Xerox University Microfilms, Ann Arbor, Michigan 48106

THIS DISSERTATION HAS BEEN MICROFILMED EXACTLY AS RECEIVED.

NONLINEAR VIBRATION OF THREE-LAYER BEAMS

by

Michael William Hyer

A dissertation submitted in partial fulfillment
of the requirements for the degree of
Doctor of Philosophy
(Aerospace Engineering)
in The University of Michigan
1974

Doctoral Committee:

Professor William J. Anderson, Co-Chairman
Associate Professor Richard A. Scott, Co-Chairman
Professor Joe G. Eisley
Professor Donald T. Greenwood
Professor Ivor K. McIvor

ODE TO A BEAM

I think that I have never seen
A picture prettier than a beam,
Gently dancing to and fro
Embraced by harmonic flow.

A. S. Wineman and M. W. Hyer, Circa 1973

ACKNOWLEDGMENTS

I would like to express my gratitude to Richard A. Scott and William J. Anderson for their guidance and the many hours they spent with me during this study. I would also like to express my gratitude to Donald T. Greenwood for his helpful discussions. I wish to express thanks to the Department of Aerospace Engineering for purchase of equipment related to the experiment and for computing funds. My appreciation goes to Richard French for helping me with the electronics and to Debbie Lurkins for her conscientious typing of the manuscript. My wife Patricia deserves special appreciation for her patience, love and understanding during this endeavor.

The financial support of NSF Grant GK-36374X1 for the purchase of material used in the experiment is also appreciated.

TABLE OF CONTENTS

ACKNOWLEDGMENTS		ii
LIST OF FIGURES		v
LIST OF SYMBOLS		vii
CHAPTER I	INTRODUCTION	1
CHAPTER II	DERIVATION OF EQUATIONS	13
2.1	REVIEW OF FINITE DEFORMATION	13
2.2	PRINCIPLE OF VIRTUAL WORK	16
2.3	APPLICATION TO LAYERED PLATE	17
2.4	ASSUMED DISPLACEMENT FIELD	21
2.5	GOVERNING EQUATIONS	23
2.6	INTERFACE CONDITIONS	30
2.7	REDUCTION TO BEAM EQUATIONS	33
CHAPTER III	NUMERICAL RESULTS	47
3.1	FORM OF APPROXIMATE SOLUTION	47
3.2	RESULTS OF NUMERICAL SOLUTION	55
3.3	EFFECT OF SYMMETRY ON DAMPING	56
CHAPTER IV	FEEDBACK CONTROL SYSTEM	59
4.1	ELECTROMAGNETIC FORCING	59
4.2	BASIC CONCEPTS OF FEEDBACK CONTROL	63
4.3	DESIGN OF FEEDBACK UNIT	69
CHAPTER V	EXPERIMENTAL RESULTS USING THE FORCING SYSTEM	90
5.1	BEAM SPECIMENS AND THE CLAMPING MECHANISM	90
5.2	BEAM AND FORCE MEASUREMENTS	91
5.3	EXPERIMENTAL RESULTS	92
5.4	DISCUSSION	94
CHAPTER VI	CONCLUSION	98
6.1	SUMMARY	98
6.2	FUTURE WORK	101

TABLE OF CONTENTS (concluded)

APPENDIX 103

REFERENCES 105

FIGURES 109

LIST OF FIGURES

FIGURE

1.1 Kovac's frequency response 109

1.2 Kovac's mode shapes 109

2.1 Deformation of a body 110

2.2 Deformation of an infinitesimal cube 110

2.3 Three-layer plate configuration 111

2.4 Assumed displacement field 112

2.5 Beam geometry 112

3.1 Response of symmetric 3-layer beam 113

3.2 Response of unsymmetric 3-layer beam - 2 values of bias force 114

4.1 Standard setup 115

4.2 Typical B vs. H relation 115

4.3 Variation of force with distance 115

4.4 Force time histories of recent investigators 116

4.5 Problem summary 117

4.6 Distortion caused by system 118

4.7 Input needed for desired output 118

4.8 Use of output to get required input 118

4.9 Simple feedback system 119

4.10 Amplifier in a feedback system 119

4.11 Effect of phase distortion on error 120

4.12 Noise entering feedback loop 120

4.13 Modified lathe bed 121

4.14 Feedback system using free floating magnet 122

4.15 Fringing of 'E' magnet 123

LIST OF FIGURES (concluded)

FIGURE

4.16 Fringing with beam in magnetic circuit 123

4.17 Fixed magnet and magnetic circuit 124

4.18 Bentley-Nevada Model 316 proximeter calibration 125

4.19 Feedback system using fixed magnet and magnetic circuit 126

4.20 Open loop phase response of magnetic circuit system 127

4.21 Differentiator in magnetic circuit system 128

4.22 System and element characteristics - elimination of magnetic circuit 129

4.23 Force spectrum 130

4.24 Amplifier circuit diagram and input-output characteristics 131

4.25 30 hz forcing spectrum 132

4.26 Final configuration of feedback system 133

5.1 Beam displacement proximeter calibration, Model 308 Bentley-Nevada 134

5.2 Force calibration procedure 135

5.3 Response of unsymmetric beam, F_0 = .15 lb., F_1 = .05 lb. 136

5.4 Response of unsymmetric beam, F_0 = .18 lb., F_1 = .073 lb. 137

5.5 Mode shapes for unsymmetric beam 138

5.6 Characteristics of feedback system 139

LIST OF SYMBOLS

A_{io}	1st moment of area of i-th layer about z=0
a(x), a(X)	assumed spatial distribution of applied load
B	physical constant, Eq. 1.2a
B_i, C_i	physical constants associated with harmonic balance
C	capacitance
C_{26}, C_{18}	coefficients of order unity, Eq. 1.1
D	ratio of differential volume element after and before deformation, $d\bar{V}/dV$
dl_i	length of differential line element after deformation, length before deformation = dx_i
E	relative elongation, Sect. 2.1, 2.2; otherwise Young's modulus
$e_1(X,t), e_2(X,t)$	force and moment imbalance associated with Galerkin's method
e_{ij}	infinitesimal strain tensor
$F, \bar{F}$	force coefficient
f	frequency, hz
G	force coefficient, Eq. 1.3c; otherwise elastic shear modulus
$G_2'(\Omega)$, $G_2''(\Omega)$	real and imaginary part, respectively, of the complex shear modulus evaluated at frequency Ω
H	force coefficient, Eq. 1.3c
$H_2, \bar{H}_2, H_3, \bar{H}_3$	physical constants, Ch. 3
h_i	thickness of i-th layer
h_T	total beam or plate thickness

h_{c_1}, h_{c_2}	z distance from neutral axis to 1st and 3rd layers, respectively
h_2	$(h_T/L)^2$, nondimensional thickness
I_{io}	2nd moment of area of i-th layer about z=0
$K, \bar{K}, K_{11}, \bar{K}_{11}, K_{12}, \bar{K}_{12}, \bar{\bar{K}}_{12}, K_{13}, \bar{K}_{13}, K_{15}, \bar{K}_{15}, K_{16}, K_T$	physical constants
L, L_x, L_y	length of beam, length of plate side; inductance, Ch.4
$\bar{L}$	physical constant, Eq. 1.2b
ℓ, m, n	direction cosines in x,y,z, directions
M,m	mass coefficients
$M_{xx}, M_{xy}, M_{yy}, M_{xz}, M_{yz}, N_{xx}, N_{xy}, N_{yy}, Q_{xz}, Q_{yz}$	stress resultants
$q(x,t)$, $\bar{q}(\chi,t)$	applied load in z direction
R	resistance, ohms
S, dS	surface area before deformation, finite and differential
$\bar{S}$, $d\bar{S}$	surface area after deformation, finite and differential
S_{km}	components of Kirchhoff stress tensor, index notation
$S_{xx}, S_{xy}, S_{xz}, S_{yx}, S_{yy}, S_{yz}, S_{zx}, S_{zy}, S_{zz}$	components of Kirchhoff stress tensor, cartesian coordinates

LIST OF SYMBOLS (continued)

T_x, T_y, T_z	surface tractions in the x,y, and z directions
$T_1(t), T_2(t)$	assumed temporal functions associated with harmonic balance
t	membrane face layer thickness, Eq.1.1; otherwise time
U	in-plane displacement in x direction of 2nd layer
u	displacement in the x direction except in Sect. 2.1 and 2.2 where it denotes displacement in general
u^0	uniform in-plane displacement in x direction
V, dV	volume before deformation, finite and differential
$\overline{V}$, $d\overline{V}$	volume after deformation, finite and differential
V, V_i	coefficients in assumed temporal functions, function of frequency
v	displacement in y direction
v^0	uniform in-plane displacement in y direction
W, W_i	coefficients in assumed temporal functions, function of frequency
$W(x), W(\chi)$	assumed spatial mode for transverse deflection of beam
w	displacement in z direction,transverse displacement of plate or beam
$\overline{w}$	(w/h_T), nondimensional displacement
X_1, X_2, X_3	Cartesian coordinate axis system
x_1, x_2, x_3	Cartesian coordinates of a point in body before deformation

LIST OF SYMBOLS (continued)

$\bar{x}_1, \bar{x}_2, \bar{x}_3$	Cartesian coordinates of a point in body after deformation, $\bar{x}_i = x_i + u_i(x_1, x_2, x_3), i=1,3$
x, y, z	Cartesian coordinates
$Y_2(t)$	shear stress relaxation function of core material
z_i	z-coordinate related to location of i-th layer
α, α_i	phase angle associated with core deformation, function of frequency, Eqs. 1.3b, 1.4b
β_i	phase angle associated with transverse deflection of beam, function of frequency, Eq. 1.4a
γ	shear strain
$\delta( )$	variation of quantity ( )
δ_{ij}	Kronecker delta
ϵ	h_T/L, small compared to unity
ε_{ij}	components of Green's strain tensor
ν_m	direction cosines of normal to deformed area element
$\bar{\nu}_m$	direction cosines of normal to undeformed area element
ρ	density before deformation
$\bar{\rho}$	density after deformation
ξ, τ	dummy time integration variables
$\phi(x,y,t)$	shear and bending deformation in y-z plane
ϕ_{ij}	shear deformation between differential line elements

LIST OF SYMBOLS (concluded)

χ	x/L nondimensional coordinate in x direction
$\Psi(x,y,t)$, $\Psi(x,t)$	shear and bending deformation in x-z plane
$\Psi(x)$, $\Psi(\chi)$	assumed spatial mode for core deformation
$\overline{\Psi}$	$(L/h_T)\Psi$
Ω	forcing frequency, radians/sec
ω_{ij}	components of local rotation tensor
ω_R	linear resonant frequency of beam
$\overline{\omega}_R$	resonant frequency of beam about statically deflected position
$( )'$	partial differentiation with respect to x, $\frac{\partial}{\partial x}$
$\dot{( )}$	partial differentiation with respect to time, $\frac{\partial}{\partial t}$

CHAPTER I

INTRODUCTION

Much theoretical and experimental work has been done investigating linear vibrations of sandwich beams and plates. A good survey of work before 1965 was written by Halbip[1]. The most often quoted work was done by Yi-Yan Yu[2,3,4]. Yu developed a flexural theory for elastic sandwich plates in a series of papers, starting with a one-dimensional theory and including the effects of transverse shear deformation and rotatory inertia in both the core and face sheets. This was for a three-layer sandwich plate and imposed no limitations on the ratios of core and face thicknesses, densities or elastic constants. This theory was extended into a simplified analysis in two dimensions for a sandwich plate with identical thin face sheets and soft core. Yu's equations were derived by assuming the form of the displacements in each layer, using these in the variational equations of elasticity and finally enforcing displacement and stress continuity across layer interfaces.

Interest has developed in using viscoelastic materials in sandwich beams to reduce vibration. The material, which usually is made of a soft elastomer, is forced into shearing deformation by sandwiching it between stiffer elastic layers. Through dissipative properties of the material, unwanted vibrations can be damped. This mechanism is referred to as constrained layer damping and Kerwin[5]

did the early work in this area investigating the damping of flexural vibrations in a three-layer bar. Later, DiTaranto[6] developed simple linear equations for elastic and viscoelastic layered beams of finite length and DiTaranto and Blasingame[7] computed loss factors and natural frequencies for such beams. Jones, Salerno and Savacchio[8] did an analytical and experimental evaluation of damping in this type of sandwich beam. They suspended layered beams on thin wires to simulate free-free conditions and excited them with an electrodynamic shaker attached to the center of the beam. The agreement between theory and experiment was at best fair; the experimental setup was crude. Yin, Kelly and Barry[9] did an experimental study of the effects of constrained layer damping on plates, beams, circular and rectangular tubes and various other shapes. Mead and Markus[10, 11] derived a sixth order equation in terms of transverse displacement for a three-layer sandwich beam with a viscoelastic core and applied this theory to get numerical results for loss factors and resonant frequencies. Mead and DiTaranto[12] determined a resonant response criterion for three-layer beams based on theories from their earlier works. Most investigators found that cores made from commonly available viscoelastic materials damped vibrations only over a limited frequency range. Grootenhuis[13], Agbasiere and Grootenhuis[14] and Nakra and Grootenhuis[15] looked at beams

with several layers of viscoelastic material. Each layer damped vibrations for a specific range of frequencies; the combination of layers damped vibrations over a wide range of frequencies. Recently, Folie[16] derived a theory of transverse bending of three-layer sandwich plates with isotropic outer layers and orthotropic cores.

All these investigations followed the same pattern of assuming a displacement field for each layer, including shear, transverse motion, and in some cases longitudinal displacements, enforcing various kinematic and stress conditions at the interfaces of the layers, assuming constitutive equations for the various layers and finally arriving at the governing equations by looking at the equilibrium of a beam element. Recently Yan and Dowell[17,18] developed general linear equations for vibrating three-layer rectangular sandwich plates by using similar ideas. The governing equations were derived, however, using the principle of virtual work. The final equations are in terms of five variables: three displacements and two shear stresses. By making the restriction that the core be much softer than the face material and dropping inertia terms except for transverse inertia, a single equation for the transverse displacement is derived. Dispersion relations from the simplified equation were compared with dispersion relations from the full set of equations as well as with the works of Mead and Markus and DiTaranto. The simplified equation and the full set of five give results that

agree quite well. Mead and Markus' results were similar but those of DiTaranto were substantially different. Yan and Dowell did experiments and the comparison between experiment and theory was quite good for beams. Their experimental work on plates was quite limited.

Krajinovic[19,20] derived variational equations for both static and dynamic analyses of symmetric three-layer elastic sandwich beams by using an approach similar to Yu. However Krajinovic's approach was unique because he chose orthogonal displacement functions for the beam as a whole. Finding solutions to the governing equations was simpler because several equations were uncoupled. Chan and Cheung[21] numerically solved problems of bending and vibration of multi-layered plates by the so-called finite strip method.

Compared to the investigation of linear bending and vibration of sandwich plates and beams, little has been done to investigate nonlinear behavior. Reissner[22] developed an explicit formula for determining the linear range of the static load-deflection relation for symmetric three-layer sandwich plates with membrane face sheets. He deduced that if the transverse plate deflections are small compared to

$$\frac{C_{26} h_T}{\sqrt{1 + C_{18}(h_T t/L^2)(E_f/G_c)}} \tag{1.1}$$

then the relation is linear, where h_T-t is the core thickness, t is the membrane thickness, L is the length of the

plate side, E_f and G_c are Young's modulus of the face sheets and shear modulus of the core, respectively, and C_{26} and C_{18} are constants of order unity. For core material whose modulus is the same order of magnitude as the face material's, the restriction is that the transverse deflections be small compared to h_T, as with homogeneous plate theory. However, as the core becomes softer and softer, compared to the face sheets, the range of linearity becomes smaller and smaller. Since Reissner did not include the individual bending resistance of the face sheets, the formulation cannot be used to determine the range of linear analysis for sandwich plates with face layers which have thicknesses comparable with the core thickness. However, based on the range of accuracy of linear theory for homogeneous plates, it would be logical to assume that for a three-layer plate whose face layers cannot be considered membranes, linear theory is accurate if the deflections are small compared to the thickness of one of the layers. This indicates that it seems necessary from the outset to consider nonlinearities when investigating the behavior of layered plates or beams in any practical structural application. This is particularly true if the edges of the plate, or ends of the beam, are restrained from in-plane motion.

Chu[23] investigated the shear effects of honeycomb cores on the moderately large deflections of sandwich beams. He concluded that shear effects in the core can be

neglected in the nonlinear analysis if they can be neglected in the linear analysis. While that basic premise is correct, due to a numerical error in his computations, he grossly underestimated the effect shear can have. Yu[24] pointed this oversight out later. In addition, Yu[25] extended his own linear analysis of flexural vibrations of sandwich plates,with identical thin face sheets,to include geometric nonlinearities. He applied his analysis to find numerical results for the one-dimensional case and the case of a rectangular sandwich plate with immovable hinged edges. Wempner and Baylor[26] derived equations in what they termed an invariant form for the large deflections of sandwich plates with weak cores. They included bending resistance of the facings and transverse deformation of the core and illustrated the use of the equations by predicting buckling loads. Habip[27] used perturbation expansion techniques to find the equations for the static deflection of a two-layer plate. The first-order terms constitute Von Karman plate equations and the second-order terms are shear effects.

In one of the few experimental investigations in the area of nonlinear vibrations of sandwich structures, Kovac, Anderson and Scott[28,29] investigated the nonlinear vibrations of a harmonically forced sandwich beam with a soft viscoelastic core and identical thin face sheets. The ends of the beam were restrained from moving toward each other and so the transverse deflections induced

axial stretching. The equations governing the motion were derived by considering force and moment equilibrium of the core and face sheets. The faces were considered as elastic membranes while the constitutive properties of the core were represented by complex moduli evaluated at the forcing frequency. The equations are

$$B\Psi'' - K(\Psi + w') - \bar{K}(\dot{\Psi} + \dot{w}') = 0 \tag{1.2a}$$

$$K(\Psi' + w'') + \bar{K}(\dot{\Psi}' + \dot{w}'') + [\bar{L}\int_0^L (w')^2 dx]\, w'' + q(x,t) - m\ddot{w} = 0 \tag{1.2b}$$

where Ψ is the shear angle in the core, w the transverse deflection of the beam, q(x,t) the applied load, B,K,$\bar{K}$,$\bar{L}$ are physical constants and L is the length of the beam. $(\,)'$ and $(\dot{})$ denotes differentiation with respect to x and time, t, respectively. Assuming a one spatial mode-one temporal mode solution of the form

$$w(x,t) = \mathbf{W}W(x)\cos(\Omega t) \tag{1.3a}$$

$$\Psi(x,t) = \mathbf{V}\Psi(x)\cos(\Omega(t-\alpha)) \tag{1.3b}$$

$$q(x,t) = a(x)(H\cos(\Omega t) + G\sin(\Omega t)) \tag{1.3c}$$

where **W, V** and α are functions of forcing frequency Ω, W(x) and Ψ(x) are the assumed spatial response, a(x) the assumed spatial distribution of the applied load, H and G the magnitude of the load. **Using Galerkin's** method and

harmonic balance, frequency response characteristics were predicted.

In general, agreement between theory and experiment was reasonable. However, the experiment revealed a super-harmonic response when forcing the beam near one-half its linear resonant frequency. The beam displacement contained a substantial component of response at twice the forcing frequency. As a result, as shown in Fig. (1.1), the actual frequency response curve deviated from the predicted one in this frequency region. In addition, the spatial mode shape deviated from the assumed mode shape in this frequency region, as shown in Fig. (1.2) . Both of these experimental observations were important deviations from expected behavior. The present investigation was motivated by the observations and was initiated to explain them.

The assumed solution, Eq.(1.3), did not allow for superharmonic response and so in this author's first attempt to account for it, a solution of the form:

$$w(x,t) = W_1(x)(W_1\cos(\Omega(t-\beta_2)) + W_2\cos(2\Omega(t-\beta_2)) + W_2(x)(W_3\cos(\Omega(t-\beta_3)) + W_4\cos(2\Omega(t-\beta_4)) \quad (1.4a)$$

$$\Psi(x,t) = \Psi_1(x)(V_1\cos(\Omega(t-\alpha_1)) + V_2\cos(2\Omega(t-\alpha_2)) + \Psi_2(x)(V_3\cos(\Omega(t-\alpha_3)) + V_4\cos(2\Omega(t-\alpha_4)) \quad (1.4b)$$

was assumed and Galerkin's method and harmonic balance used to determine $W_1, \ldots, V_4, \alpha_1, \ldots, \beta_4$. The different spatial mode shapes $W_1(x)$ and $W_2(x)$, as well as $\Psi_1(x)$ and $\Psi_2(x)$, were chosen to account for the spatial behavior while the frequency 2Ω was included to account for the temporal response. Since the governing equations represent a cubic hardening system which will respond with only the odd harmonics when excited by a single harmonic, the approach failed to predict the observed response. It was obvious there were other causes for the observed behavior. Perhaps there were important structural effects in the layered construction not included in the theory or there were effects present in the experiment not accounted for in the theory. In Kovac's experiment the force on the beam, which was produced by an electromagnet, was actually a constant plus a harmonic. However, Kovac did not include the constant term in arriving at his theoretical results. Stoker[30] and Meirovitch[31] show the existence of response at more than one frequency when exciting a cubic hardening spring-mass system with a constant plus a harmonic force. The results are derived as a perturbation on a linear spring but they are important because they predict the existence of response at twice the forcing frequency. This then raises the question that if the beam is expected to respond at more than one frequency, which frequency should be used to evaluate the complex moduli properties of the core?

In an effort to resolve these issues, a theory is developed in Chapter 2 to determine the vibratory behavior of three-layer axially restrained beams when the transverse deflections are the same order as the total beam thickness. All important structural effects are accounted for, including the bending resistance of the individual face layers, and the derivation follows some of the ideas used in the aforementioned investigations but extends the ideas to include the effects of multiple frequency response in the viscoelastic core and dissimilar face layers. First a plate theory is developed and the beam equations are considered as a special case. Certain approximations are made for soft cores and other effects and the equations simplify in a systematic way to include only those effects which are important to the analysis. These equations are compared to Eqs. (1.2) and in Chapter 3 an attempt is made to explain the superharmonic response by finding approximate solutions to the equations for a constant plus a harmonic force.

Based on observations from Kovac's experiment, it was necessary to assume that the superharmonic component of the response was the same order of magnitude as the response at the forcing frequency and could not be treated as a perturbation. This assumption led to 14 nonlinear algebraic equations and, although a certain amount of superharmonic was predicted, the analysis failed to predict the magnitude observed.

It was then felt necessary to repeat some of Kovac's experiments to verify his measurements. It was found that an interaction between the beam displacement measuring device - a Bentley-Nevada proximeter - and the magnetic field, used to excite the beam, was causing an error in the measurement of the beam displacement. Further investigation with the proximeter indicated that inaccurate readings can result if the displacement of a ferromagnetic material is being measured and the material is approaching magnetic saturation. Operation of the proximeter depends on the electrical conductivity of the material whose displacement is being measured and a magnetic field will alter the conductivity. This is what happened near the center of the beam, where it was being forced, resulting in inaccurate measurements in this region. Even though an accurate measurement of spatial mode shape was impossible with Kovac's specimens, measurements of beam displacement time histories away from the location of the magnet indicated that superharmonic response of the beam did really occur with the magnitude reported by Kovac.

Since the structural theory and the approximate solution were felt to accurately represent the physics of the beam and yet had failed to account for the observed behavior, attention was turned to the forcing method. Further investigation indicated that part of the observed response was probably caused by the magnetic forcing system. The nonlinear relation between the magnetic

induction, B, which produces the force, and the magnetic intensity, H, which is directly related to the current in the windings of the magnet, caused the force to contain harmonics of the forcing frequency. In addition, spatial nonuniformities in the field strength near the pole of the magnet added harmonics to the beam response. Chapter 4 elaborates on these effects and details the design of a feedback control system used to insure that the force on the beam is a harmonic plus a constant bias. Chapter 5 then presents experimental results and compares them with the results of Chapter 3. Chapter 6 summarizes the results of this investigation and makes recommendations for future work.

CHAPTER II

DERIVATION OF EQUATIONS

The principle of virtual work states that at equilibrium, the total work done by the internal and external forces during an arbitrary virtual displacement, satisfying the prescribed kinematic boundary conditions and geometric constraints, is zero. It is important to note that the principle holds irrespective of the constitutive equations and refers to the body in the equilibrium position. The work terms involve integrals over the deformed shape, which is unknown a priori. To circumvent this, the equilibrium stresses, strains and displacements are described in terms of the body before deformation (Lagrangian coordinates). When this is done, the integrals are over known regions.

2.1 REVIEW OF FINITE DEFORMATION

For completeness and review purposes, a brief description of large deformations is now presented. For a comprehensive description, see Novozhilov[32].

Referring to Fig. 2.1, suppose before deformation that a body occupies a region V enclosed by a surface S. After deformation the body occupies a region $\bar{V}$ and is enclosed by a surface $\bar{S}$. Referred to the same set of rectangular cartesian coordinates, a point in the body at position x_1, x_2, x_3 before deformation is located at $\bar{x}_1$, $\bar{x}_2$, $\bar{x}_3$ after deformation. The displacement components u_i are given by

$$\bar{x}_i = x_i + u_i(x_1, x_2, x_3), \quad i = 1,2,3 \tag{2.1}$$

Referring to Fig. 2.2, a rectangular volume element dx_1 by dx_2 by dx_3 whose sides, before deformation, are parallel to the X_1, X_2, X_3 axis, respectively, becomes an oblique parallelepiped with edges $dl_1 = (1+E_1)dx_1$, $dl_2 = (1+E_2)dx_2$ and $dl_3 = (1+E_3)dx_3$. E_k is the relative elongation of a differential line element originally in the X_k direction and is related to the Green's strain tensor, ε_{ij}, by

$$E_k(1 + \tfrac{1}{2}E_k) = \varepsilon_{kk} \quad \text{(no sum)} \tag{2.2}$$

where

$$\varepsilon_{ij} = e_{ij} + \tfrac{1}{2}(e_{ki} + \omega_{ki})(e_{kj} + \omega_{kj}) \tag{2.3}$$

and

$$e_{ij} = \tfrac{1}{2}\left(\frac{\partial u_i}{\partial x_j} + \frac{\partial u_j}{\partial x_i} \right), \quad \omega_{ij} = \tfrac{1}{2}\left(\frac{\partial u_i}{\partial x_j} - \frac{\partial u_j}{\partial x_i} \right) \tag{2.4}$$

The angles between dl_1 and dl_2, and dl_1 and dl_3, and dl_2 and dl_3 are given by $\frac{\pi}{2} - \phi_{12}$, $\frac{\pi}{2} - \phi_{13}$ and $\frac{\pi}{2} - \phi_{23}$, respectively, where ϕ_{ij} is given by

$$\sin(\phi_{ij}) = \frac{\varepsilon_{ij}}{(1 + E_i)(1 + E_j)} \tag{2.5}$$

The ratio of volume before and after deformation is given by

$$d\bar{V}/dV = D \tag{2.6}$$

where

$$D = \begin{vmatrix} 1+\frac{\partial u_1}{\partial x_1} & \frac{\partial u_1}{\partial x_2} & \frac{\partial u_1}{\partial x_3} \\ \frac{\partial u_2}{\partial x_1} & 1+\frac{\partial u_2}{\partial x_2} & \frac{\partial u_2}{\partial x_3} \\ \frac{\partial u_3}{\partial x_1} & \frac{\partial u_3}{\partial x_2} & 1+\frac{\partial u_3}{\partial x_3} \end{vmatrix} = \begin{vmatrix} 1+e_{11} & e_{12}+\omega_{12} & e_{13}+\omega_{13} \\ e_{21}+\omega_{21} & 1+e_{22} & e_{23}+\omega_{23} \\ e_{31}+\omega_{31} & e_{32}+\omega_{32} & 1+e_{33} \end{vmatrix} \tag{2.7}$$

and the ratio of density before deformation, ρ, and the density after deformation, $\bar{\rho}$, is given by

$$\rho/\bar{\rho} = D \tag{2.8}$$

The area of the side originally parallel to the X_1X_2 plane, dS_3, becomes $d\bar{S}_3$ after deformation and they are related by

$$d\bar{S}_3/dS_3 = \sqrt{(1+2\varepsilon_{11})(1+2\varepsilon_{22}) - 4\varepsilon_{12}^2} \tag{2.9a}$$

Similarily

$$d\bar{S}_2/dS_2 = \sqrt{(1+2\varepsilon_{11})(1+2\varepsilon_{33}) - 4\varepsilon_{13}^2} \tag{2.9b}$$

$$d\bar{S}_1/dS_1 = \sqrt{(1+2\varepsilon_{22})(1+2\varepsilon_{33}) - 4\varepsilon_{23}^2} \tag{2.9c}$$

The relation between a deformed area element, $d\bar{S}$, with

arbitrarily directed normal $\bar{\nu}_m$ and an undeformed area element, dS, with normal ν_k is given by

$$\bar{\nu}_m d\bar{S} = D \frac{\partial x_k}{\partial \bar{x}_m} \nu_k dS \tag{2.10}$$

where $\bar{\nu}_m$ and ν_k are the direction cosines of the normal to the deformed and undeformed areas, respectively.

2.2 PRINCIPLE OF VIRTUAL WORK

The principle of virtual work can be written as

$$\int_V \{\rho_i F_i + \frac{\partial}{\partial x_k} (S_{km}(\delta_{im} + e_{im} + \omega_{im}))\} \delta u_i dV +$$

$$\int_S \{T_i - S_{km}(\delta_{im} + e_{im} + \omega_{im}) \nu_k\} \delta u_i dS = 0 \tag{2.11}$$

where summation convention is being used and δ_{im} is the kronecker delta, F_i is the body force per unit mass and S_{km} are the Kirchhoff stress components. The Kirchhoff stresses are not physical stresses because they are forces per unit undeformed area; however, they are symmetric. T_i are the surface tractions per unit undeformed area. The transformation from surface tractions in terms of deformed areas to tractions in terms of undeformed areas is complicated and care must be used in computing the virtual work from these forces. The transformation simplifies

when certain loadings, e.g. constant direction, and geometries, e.g. rectangular bodies, are considered.

2.3 APPLICATION TO LAYERED PLATE

Equation 2.11 will be applied to a three-layer plate whose configuration is shown in Fig. 2.3. The plate is, in general, made from three different materials perfectly bonded at the interface. It has much smaller dimensions in the thickness direction than in the other directions. The plate can be loaded by forces parallel and/or perpendicular to the upper and lower surface. It will be assumed that in the interior of the plate the normal stress in the thickness direction is small compared to the normal stresses in the plane of the plate and will be assumed zero. Also it will be assumed that normal strains in the thickness direction are negligible compared to other strains. The body forces will be strictly inertial with the effects of gravity being ignored.

When considering transverse deflections of the plate that are limited to the same order of magnitude as the total plate thickness, it can be assumed that the elongations, E_i, and the shear deformations, ϕ_{ij}, are small compared to unity. Then Eqs. 2.2 and 2.5 yield

$$E_i = \epsilon_{ii} \qquad i = 1,2,3 \tag{2.12}$$

$$\phi_{ij} = \epsilon_{ij} \qquad i,j = 1,2,3 \qquad i \neq j \tag{2.13}$$

Also, for transverse deflections of this magnitude, the local rotations, ω_{ij}, are small compared to unity. However, the majority of the plate deflection is due to these local rotations and so the elongations and shear strains can be considered negligible compared to these rotations. For the magnitude of deflections considered here, if L is the plate's longest dimension and its total thickness is h_T, then

$$\varepsilon_{ij} = O(\epsilon^2) \quad i,j = 1,2,3 \tag{2.14}$$

$$\omega_{ij} = O(\epsilon) \quad i,j = 1,2,3 \tag{2.15}$$

where $\epsilon = h_T/L$. Using Eq. 2.3

$$e_{ij} = O(\epsilon^2) \quad i,j = 1,2,3 \tag{2.16}$$

When appropriate, e_{ij} can be dropped compared to ω_{ij} and both can be dropped compared to unity. Using Eqs. 2.14, 2.15 and 2.16,

$$D = 1 \quad \text{and} \quad d\bar{S}_i/dS_i = 1, \quad i = 1,2,3 \tag{2.17}$$

Thus, restricting the plate deflections to the same order as total plate thickness means that the distinction between volumes and areas before and after deformation can be ignored and that the Kirchhoff stress components

represent true stresses. The deformations are small enough so that linear materials will not deform beyond their linear range and nonlinearities in the problem will be strictly geometric. One further simplification can be introduced at this point. Since transverse loadings and deflections are of prime concern, it is fair to assume that local rotations about the X_3 axis are small compared to local rotations about the X_1 and X_2 axis. Thus

$$\omega_{21} , \omega_{12} \cong 0 \tag{2.18}$$

Since the plate is made of three different materials, certain material properties are discontinuous at the interfaces between layers. This should not affect the application of the principle of virtual work since the principle does not depend on constitutive laws. However, since the material properties are discontinuous, certain kinematic quantities and stresses could be discontinuous at the interfaces and the question arises as to whether the principle in the form 2.11 can be applied in situations where discontinuities exist. This is a question which deserves a rigorous investigation and shall not be explored here. To avoid any problems associated with the application of the principle in these situations, the principle will be applied as if each layer, within which all quantities are continuous, is independent and the layers will be related by certain interface conditions.

Using the simplifications mentioned above, changing notation such that $x_1 = x$, $x_2 = y$, $x_3 = z$, $u_1 = u$, $u_2 = v$, $u_3 = w$ and with the subscripts 1=x, 2=y, 3=z and expanding Eq. 2.11, one gets a new equation of motion.

$$\sum_{i=1}^{3} \int_V [\{-\rho_i \ddot{u} + \frac{\partial}{\partial x}(S_{xxi}+S_{xzi}\omega_{xzi}) + \frac{\partial}{\partial y}(S_{yxi}+S_{yzi}\omega_{xzi}) + \frac{\partial}{\partial z}(S_{zxi}+S_{zzi}\omega_{xzi})\}\delta u_i + \{-\rho_i \ddot{v}_i + \frac{\partial}{\partial x}(S_{xyi}+S_{xzi}\omega_{yzi}) + \frac{\partial}{\partial y}(S_{yyi}+S_{yzi}\omega_{yzi}) + \frac{\partial}{\partial z}(S_{zyi}+S_{zzi}\omega_{yzi})\}\delta v_i + \{-\rho_i \ddot{w}_i + \frac{\partial}{\partial x}(S_{xxi}\omega_{zxi}+S_{xyi}\omega_{zyi}+S_{xzi}) + \frac{\partial}{\partial y}(S_{yxi}\omega_{zxi}+S_{yyi}\omega_{zyi} + S_{yzi}) + \frac{\partial}{\partial z}(S_{zxi}\omega_{zxi}+S_{zyi}\omega_{zyi}+S_{zzi})\}\delta w_i] \, dxdydz +$$

$$\sum_{i=1}^{3} \int_S [\{T_{xi}-(S_{xxi}+S_{xzi}\omega_{xzi})\ell_i-(S_{yxi}+S_{yzi}\omega_{xzi})m_i - (S_{zxi}+S_{zzi}\omega_{xzi})n_i\}\delta u_i + \{T_{yi} - (S_{xyi}+S_{xzi}\omega_{yzi})\ell_i - (S_{yyi}+S_{yzi}\omega_{yzi})m_i-(S_{zyi}+S_{zzi}\omega_{yzi})n_i\}\delta v_i + \{T_{zi}-(S_{xxi}\omega_{zxi} + S_{xyi}\omega_{zyi}+S_{xzi})\ell_i - (S_{yxi}\omega_{zxi}+S_{yyi}\omega_{zyi}+ S_{yzi}) m_i - (S_{zxi}\omega_{zxi}+S_{zyi}\omega_{zyi}+S_{zzi})n_i\}\delta w_i] dS = 0 \qquad (2.19)$$

where the summation is over the three layers and the

subscript i refers to a particular quantity in the i-th layer and ℓ_i, m_i and n_i are the direction cosines, in the x, y and z directions respectively, of the normal to the outer surface and take values of ± 1 or 0, depending on the surface. This equation will be used directly to derive the equations governing the transverse motions of a three layer plate.

2.4 ASSUMED DISPLACEMENT FIELD

It will be assumed, in common with other workers, that in each layer, plane sections remain plane. Because of shear deformation, plane sections perpendicular before deformation will not necessarily be perpendicular after deformation. In any one layer the displacements in the plane of the plate will be due to extension, shear and bending deformation. The extensional displacement is assumed uniform across the thickness of the layer while the shear and bending effects cause the displacements to vary linearly in the thickness direction. In keeping with the assumption of neglecting strain in the thickness direction, the out-of-plane displacement, w, will not vary with thickness and is the same in each layer. Referring to Fig. 2.4a, the assumed displacements can be written in the form

$$u_i(x,y,z,t) = u_i^0(x,y,t) + z\Psi_i(x,y,t) \qquad (2.20a)$$

$$v_i(x,y,z,t) = v_i^0(x,y,t) + z\phi_i(x,y,t) \qquad (2.20b)$$

$$w_i(x,y,z,t) = w(x,y,t) \qquad (2.20c)$$

$u_i^0(x,y,t)$ and $v_i^0(x,y,t)$ represent uniform extension of the i-th layer in the x and y direction, respectively, while $\Psi_i(x,y,t)$ represents the combined effect of shear and bending deformation in the xz plane and $\phi_i(x,y,t)$ represents the same effect in the yz plane. The form of Eq. 2.20 leads to a uniform shear stress across each layer and ultimately, after interface conditions are enforced, across the entire thickness. This can lead to difficulties since, for no shearing tractions on the upper and lower surfaces of the plate, the shear stress is physically zero at the outer edges of the plate but could take on a non-zero value in the interior of the plate. Perhaps a displacement field involving higher order powers of z could be used to allow the shear to vanish on the outer edges but not in the interior. Equation 2.20 accounts for shearing deformation but produces a shear stress distribution in an average sense. When interface continuity conditions are enforced, the deformation of the composite plate will be as shown in Fig. 2.4b. Substituting the assumed displacements 2.20 into the definition of rotation 2.4 gives

$$\omega_{xzi} = \tfrac{1}{2}(\Psi_i - \frac{\partial w}{\partial x}) = -\omega_{zxi} \qquad (2.21a)$$

$$\omega_{yzi} = \tfrac{1}{2}(\phi_i - \frac{\partial w}{\partial y}) = -\omega_{yzi} \qquad (2.21b)$$

Note that ω_{xzi} and ω_{yzi} are not functions of z. This will help simplify integration with respect to z in the next section.

2.5 GOVERNING EQUATIONS

The assumed displacement field, Eq. 2.20, is now substituted into the principle of virtual work, Eq. 2.19, giving

$$\sum_{i=1}^{3} \int_{-\frac{L_x}{2}}^{\frac{L_x}{2}} \int_{-\frac{L_y}{2}}^{\frac{L_y}{2}} \int_{z_{i-1}}^{z_i} [\{-\rho_i(\ddot{u}_i^0+z\ddot{\Psi}_i)+ \frac{\partial}{\partial x}(S_{xxi}+S_{xzi}\omega_{xzi})+\frac{\partial}{\partial y}(S_{yxi} +$$

$$S_{yzi}\omega_{xzi})+ \frac{\partial}{\partial z}(S_{zxi}+S_{zzi}\omega_{xzi})\}\{\delta u_i^0+z\delta\Psi_i\}+\{-\rho_i(\ddot{v}_i+z\ddot{\phi}_i) +$$

$$\frac{\partial}{\partial x}(S_{xyi}+S_{xzi}\omega_{yzi})+ \frac{\partial}{\partial y}(S_{yyi}+S_{yzi}\omega_{yzi})+ \frac{\partial}{\partial z}(S_{zyi}+S_{zzi}\omega_{yzi})\} \times$$

$$\{\delta\ddot{v}_i+z\delta\ddot{\phi}_i\}+\{-\rho_i\ddot{w}+ \frac{\partial}{\partial x}(S_{xxi}\omega_{zxi}+S_{xyi}\omega_{zyi}+S_{xzi})+ \frac{\partial}{\partial y}(S_{yxi}\omega_{zxi}+$$

$$S_{yyi}\omega_{zyi}+S_{yzi})+ \frac{\partial}{\partial z}(S_{zxi}\omega_{zxi}+S_{zyi}\omega_{zyi}+S_{zzi})\}\delta w]dxdydz +$$

$$\sum_{i=1}^{3} \int_S [\{T_{xi}-(S_{xxi}+S_{xzi}\omega_{xzi})\ell_i - (S_{yxi}+S_{yzi}\omega_{xzi})m_i -$$

$$(S_{zxi}+S_{zzi}\omega_{xzi})n_i\}\delta u_i + \{T_{yi}-(S_{xyi}+S_{xzi}\omega_{yzi})\ell_i -$$

$$(S_{yyi}+S_{yzi}\omega_{yzi})m_i - (S_{zyi}+S_{zzi}\omega_{yzi})n_i\}\delta v_i + \{T_{zi} -$$

$$(S_{xxi}\omega_{zxi}+S_{xyi}\omega_{zyi}+S_{xzi})\ell_i - (S_{yxi}\omega_{zxi}+S_{yyi}\omega_{zyi}+S_{yzi})m_i -$$

$$(S_{zxi}\omega_{zxi}+S_{zyi}\omega_{zyi}+S_{zzi})n_i\}\delta w_i]dS = 0 \qquad (2.22)$$

where all layers extend from $-L_x/2$ to $+L_x/2$ in the x direction, $-L_y/2$ to $+L_y/2$ in the y direction and the i-th layer extends from z_{i-1} to z_i in the z direction.

Integrating with respect to z, one gets

$$\sum_{i=1}^{3} \int_{-\frac{L_x}{2}}^{\frac{L_x}{2}} \int_{-\frac{L_y}{2}}^{\frac{L_y}{2}} [\{-\rho_i(h_i\ddot{u}_i^0+A_{io}\ddot{\Psi}_i)+\frac{\partial}{\partial x}(N_{xxi}+Q_{xzi}\omega_{xzi})+\frac{\partial}{\partial y}(N_{yxi}+$$

$$Q_{yzi}\omega_{xzi})+(S_{zxi}+S_{zzi}\omega_{xzi})\Big|_{z=z_{i-1}}^{z=z_i}\}\delta u_i^0+\{-\rho_i(A_{io}\ddot{u}_i^0+I_{io}\ddot{\Psi}_i)+\frac{\partial}{\partial x}(M_{xxi}+$$

$$M_{xzi}\omega_{xzi})+\frac{\partial}{\partial y}(M_{yxi}+M_{yzi}\omega_{xzi})+(z(S_{zxi}+S_{zzi}\omega_{xzi}))\Big|_{z=z_{i-1}}^{z=z_i}-Q_{xzi}\}\delta\Psi_i+$$

$$\{-\rho_i(h_i\ddot{v}_i^0+A_{io}\ddot{\phi}_i)+\frac{\partial}{\partial x}(N_{xyi}+Q_{xzi}\omega_{yzi})+\frac{\partial}{\partial y}(N_{yyi}+Q_{yzi}\omega_{yzi})+$$

$$(S_{zyi}+S_{zzi}\omega_{yzi})\Big|_{z=z_{i-1}}^{z=z_i}\}\delta v_i^0+\{-\rho_i(A_{io}\ddot{v}_i^0+I_{io}\ddot{\phi}_i)+\frac{\partial}{\partial x}(M_{xyi}+$$

$$M_{xzi}\omega_{yzi})+\frac{\partial}{\partial y}(M_{yyi}+M_{yzi}\omega_{yzi})+(z(S_{zyi}+S_{zzi}\omega_{yzi}))\Big|_{z=z_{i-1}}^{z=z_i}-$$

$$Q_{yzi}\}\delta\phi_i+\{-\rho_i h_i\ddot{w}_i+\frac{\partial}{\partial x}(N_{xxi}\omega_{zxi}+N_{xyi}\omega_{zyi}+Q_{xzi})+\frac{\partial}{\partial y}(N_{yxi}\omega_{zxi}+$$

$$N_{yyi}\omega_{zyi}+Q_{yzi})+(S_{zxi}\omega_{zxi}+S_{zyi}\omega_{zyi}+S_{zzi})\Big|_{z=z_{i-1}}^{z=z_i}\}\delta w]dxdz +$$

$$\int_S [\{T_{xi}-(S_{xxi}+S_{xzi}\omega_{xzi})\ell_i -(S_{yxi}+S_{yzi}\omega_{xzi})m_i -(S_{zxi} +$$

$$S_{zzi}\omega_{xzi})n_i\}\delta u_i +\{T_{yi}-(S_{xyi}+S_{xzi}\omega_{yzi})\ell_i -(S_{yyi} +$$

$$S_{yzi}\omega_{yzi})m_i-(S_{zyi}+S_{zzi}\omega_{yzi})n_i\}\ \delta v_i+\ \{T_{zi}-\ (S_{xxi}\omega_{zxi} +$$

$$S_{xyi}\omega_{zyi}+S_{xzi})\ell_i - (S_{yxi}\omega_{zxi}+S_{yyi}\omega_{zyi}+S_{yzi})m_i-(S_{zxi}\omega_{zxi}+$$

$$S_{zyi}\omega_{zyi}+S_{zzi})n_i\}\delta w]dS = 0 \qquad (2.23a)$$

where

$$h_i = \int_{z_{i-1}}^{z_i} dz \qquad A_{io}= \int_{z_{i-1}}^{z_i} zdz \qquad I_{io}= \int_{z_{i-1}}^{z_i} z^2dz \qquad (2.23b)$$

and the stress resultants are defined by

$$N_{xxi} = \int_{z_{i-1}}^{z_i} S_{xxi}dz \qquad N_{yyi} = \int_{z_{i-1}}^{z_i} S_{yyi}dz$$

$$M_{xxi} = \int_{z_{i-1}}^{z_i} zS_{xxi}dz \qquad M_{yyi} = \int_{z_{i-1}}^{z_i} zS_{yyi}dz$$

$$N_{xyi} = \int_{z_{i-1}}^{z_i} S_{xyi}\,dz \qquad M_{xyi} = \int_{z_{i-1}}^{z_i} zS_{xyi}\,dz$$

$$Q_{xzi} = \int_{z_{i-1}}^{z_i} S_{xzi}\,dz \qquad M_{xzi} = \int_{z_{i-1}}^{z_i} zS_{xzi}\,dz \qquad (2.23c)$$

$$Q_{yzi} = \int_{z_{i-1}}^{z_i} S_{yzi}\,dz \qquad M_{yzi} = \int_{z_{i-1}}^{z_i} zS_{yzi}\,dz$$

It is important to note that integration on the z variable has produced quantities evaluated at the interfaces, e.g. $(S_{zxi}+S_{zzi}\omega_{xzi})$. It is at the interfaces the question of discontinuities arises and treating each layer individually has exposed all legitimate contributions to the virtual work. This approach appears to negate the most convenient feature of variational methods of not involving internal forces. However, this approach, while not as elegant, has a firm basis.

Noting that δu_i^0, $\delta \Psi_i$, ..., δw are independent, Eq.2.23 gives

$$\frac{\partial}{\partial x}(N_{xxi}+Q_{xzi}\omega_{xzi})+\frac{\partial}{\partial y}(N_{yxi}+Q_{yzi}\omega_{xzi})+(S_{zxi}+S_{zzi}\omega_{xzi})\Big|_{z_{i-1}}^{z_i}$$

$$-\rho_i(h_i\ddot{u}_i^0 + A_{io}\ddot{\Psi}_i) = 0 \qquad (2.24a)$$

$$\frac{\partial}{\partial x}(M_{xxi}+M_{xzi}\omega_{xzi})+\frac{\partial}{\partial y}(M_{yxi}+M_{yzi}\omega_{xzi})+(z(S_{zxi}+S_{zzi}\omega_{xzi}))\Big|_{z_{i-1}}^{z_i}$$

$$-Q_{xzi}-\rho_i(A_{io}\ddot{u}_i^0+I_{io}\ddot{\Psi}_i)=0 \qquad (2.24b)$$

$$\frac{\partial}{\partial x}(N_{xyi}+Q_{xzi}\omega_{yzi})+\frac{\partial}{\partial y}(N_{yyi}+Q_{yzi}\omega_{yzi})+(S_{zyi}+S_{zzi}\omega_{yzi})\Big|_{z_{i-1}}^{z_i}$$

$$-\rho_i(h_i\ddot{v}_i^0+A_{io}\ddot{\phi}_i)=0 \qquad (2.24c)$$

$$\frac{\partial}{\partial x}(M_{xyi}+M_{xzi}\omega_{yzi})+\frac{\partial}{\partial y}(M_{yyi}+M_{yzi}\omega_{yzi})+(z(S_{zyi}+S_{zzi}\omega_{yzi}))\Big|_{z_{i-1}}^{z_i}$$

$$-Q_{yzi}-\rho_i(A_{io}\ddot{v}_i^0+I_{io}\ddot{\phi}_i)=0 \qquad (2.24d)$$

$$\frac{\partial}{\partial x}(N_{xxi}\omega_{zxi}+N_{xyi}\omega_{zyi}+Q_{xzi})+\frac{\partial}{\partial y}(N_{yxi}\omega_{zxi}+N_{yyi}\omega_{zyi}+Q_{yzi})$$

$$+(S_{zxi}\omega_{zxi}+S_{zyi}\omega_{zyi}+S_{zzi})\Big|_{z_{i-1}}^{z_i}-\rho_i h_i\ddot{w}=0 \qquad (2.24e)$$

and

$$\sum_{i=1}^{3}\Bigg[\Bigg\{\int_{-\frac{L_x}{2}}^{\frac{L_x}{2}}\int_{-\frac{L_y}{2}}^{\frac{L_y}{2}}[\{T_{xi}-(S_{zxi}+S_{zzi}\omega_{xzi})n_i\}\delta u_i+\{T_{yi}-$$

$$(S_{zyi}+S_{zzi}\omega_{yzi})n_i\}\delta v_i+\{T_{zi}-(S_{zxi}\omega_{zxi}+S_{zyi}\omega_{zyi}+$$

$$S_{zzi})n_i\}\delta w]dxdy\Big|_{z=z_{i-1}}^{z=z_i} + \int_{-\frac{L_y}{2}}^{\frac{L_y}{2}}\int_{z_{i-1}}^{z_i}[\{T_{xi}-(S_{xxi}+S_{xzi}\omega_{xzi})\ell_i\}\delta u_i+$$

$$\{T_{yi}-(S_{xyi}+S_{xzi}\omega_{yzi})\ell_i\}\delta v_i+\{T_{zi}-(S_{xxi}\omega_{zxi}+S_{xyi}\omega_{zyi}+$$

$$S_{xzi})\ell_i\}\delta w]dydz\Big|_{x=-\frac{L_x}{2}}^{x=\frac{L_x}{2}} + \int_{-\frac{L_x}{2}}^{\frac{L_x}{2}}\int_{z_{i-1}}^{z_i}[\{T_{xi}-(S_{yxi}+S_{yzi}\omega_{xzi})m_i\}\delta u_i+$$

$$\{T_{yi}-(S_{yyi}+S_{yzi}\omega_{yzi})m_i\}\delta v_i+\{T_{zi}-(S_{yxi}\omega_{zxi}+S_{yyi}\omega_{zyi}+$$

$$S_{yzi})m_i\}\delta w]dxdz\Big|_{y=-\frac{L_y}{2}}^{y=\frac{L_y}{2}} = 0 \qquad (2.24f)$$

Several terms in the final equations are interesting. The products $Q_{xzi}\omega_{xzi}$, $Q_{yxi}\omega_{yzi}$ are projections of the shear stress resultant, a force in the thickness direction, in the x direction. The terms which result,

$$Q_{xzi}\frac{\partial\omega_{xzi}}{\partial x}, \frac{\partial Q_{xzi}}{\partial x}\omega_{xzi}, \text{ etc.} \qquad (2.25)$$

are refered to by Herrmann[33] as "shear curvature" and "shear buoyancy" terms. The terms such as

$$M_{xzi} \frac{\partial \omega_{xzi}}{\partial x}, \frac{\partial M_{xzi}}{\partial x} \omega_{xzi}, \text{ etc.} \tag{2.26}$$

are moments due to shear and are the counterparts of the shear curvature and shear buoyancy terms. The terms

$$N_{xxi}\omega_{zxi}, N_{xyi}\omega_{zyi}, \text{ etc.} \tag{2.27}$$

are projections of the in-plane stress resultant in the z direction.

If rotatory inertia is ignored and there are no applied forces, the equations for a single layer become, on locating the origin of the coordinates at the center of the plate so that $A_{10} = 0$ and $I_{10} = h^3/12$, h being the plate thickness,

$$\begin{aligned}
&\frac{\partial}{\partial x}(N_{xx} + Q_{xz}\omega_{xz}) + \frac{\partial}{\partial y}(N_{yx} + Q_{yz}\omega_{xz}) - \rho h\ddot{u}^0 = 0 \\
&\frac{\partial}{\partial x}(M_{xx} + M_{xz}\omega_{xz}) + \frac{\partial}{\partial y}(M_{yx} + M_{yz}\omega_{xz}) - Q_{xz} = 0 \\
&\frac{\partial}{\partial x}(N_{xy} + Q_{xz}\omega_{yz}) + \frac{\partial}{\partial y}(N_{yy} + Q_{yz}\omega_{yz}) - \rho h\ddot{v}^0 = 0 \\
&\frac{\partial}{\partial x}(M_{xy} + M_{xz}\omega_{yz}) + \frac{\partial}{\partial y}(M_{yy} + M_{yz}\omega_{yz}) - Q_{yz} = 0 \\
&\frac{\partial}{\partial x}(N_{xx}\omega_{zx}+N_{xy}\omega_{zy}+Q_{xz}) + \frac{\partial}{\partial y}(N_{yx}\omega_{zx}+N_{yy}\omega_{zy}+Q_{yz}) - \rho h\ddot{w} = 0
\end{aligned} \tag{2.28}$$

if shear motion is suppressed, so that $\omega_{xz} = -\frac{\partial w}{\partial x}$ and $\omega_{yz} = -\frac{\partial w}{\partial y}$ Eqs. 2.28 can be written as

$$\frac{\partial}{\partial x}(N_{xx}-Q_{xz}\frac{\partial w}{\partial x}) + \frac{\partial}{\partial y}(N_{yx}-Q_{yz}\frac{\partial w}{\partial x}) - \rho h\ddot{u}^0 = 0$$

$$\frac{\partial}{\partial x}(N_{xy}-Q_{xz}\frac{\partial w}{\partial y}) + \frac{\partial}{\partial y}(N_{yy}-Q_{yz}\frac{\partial w}{\partial y}) - \rho h\ddot{v}^0 = 0$$

$$\frac{\partial}{\partial x}(N_{xx}\frac{\partial w}{\partial x}) + \frac{\partial}{\partial x}(N_{xy}\frac{\partial w}{\partial y}) + \frac{\partial}{\partial y}(N_{yx}\frac{\partial w}{\partial y}) + \frac{\partial}{\partial y}(N_{yy}\frac{\partial w}{\partial y}) + \tag{2.29}$$

$$\frac{\partial^2 M_{xx}}{\partial x^2} + \frac{\partial^2 M_{yx}}{\partial y \partial x} + \frac{\partial^2 M_{xy}}{\partial y \partial x} + \frac{\partial^2 M_{yy}}{\partial y^2} - \frac{\partial^2}{\partial x^2}(M_{xz}\frac{\partial w}{\partial x}) - \frac{\partial^2}{\partial x \partial y}(M_{yz}\frac{\partial w}{\partial x}) -$$

$$\frac{\partial^2}{\partial y \partial x}(M_{xz}\frac{\partial w}{\partial y}) - \frac{\partial}{\partial y}(M_{yz}\frac{\partial w}{\partial y}) - \rho h\ddot{w} = 0$$

These are identical to Herrmann's Eq. 66 except for the terms $\frac{\partial}{\partial x}(M_{xz}\frac{\partial^2 w}{\partial x^2})$ which he does not include. The present author can see no reason for excluding them at this point. However, they are ultimately deleted.

2.6 INTERFACE CONDITIONS

The thirteen equations 2.24 are not independent, thanks to the interface conditions. For perfect bonds, the displacements are continuous across the interfaces. Since $w(x,y,z,t) = w(x,y,t)$, part of the requirement is automatically satisfied. Continuity of the u and v displacements requires

$$u_1(x,y,z_1,t) = u_2(x,y,z_1,t) \tag{2.30a}$$

$$v_1(x,y,z_1,t) = v_2(x,y,z_1,t) \tag{2.30b}$$

$$u_2(x,y,z_2,t) = u_3(x,y,z_2,t) \tag{2.30c}$$

$$v_2(x,y,z_2,t) = v_3(x,y,z_2,t) \tag{2.30d}$$

Examination of the dxdy portion of the surface integral, Eq. 2.24f, reveals that certain combinations of stresses must be continuous across the interfaces, specifically,

$$(S_{zx_1}+S_{zz_1}\omega_{xz_1})_{z=z_1} = (S_{zx_2}+S_{zz_2}\omega_{xz_2})_{z=z_1} \tag{2.31a}$$

$$(S_{zx_2}+S_{zz_2}\omega_{xz_2})_{z=z_2} = (S_{zx_3}+S_{zz_3}\omega_{xz_3})_{z=z_2} \tag{2.31b}$$

$$(S_{zy_1}+S_{zz_1}\omega_{yz_1})_{z=z_1} = (S_{zy_2}+S_{zz_2}\omega_{yz_2})_{z=z_1} \tag{2.31c}$$

$$(S_{zy_2}+S_{zz_2}\omega_{yz_2})_{z=z_2} = (S_{zy_3}+S_{zz_3}\omega_{yz_3})_{z=z_2} \tag{2.31d}$$

$$(S_{zx_1}\omega_{zx_1}+S_{zy_1}\omega_{zy_1}+S_{zz_1})_{z=z_1} =$$

$$(S_{zx_2}\omega_{zx_2}+S_{zy_2}\omega_{zy_2}+S_{zz_2})_{z=z_1} \tag{2.31e}$$

$$(S_{zx_2}\omega_{zx_2}+S_{zy_2}\omega_{zy_2}+S_{zz_2})_{z=z_2} =$$

$$(S_{zx_3}\omega_{zx_3}+S_{zy_3}\omega_{zy_3}+S_{zz_3})_{z=z_2} \tag{2.31f}$$

Since S_{zz} has been assumed to be zero on the interior of the plate, the stress interface conditions, Eq. 2.31, reduce to

$$(S_{zx_1})_{z=z_1} = (S_{zx_2})_{z=z_1} \tag{2.32a}$$

$$(S_{zx_2})_{z=z_2} = (S_{zx_3})_{z=z_2} \tag{2.32b}$$

$$(S_{zy_1})_{z=z_1} = (S_{zy_2})_{z=z_1} \tag{2.32c}$$

$$(S_{zy_2})_{z=z_2} = (S_{zy_3})_{z=z_2} \tag{2.32d}$$

and

$$(S_{zx_1}\omega_{xz_1}+S_{zy_1}\omega_{zy_1})_{z=z_1} = (S_{zx_2}\omega_{zx_2}+S_{zy_2}\omega_{zy_2})_{z=z_1} \tag{2.33a}$$

$$(S_{zx_2}\omega_{zx2}+S_{zy2}\omega_{zy2})_{z=z_2} = (S_{zx3}\omega_{zx3}+S_{zy3}\omega_{zy3})_{z=z_2} \qquad (2.33b)$$

As a result, Eqs. 2.32 and 2.33 require that the shear stress be continuous and that a relation exist among the local rotations, ω_{xzi} and ω_{yzi}, across the interfaces.These relations for the local rotations at the interface are kinematic constraints which result from enforcing force equilibrium. They physically exist, but to enforce them with the assumed approximate displacement field would constrain the shearing effect in the core. Enforcing only Eq. 2.32 instead of Eqs. 2.32 and 2.33 leaves a force imbalance in the thickness direction at the interface which is an order of magnitude less than the shear force at the interface, the dominant force there. Using the more sophisticated displacement field, mentioned previously, would allow more mathematical freedom to match all constraints at the interfaces.

Thus the eight interface conditions, Eqs. 2.30 and 2.32, applied to the thirteen variables u_i^0, Ψ_i, ..., w lead to five independent variables to describe the vibrational behavior of a three-layer plate. Even though the plate equations have lost generality by restricting the elongations and rotations, they are still difficult to solve. Further simplifications must be made in order to get the equations into manageable form but at the expense of limiting the physical applications.

In the next section the equations will be reduced to a form appropriate for sandwich beams with linear isotropic elastic outer layers and linear isotropic viscoelastic cores.

2.7 REDUCTION TO BEAM EQUATIONS

By setting to zero in Eqs. 2.24 $\partial/\partial y$ and any stress or displacement associated with y, the differential equations for a beam are:

$$\frac{\partial}{\partial x}(N_{xxi}+Q_{xzi}\omega_{xzi}) + (S_{zxi}+S_{zzi}\omega_{xzi}) \Big|_{z=z_{i-1}}^{z=z_i}$$

$$-\rho_i(h_i\ddot{u}_i^0 + A_{io}\ddot{\Psi}_i) = 0 \qquad (2.34a)$$

$$\frac{\partial}{\partial x}(M_{xxi}+M_{xzi}\omega_{xzi}) + (z(S_{zxi}+S_{zzi}\omega_{xzi})) \Big|_{z=z_{i-1}}^{z=z_i} -Q_{xzi}$$

$$-\rho_i(A_{io}\ddot{u}_i^0 + I_{io}\ddot{\Psi}_i) = 0 \qquad (2.34b)$$

$$\frac{\partial}{\partial x}(N_{xxi}\omega_{zxi}+Q_{xzi}) + (S_{zxi}\omega_{zxi}+S_{zzi}) \Big|_{z=z_{i-1}}^{z=z_i}$$

$$-\rho_i h_i\ddot{w} = 0 \qquad (2.34c)$$

The boundary integral becomes, for a beam of length L,

$$\sum_{i=1}^{3} \left[\int_{-L/2}^{L/2} \{T_{xi}-(S_{zxi}+S_{zzi}\omega_{xzi})\}\delta u_i + \{T_{zi}-(S_{zxi}\omega_{zxi} + S_{zzi})\}\delta w \right] dx \Big|_{z=z_{i-1}}^{z=z_i} + \int_{z_{i-1}}^{z_i} \{T_{xi}-(S_{xxi}+S_{xzi}\omega_{xzi})\}\delta u_i +$$

$$\{T_{zi}-(S_{xxi}\omega_{zxi}+S_{xzi})\}\delta w \quad dz \Big|_{x=-L/2}^{x=L/2} \tag{2.35}$$

and the interface conditions become,

$$u_1(x,z_1,t) = u_2(x,z_1,t) \tag{2.36a}$$

$$u_2(x,z_2,t) = u_3(x,z_2,t) \tag{2.36b}$$

$$(S_{zx1})_{z=z_1} = (S_{zx2})_{z=z_2} \tag{2.36c}$$

$$(S_{xz2})_{z=z_2} = (S_{zx3})_{z=z_2} \tag{2.36d}$$

For a beam with a soft core, the normal stress in the core, S_{xx2}, is negligible compared with the corresponding stress in the outer layers. Setting $S_{xx2}= 0$, summing on i in each of Eqs. 2.34 and using the interface conditions, one gets

$$\frac{\partial}{\partial x}(N_{xx1}+N_{xx3}+Q_{xz1}\omega_{xz1}+Q_{xz2}\omega_{xz2}+Q_{xz3}\omega_{xz3}) +$$

$$(S_{zx3}+S_{zz3}\omega_{xz3})_{z=z_3} - (S_{zx1}+S_{zz1}\omega_{xz1})_{z=z_0} - \rho_1(h_1\ddot{u}_1^0 + A_{10}\ddot{\Psi}_1) -$$

$$\rho_2\ (h_2\ddot{u}_2^0 + A_{20}\ddot{\Psi}_2) - \rho_3(h_3\ddot{u}_3^0 + A_{30}\ddot{\Psi}_3) = 0 \tag{2.37a}$$

$$\frac{\partial}{\partial x}(M_{xx1}+M_{xx3}+M_{xz1}\omega_{xz1}+M_{xz2}\omega_{xz2}+M_{xz3}\omega_{xz3}) +$$

$$(z(S_{zx3}+S_{zz3}\omega_{xz3}))_{z=z_3} - (z(S_{zx1}+S_{zz1}\omega_{xz1}))_{z=z_0} - (Q_{xz1}+Q_{xz2}+Q_{xz3}) -$$

$$\rho_1(A_{10}\ddot{u}_1^0 + I_{10}\ddot{\Psi}_1) - \rho_2(A_{20}\ddot{u}_2^0 + I_{20}\ddot{\Psi}_2) - \rho_3(A_{30}\ddot{u}_3^0 + I_{30}\ddot{\Psi}_3) = 0 \tag{2.37b}$$

$$\frac{\partial}{\partial x}(N_{xx1}\omega_{xz1}+N_{xx3}\omega_{zx3}+Q_{xz1}+Q_{xz2}+Q_{xz3}) + (S_{zx3}\omega_{zx3}+S_{zz3})_{z=z_3} -$$

$$(S_{zx1}\omega_{zx1}+S_{zz1})_{z=z_0} - (\rho_1 h_1+\rho_2 h_2+\rho_3 h_3)\ddot{w} = 0 \tag{2.37c}$$

where the terms $(S_{zx_3}+S_{zz_3}\omega_{xz_3})_{z=z_3}$, etc. are related to the applied loadings, T_{x_3}, etc., through the x integral in the boundary term, Eq. 2.35.

If the two outer layers are linear elastic and the core is linear viscoelastic, the stress-strain relations become, for the outer layers, recalling that $S_{yyi}= 0$, $S_{zzi}= 0$

$$S_{xxi}=E_i\varepsilon_{xxi} \quad \text{and} \quad S_{xzi}=2G_i\varepsilon_{xzi} \qquad i=1 \text{ and } 3 \tag{2.38a}$$

where E_i and G_i are Young's modulus and the shear modulus, respectively, and for the core,

$$S_{xz_2} = 2\int_{-\infty}^{t} Y_2(t-\tau)d\varepsilon_{xz_2}(\tau) \tag{2.38b}$$

where $Y_2(t)$ is the shear stress relaxation function of the core material. The stress interface conditions become, using Eqs. 2.3, 2.14, 2.15, 2.16, 2.20, 2.36 and 2.38,

$$G_1(\Psi_1+\frac{\partial w}{\partial x}) = \int_{-\infty}^{t} Y_2(t-\tau)d(\Psi_2+\frac{\partial w}{\partial x}) \tag{2.39a}$$

$$G_3(\Psi_3+\frac{\partial w}{\partial x}) = \int_{-\infty}^{t} Y_2(t-\tau)d(\Psi_2+\frac{\partial w}{\partial x}) \tag{2.39b}$$

The displacement interface conditions, Eqs. 2.36a and b, become, using Eq. 2.20,

$$u_1^0 + z_1\Psi_1 = u_2^0 + z_1\Psi_2 \tag{2.40a}$$

$$u_3^0 + z_2\Psi_3 = u_2^0 + z_2\Psi_2 \tag{2.40b}$$

Defining $u_2^0 = U$ and $\Psi_2 = \Psi$ and solving Eqs. 2.39 and 2.40 for u_1^0, u_3^0, Ψ_1 and Ψ_3, the displacement field becomes,

$$u_1 = U + z_1\left(\Psi + \frac{\partial w}{\partial x} - \frac{1}{G_1}\int_{-\infty}^{t} Y_2(t-\tau)\,d\left(\Psi + \frac{\partial w}{\partial x}\right) + z\left(\frac{1}{G_1}\int_{-\infty}^{t} Y_2(t-\tau)\,d\left(\Psi + \frac{\partial w}{\partial x}\right) - \frac{\partial w}{\partial x}\right)\right. \tag{2.41a}$$

$$u_2 = U + z\Psi \tag{2.41b}$$

$$u_3 = U + z_2\left(\Psi + \frac{\partial w}{\partial x} - \frac{1}{G_3}\int_{-\infty}^{t} Y_2(t-\tau)\,d\left(\Psi + \frac{\partial w}{\partial x}\right) + z\left(\frac{1}{G_3}\int_{-\infty}^{t} Y_2(t-\tau)\,d\left(\Psi + \frac{\partial w}{\partial x}\right) - \frac{\partial w}{\partial x}\right)\right. \tag{2.41c}$$

$$\Psi_1 = \frac{1}{G_1}\int_{-\infty}^{t} Y_2(t-\tau)\,d\left(\Psi + \frac{\partial w}{\partial x}\right) - \frac{\partial w}{\partial x} \tag{2.41d}$$

$$\Psi_3 = \frac{1}{G_3}\int_{-\infty}^{t} Y_2(t-\tau)\,d\left(\Psi + \frac{\partial w}{\partial x}\right) - \frac{\partial w}{\partial x} \tag{2.41e}$$

For an elastic core

$$\int_{-\infty}^{t} Y_2(t-\tau)\,d\left(\Psi + \frac{\partial w}{\partial x}\right) = G_2\left(\Psi + \frac{\partial w}{\partial x}\right)$$

where G_2 is the shear modulus of the material. For a soft elastic core material $(G_2/G_1)<<1$ and

$$(\Psi+\frac{\partial w}{\partial x}) - (G_2/G_1)(\Psi+\frac{\partial w}{\partial x}) \cong (\Psi+\frac{\partial w}{\partial x}) \tag{2.42}$$

Thus for a soft viscoelastic core with damping properties the same order of magnitude as its elastic properties, the following approximation is justified:

$$\Psi+\frac{\partial w}{\partial x} - \frac{1}{G_1}\int_{-\infty}^{t} Y_2(t-\tau)\,d(\Psi+\frac{\partial w}{\partial x}) \cong \Psi+\frac{\partial w}{\partial x} \tag{2.43}$$

Using this and similar approximations in Eqs. 2.41, one obtains a simplified displacement field:

$$u_1 = U + z_1\Psi + (z_1 - z)\frac{\partial w}{\partial x} \tag{2.44a}$$

$$u_2 = U + z\Psi \tag{2.44b}$$

$$u_3 = U + z_2\Psi + (z_2 - z)\frac{\partial w}{\partial x} \tag{2.44c}$$

$$\Psi_1 = -\frac{\partial w}{\partial x} = \Psi_3 \tag{2.44d}$$

The rotations become

$$\omega_{xz1} = \omega_{xz3} = -\frac{\partial w}{\partial x} \text{ and } \omega_{xz2} = \tfrac{1}{2}(\Psi-\frac{\partial w}{\partial x}) \tag{2.45}$$

The Green's strains become, using Eq. 2.41,

$$\varepsilon_{xx1} = \frac{\partial U}{\partial x} + z_1\frac{\partial \Psi}{\partial x} + (z_1 - z)\frac{\partial^2 w}{\partial x^2} + \tfrac{1}{2}(\frac{\partial w}{\partial x})^2 \tag{2.46a}$$

$$\varepsilon_{xx3} = \frac{\partial U}{\partial x} + z_2 \frac{\partial \Psi}{\partial x} + (z_2 - z)\frac{\partial^2 w}{\partial x^2} + \frac{1}{2}\left(\frac{\partial w}{\partial x}\right)^2 \tag{2.46b}$$

$$\varepsilon_{xz1} = \frac{1}{2G_1}\int_{-\infty}^{t} Y_2(t-\tau)\, d\left(\Psi + \frac{\partial w}{\partial x}\right) \tag{2.46c}$$

$$\varepsilon_{xz2} = \frac{1}{2}\left(\Psi + \frac{\partial w}{\partial x}\right) \tag{2.46d}$$

$$\varepsilon_{xz} = \frac{1}{2G_3}\int_{-\infty}^{t} Y_2(t-\tau)\, d\left(\Psi + \frac{\partial w}{\partial x}\right) \tag{2.46e}$$

Using Eqs.2.23c, 2.25, 2.38 and 2.46, one obtains the stress resultants,

$$N_{xx1} = E_1\left\{h_1 \frac{\partial U}{\partial x} + h_1 z_1\left(\frac{\partial \Psi}{\partial x} + \frac{\partial^2 w}{\partial x^2}\right) - A_{10}\frac{\partial^2 w}{\partial x^2} + (h_1/2)\left(\frac{\partial w}{\partial x}\right)^2\right\} \tag{2.47a}$$

$$N_{xx3} = E_3\left\{h_3 \frac{\partial U}{\partial x} + h_3 z_3\left(\frac{\partial \Psi}{\partial x} + \frac{\partial^2 w}{\partial x^2}\right) - A_{30}\frac{\partial^2 w}{\partial x^2} + (h_3/2)\left(\frac{\partial w}{\partial x}\right)^2\right\} \tag{2.47b}$$

$$Q_{xz1} = h_1\int_{-\infty}^{t} Y_2(t-\tau)\, d\left(\Psi + \frac{\partial w}{\partial x}\right) \tag{2.47c}$$

$$Q_{xz2} = h_2\int_{-\infty}^{t} Y_2(t-\tau)\, d\left(\Psi + \frac{\partial w}{\partial x}\right) \tag{2.47d}$$

$$Q_{xz3} = h_3\int_{\infty}^{t} Y_2(t-\tau)\, d\left(\Psi + \frac{\partial w}{\partial x}\right) \tag{2.47e}$$

$$M_{xx1} = E_1\left\{A_{10}\frac{\partial U}{\partial x} + z_1 A_{10}\left(\frac{\partial \Psi}{\partial x} + \frac{\partial^2 w}{\partial x^2}\right) - I_{10}\frac{\partial^2 w}{\partial x^2} + (A_{10}/2)\left(\frac{\partial w}{\partial x}\right)^2\right\} \tag{2.47f}$$

$$M_{xx3} = E_3\left\{A_{30}\frac{\partial U}{\partial x} + z_2 A_{30}\left(\frac{\partial \Psi}{\partial x} + \frac{\partial^2 w}{\partial x^2}\right) - I_{30}\frac{\partial^2 w}{\partial x^2} + (A_{30}/2)\left(\frac{\partial w}{\partial x}\right)^2\right\} \tag{2.47g}$$

$$M_{xz1} = A_{10}\int_{-\infty}^{t} Y_2(t-\tau)\, d\left(\Psi + \frac{\partial w}{\partial x}\right) \tag{2.47h}$$

$$M_{xz_2} = A_{20}\int_{-\infty}^{t} Y_2(t-\tau)\,d\left(\Psi+\frac{\partial w}{\partial x}\right) \tag{2.47i}$$

$$M_{xz_3} = A_{30}\int_{-\infty}^{t} Y_2(t-\tau)\,d\left(\Psi+\frac{\partial w}{\partial x}\right) \tag{2.47j}$$

Further simplifications can be made which result in a hierarchy of theories for three-layer beams. For motion with frequencies at which transverse motion dominates, rotatory and axial inertia can be ignored. Since the study will concentrate on axially restrained beams, the axial forces N_{xx_1} and N_{xx_3}, will be large compared to the shear forces. Thus the curvature and buoyancy terms in Eqs. 2.37a and 2.37b will be dropped compared to the other terms in the equations while in 2.37c the products $N_{xx_1}\omega_{zx_1}$ and $N_{xx_3}\omega_{zx_3}$ will be retained as the dominant nonlinear effect. Using these simplifications and considering loadings in the z direction only, one obtains a simplified set of equations:

$$\frac{\partial}{\partial x}(N_{xx_1}+N_{xx_3}) = 0 \tag{2.48a}$$

$$\frac{\partial}{\partial x}(M_{xx_1}+M_{xx_3}) - (Q_{xz_1}+Q_{xz_2}+Q_{xz_3}) = 0 \tag{2.48b}$$

$$\frac{\partial}{\partial x}(N_{xx_1}\omega_{zx_1}+N_{xx_3}\omega_{zx_3}+Q_{xz_1}+Q_{xz_2}+Q_{xz_3}) + q(x,t) - (\rho_1 h_1+\rho_2 h_2+\rho_3 h_3)\ddot{w} = 0 \tag{2.48c}$$

where q(x,t) is the loading, per unit length, in the z direction and is given by $q(x,t)=(S_{zx_3}\omega_{zx_3}+S_{zz_3})_{z=z_3}$

$$-(S_{zx_3}\omega_{zx3}+S_{zz3})_{z=z_0} = T_{z3}(z=z_3,x,t) - T_{z1}(z=z_1,x,t).$$

Referring to Fig. 2.5, which shows the location of the coordinate system relative to the beam, the geometric quantities can be written as:

$$z_0 = -(h_{c1}+h_1),\ z_1 = -h_{c1},\ z_2 = h_{c2},\ z_3 = (h_{c2}+h_3)$$

$$A_{10} = -h_{c1}h_1(1+\tfrac{1}{2}h_1/h_{c1}),\ A_{20} = \tfrac{1}{2}(h_{c1}^2 - h_{c2}^2),\ A_{30} = h_{c2}h_3(1+h_3/2h_{c2})$$

$$I_{10} = h_1h_{c1}^2(1+(h_1/h_{c1}) + (1/3)(h_1/h_{c1})^2),\ I_{20} = (h_{c2}^2+h_{c1}^2)/3$$

$$I_{20} = h_3h_{c2}^2(1+(h_3/h_{c3}) + (1/3)(h_3/h_{c3})^2)$$

Using these in the stress resultants, Eq. 2.47, substituting into the simplified equations, Eq. 2.48, and choosing the origin of the z coordinate at the neutral axis in bending so that $E_3h_3h_{c2} = E_1h_1h_{c1}$, one obtains

$$\frac{\partial}{\partial x}\{(E_3h_3+E_1h_1)(\frac{\partial U}{\partial x} + \tfrac{1}{2}(\frac{\partial w}{\partial x})^2) - (E_3h_3h_{c2}(1+h_3/2h_{c2}) -$$

$$E_1h_1h_{c1}(1+h_1/2h_{c1}))\frac{\partial^2 w}{\partial x^2}\} = 0 \qquad (2.49a)$$

$$\frac{\partial}{\partial x}\{(E_3h_3h_{c2}(1+h_3/2h_{c2}) - E_1h_1h_{c1}(1+h_1/2h_{c1}))(\frac{\partial U}{\partial x} + \tfrac{1}{2}(\frac{\partial w}{\partial x})^2) +$$

$$(E_3h_3h_{c2}^2(1+h_3/2h_{c2}) + E_1h_1h_{c1}^2(1+h_1/2h_{c1}))(\frac{\partial \Psi}{\partial x} + \frac{\partial^2 w}{\partial x^2}) -$$

$$(E_3h_3h_{c2}^2(1+(h_3/h_{c2}) + (1/3)(h_3/h_{c2})^2) + E_1h_1h_{c1}^2(1+(h_1/h_{c1}) +$$

$$(\tfrac{1}{3})(h_1/h_{c1})^2)\frac{\partial^2 w}{\partial x^2} - h_2(1+(h_1/h_2)+(h_3/h_2))\int_{-\infty}^{t} Y_2(t-\tau)\,d(\Psi+\frac{\partial w}{\partial x}) = 0 \qquad (2.49b)$$

$$\frac{\partial}{\partial x}\{((E_3h_3+E_1h_1)(\frac{\partial U}{\partial x} + \tfrac{1}{2}(\frac{\partial w}{\partial x})^2) - (E_3h_3h_{c2}(1+h_3/2h_{c2}) -$$

$$E_1 h_1 h_{c1} (1+h_1/2h_{c1}))\frac{\partial^2 w}{\partial x^2})(\frac{\partial w}{\partial x})+h_2 (1+h_1/h_2+h_3/h_2)\int_{-\infty}^{t} Y_2(t-\tau)d(\Psi +$$

$$\frac{\partial w}{\partial x})\} + q(x,t)-(\rho_1 h_1+\rho_2 h_2+\rho_3 h_3)\ddot{w} = 0 \qquad (2.49c)$$

The boundary term, Eq. 2.35, becomes:

$$\Big[\{\int_{z_0}^{z_1} T_{x_1}dz+\int_{z_1}^{z_2} T_{x_2}dz+\int_{z_2}^{z_3} T_{x_3}dz-(N_{xx1}+N_{xx2}+N_{xx3}-(Q_{xz_1} +$$

$$Q_{xz2}+Q_{xz3})\frac{\partial w}{\partial x}\}\{\delta U\} + \{z_1\int_{z_0}^{z_1} T_{x_1}dz+\int_{z_1}^{z_2} zT_{x_2}dz+ z_2\int_{z_2}^{z_3} T_{x_3}dz -$$

$$z_1 (N_{xx1}-Q_{xz_1}\frac{\partial w}{\partial x})+(M_{xx2}-M_{xz2}\frac{\partial w}{\partial x})-z_2 (N_{xx_3}-Q_{xz_3}\frac{\partial w}{\partial x})\}\{\delta\Psi\} +$$

$$\{z_1\int_{z_0}^{z_1} T_{x_1}dz-\int_{z_0}^{z_1} zT_{x1}dz+ z_2\int_{z_2}^{z_3} T_{x_3}dz-\int_{z_2}^{z_3} zT_{x_3}dz - z_1 (N_{xx_1}-$$

$$Q_{xz_1}\frac{\partial w}{\partial x})+(M_{xx1}-M_{xz_1}\frac{\partial w}{\partial x})-z_2 (N_{xx_3}-Q_{xz_3}\frac{\partial w}{\partial x})+(M_{xx_3} -$$

$$M_{xz_3}\frac{\partial w}{\partial x})\}\{\delta(\frac{\partial w}{\partial x})\}+\{\int_{z_0}^{z_1} T_{z_1}dz+\int_{z_1}^{z_2} T_{z2}dz+\int_{z_2}^{z_3} T_{z_3}dz-((N_{xx_1} +$$

$$N_{xx_3}+N_{xx_3})\frac{\partial w}{\partial x}-Q_{xz_1}-Q_{xz_2}-Q_{xz_3})\}\{\delta w\}\Big]_{x=-L/2}^{x=L/2} \qquad (2.50)$$

where the x integral portion of the boundary term has disappeared because of interface conditions and matching the applied tractions with the stresses at $z=z_0$ and $z=z_3$. This remaining part of the integral gives the boundary conditions at $x = \pm(L/2)$. It is important to note that the boundary conditions at $z=z_0$ and $z=z_3$ have not been truly satisfied. Matching the stresses to the applied tractions

in the x direction requires

$$T_{x1} = (S_{zx1} - S_{zz1}\frac{\partial w}{\partial x}) \text{ at } z=z_0$$

and

$$T_{x3} = (S_{zx3} - S_{zz3}\frac{\partial w}{\partial x}) \text{ at } z=z_3$$

Since S_{zz} has been assumed to be zero, the requirements become

$$T_{x1} = S_{zx1} \text{ at } z=z_0$$

and

$$T_{x3} = S_{zx3} \text{ at } z=z_1$$

No tractions in the x direction requires

$$S_{zx1} = 0 \text{ at } z=z_0$$

and

$$S_{zx3} = 0 \text{ at } z=z_3$$

By virtue of the assumed displacement field, this would force S_{zx} to be zero throughout the thickness of the beam, a condition which will not be true for the problems considered. Thus, the traction boundary condition on the upper and lower surface must be violated to get meaningful results from this theory.

A common simplification is to assume the outer layers are much thinner than the core, i.e.

$$h_1/h_{c1} << 1 \quad \text{and} \quad h_3/h_{c2} << 1 \tag{2.51a}$$

Using this simplification in Eq. 2.49 gives

$$\frac{\partial}{\partial x}\{(E_3h_3+E_1h_1)(\frac{\partial U}{\partial x}+\frac{1}{2}(\frac{\partial w}{\partial x})^2)\} = 0 \qquad (2.51b)$$

$$\frac{\partial}{\partial x}\{(E_3h_3h_{C2}^2+E_1h_1h_{C1}^2)\frac{\partial \Psi}{\partial x}\} - h_2\int_{-\infty}^{t} Y_2(t-\tau)\,d(\Psi+\frac{\partial w}{\partial x}) = 0 \qquad (2.51c)$$

$$\frac{\partial}{\partial x}\{((E_3h_3+E_1h_1)(\frac{\partial U}{\partial x}+\frac{1}{2}(\frac{\partial w}{\partial x})^2)+h_2\int_{-\infty}^{t} Y_2(t-\tau)\,d(\Psi+\frac{\partial w}{\partial x})\}$$

$$+ q(x,t)-(\rho_1h_1+\rho_2h_2+\rho_3h_3)\ddot{w} = 0 \qquad (2.51d)$$

It is interesting to note that for beams with face layers of dissimiliar materials but of the same thickness, the thin face sheet assumption is not as accurate for a given thickness as it is for beams with identical face layers. Since the condition for locating the coordinate axis, $E_3h_3h_{C2} = E_1h_1h_{C1}$, leads to

$$h_{C1} = \{\frac{E_3h_3}{E_1h_1 + E_3h_3}\}\ h_2$$

$$h_{C2} = \{\frac{E_1h_1}{E_1h_1 + E_3h_3}\}\ h_3$$

The restriction 2.51a becomes difficult to meet for all but very thin face layers if E_1 and E_3 differ by even a factor of two or three. Conditions 2.51a are a generalization of Yu's thin face sheet condition for symmetric beams which states that the face thickness divided by one-half the core thickness must be much less than unity.

The thin face sheet assumption is equivalent to assuming that the outer layers act as membranes and offer no individual resistance to bending. This is evident by the absence of spatial derivatives of w higher than 2nd order in the differential equations.

Integrating Eq. 2.49a twice with respect to x, and considering a beam with axially restrained ends, i.e. $U(L/2,t) = U(-L/2,t) = 0$, yields

$$\left(\frac{\partial U}{\partial x} + \frac{1}{2}\left(\frac{\partial w}{\partial x}\right)^2\right) = \left(\left(E_3 h_3^2 - E_1 h_1^2\right)/2\left(E_1 h_1 + E_3 h_3\right)\right) \frac{\partial^2 w}{\partial x^2} + \left(\frac{1}{2}L\right)\int_{-L/2}^{L/2} \left(\frac{\partial w}{\partial x}\right)^2 dx + \left\{\left(E_3 h_3^2 - E_1 h_1^2\right)/2\left(E_1 h_1 + E_3 h_3\right)\right\}\left(\frac{\partial w}{\partial x}\right)\Bigg|_{x=-L/2}^{x=L/2} \tag{2.52}$$

Using this in Eqs. 2.49b and c and defining

$$h_T = h_1 + h_2 + h_3, \quad \bar{w} = w/h_T, \quad \bar{\Psi} = (L/h_T)\Psi, \quad \chi = x/L$$

$$K_{11} = \left(\left(E_3 (h_3/h_T)^2 - E_1 (h_1/h_T)^2\right)^2/4\left(E_1 (h_1/h_T) + E_3 (h_3/h_T)\right)\right)(h_T/L)^4$$

$$K_{12} = \left(E_3 (h_3/h_T)(h_{C2}/h_T)^2\left(1 + \frac{1}{2}(h_3/h_{C2})\right) + E_1 (h_1/h_T)(h_{C1}/h_T)^2\left(1 + \frac{1}{2}(h_1/h_{C1})\right)\right)(h_T/L)^4$$

$$K_{13} = \left(E_3 (h_3/h_T)(h_{C2}/h_T)^2\left(1 + (h_3/h_{C2}) + (1/3)(h_3/h_{C2})^2\right) + \left(E_1 (h_1/h_T)(h_{C1}/h_T)^2\left(1 + (h_1/h_{C1}) + (1/3)(h_1/h_{C1})^2\right)\right)(h_T/L)$$

$$K_{15} = \left(E_1 (h_1/2h_T) + E_3 (h_3/2h_T)\right)(h_T/L)^4$$

$$K_{16} = \left(\left(E_1 (h_1/h_T)^2 - E_3 (h_3/h_T)^2\right)/2\right)(h_T/L)^4$$

$m = (\rho_1 h_1 + \rho_2 h_2 + \rho_3 h_3) h_T$, $\bar{h}_2 = (h_T/L)^2$ and $q(\chi L, t) = \bar{q}(\chi, t)$, one gets

$$\frac{\partial}{\partial x}\{K_{11}\frac{\partial^2 w}{\partial \chi^2} + K_{12}(\frac{\partial \bar{\Psi}}{\partial \chi} + \frac{\partial^2 w}{\partial \chi^2}) - K_{13}\frac{\partial^2 w}{\partial \chi^2}\}$$

$$-\bar{h}_2\int_{-\infty}^{t} Y_2(t-\tau)\,d(\bar{\Psi} + \frac{\partial w}{\partial \chi}) = 0 \qquad (2.53a)$$

$$\{K_{15}\int_{-\frac{1}{2}}^{\frac{1}{2}}(\frac{\partial \bar{w}}{\partial \chi})^2 d\chi + K_{16}(\frac{\partial \bar{w}}{\partial \chi}\Big|_{\chi=-\frac{1}{2}}^{\chi=\frac{1}{2}})\frac{\partial \bar{w}}{\partial \chi} + \bar{h}_2\int_{-\infty}^{t} Y_2(t-\tau)\,d(\frac{\partial \bar{\Psi}}{\partial \chi} + \frac{\partial^2 \bar{w}}{\partial \chi^2})$$

$$+ \bar{q}(\chi, t) - m\ddot{w} = 0 \qquad (2.53b)$$

Equations 2.53a and b constitute a set of partial differential-integral equations which will be used to predict the response of the three-layer beams to a constant plus a harmonic force.

Equation 2.52 is interesting because it shows that in general, for three-layer beams, the axial displacement is coupled to the transverse displacement through first-order terms. However, for symmetric three-layer beams, i.e. $E_1 = E_3$ and $h_1 = h_3$, the coupling is similar to homogeneous beams, namely, that the axial displacement is coupled to the transverse displacement through a second-order effect.

Integrating Eq. 2.51b twice, considering beams with axially restrained ends and substituting the results into Eqs. 2.51c and d, yields equations that are identical to

Kovac's equations, Eq. 1.2, the thin face sheet counterpart of Eqs. 2.53.

Equations 2.53 will be used to determine the effect of including a bias force, in addition to a harmonic force, on the response of three-layer beams with soft, viscoelastic cores.

CHAPTER III

NUMERICAL RESULTS

Approximate methods will be used to predict the behavior of a three-layer beam to a harmonic force plus a constant bias. In Kovac's investigation and in the experiment described later in this work, the beams were clamped on both ends with the clamping mechanism also providing the axial restraint. This beam configuration motivated some of the assumptions used to arrive at an approximate solution. By assuming separation of variables and using harmonic balance, numerical results are obtained.

3.1 FORM OF APPROXIMATE SOLUTION

Assuming separation of temporal and spatial variables gives

$$\bar{w}(\chi,t) = W(\chi)T_1(t) \tag{3.1a}$$

$$\bar{\Psi}(\chi,t) = \Psi(\chi)T_2(t) \tag{3.1b}$$

To implement Galerkin's method, the spatial parts of the solution are chosen to be

$$W(\chi) = 16(\chi^2 - \tfrac{1}{4})^2 \tag{3.2a}$$

$$\Psi(\chi) = 12\sqrt{3}\chi(\chi - \tfrac{1}{4}) \tag{3.2b}$$

For forcing at the center of the beam, the motion is expected to be synchronous and spatially distributed in the manner approximated by Eqs. 3.2, $\bar{w}(\chi,t)$ an even function of χ and $\bar{\Psi}(\chi,t)$ an odd function. In addition, Eqs. 3.2

renders the boundary term, Eq. 2.50 zero. $\bar{q}(\chi,t)$ is assumed to be of the form

$$\bar{q}(\chi,t) = a(\chi)(F_0 + F_1 \sin\Omega t) \tag{3.3}$$

where Ω is the forcing frequency and $a(\chi)$ is the spatial distribution of the load and is given by

$$\begin{aligned} a(\chi) &= 0, \quad -(1/2) < \chi < -(1/4L) \\ a(\chi) &= 2, \quad -(1/4L) \leq \chi \leq (1/4L) \\ a(\chi) &= 0, \quad (1/4L) < \chi < (1/2) \end{aligned} \tag{3.4}$$

Substituting these displacements and forces into the equations of motion, 2.53, results in

$$K_{11}(384\chi)T_1(t) + K_{12}(+72\sqrt{3}\chi T_2(5) + (384\chi)T_1(t)) -$$

$$K_{13}(384\chi)T_1(t) - \bar{h}_2 \int_{-\infty}^{t} Y_2(t-\tau)\, d\{+12\sqrt{3}(\chi^3 - (\chi/4))T_2(\tau) +$$

$$(64\chi^3 - 16)T_1(\tau) = e_1(\chi,t) \tag{3.5a}$$

$$K_{15}\{\int_{-\frac{1}{2}}^{\frac{1}{2}} \{(64\chi^3 - 16\chi)T_1(t)\}^2 dx\}\}(192\chi^2 - 16)T_1(t) +$$

$$\bar{h}_2 \int_{-\infty}^{t} Y_2(t-\tau)\, d\{+12\sqrt{3}(3\chi^2 - (1/4))T_2(\tau) + (192\chi^2 - 16)T_1(\tau) -$$

$$m(16\chi^4 - 8\chi^2 + 1)T_1(t) + a(\chi)(F_0 + F_1 \sin(\Omega t) = e_2(\chi,t) \tag{3.5b}$$

$e_1(\chi,t)$ and $e_2(\chi,t)$ are the moment and force imbalance in the equilibrium equations as a result of not using the

exact solution. Galerkin's method requires

$$\int_{-\frac{1}{2}}^{\frac{1}{2}} e_1(\chi,t)\Psi(\chi)d\chi = 0 \tag{3.6a}$$

$$\int_{-\frac{1}{2}}^{\frac{1}{2}} e_2(\chi,t)W(\chi)d\chi = 0 \tag{3.6b}$$

Since $e_2(\chi,t)$ is a force and $W(\chi)$ a displacement, $e_2(\chi,t)W(\chi)$ is the work done by the force imbalance. Galerkin's method can be interpreted as requiring this work, as well as the work done by the moment imbalance $e_1(\chi,t)\Psi(\chi)$, to be zero. Carrying out Eqs. 3.6 results in

$$\bar{K}_{11}T_1(t)+\bar{K}_{12}T_2(t)+\bar{\bar{K}}_{12}T_1(t)-\bar{K}_{13}T_1(t) - H_2\int_{-\infty}^{t} Y_2(t-\tau)dT_2(\tau) - \bar{H}_2\int_{-\infty}^{t} Y_2(t-\tau)dT_1(\tau) = 0 \tag{3.7a}$$

$$\bar{K}_{15}T_1(t)+H_3\int_{-\infty}^{t} Y_2(t-\tau)dT_2(\tau)+\bar{H}_3\int_{-\infty}^{t} Y_2(t-\tau)dT_1(\tau)-MT_1(t) + \bar{F}_0+\bar{F}_1\sin(\Omega t) = 0 \tag{3.7b}$$

where

$$\bar{K}_{11} = -64.5\,K_{11}, \quad \bar{K}_{12} = -21.7\,K_{12}, \quad \bar{\bar{K}}_{12} = -66.5\,K_{12}$$

$$\bar{K}_{13} = -66.5\,K_{13}, \quad H_2 = .514\,\bar{h}_2, \quad \bar{H}_2 = 1.58\,\bar{h}_2$$

$$\bar{K}_{15} = -23.8\,K_{15}, \quad H_3 = 1.58\,\bar{h}_2, \quad \bar{H}_3 = -4.88\,\bar{h}_2$$

$$M = .406\ m, \quad \bar{F}_0 = F_0\int_{-\frac{1}{2}}^{\frac{1}{2}} a(\chi)W(\chi)d\chi \text{ and } \bar{F}_1 = F_1\int_{-\frac{1}{2}}^{\frac{1}{2}} a(\chi)W(\chi)d\chi$$

Harmonic balance will be used on the two temporal equations, 3.7a and b. This will lead to a set of nonlinear algebraic equations.

Because the load is a constant force plus a harmonic variation, it is reasonable to assume the temporal response as

$$T_1(t) = W_0 + W_1\sin(\Omega t) + W_2\cos(\Omega t) + W_3\sin(2\Omega t) + W_4\cos(2\Omega t) + W_5\sin(3\Omega t) + W_6\cos(3\Omega t) \qquad (3.8a)$$

$$T_2(t) = V_0 + V_1\sin(\Omega t) + V_2\cos(\Omega t) + V_3\sin(2\Omega t) + V_4\cos(2\Omega t) + V_5\sin(3\Omega t) + V_6\cos(3\Omega t) \qquad (3.8b)$$

where W_i and V_i, i=0,6, are functions of frequency and are the unknowns. Substituting these into the temporal equations, 3.7, and retaining harmonics to order three gives

$$(\overline{K}_{11} + \overline{\overline{K}}_{12} - \overline{K}_{13})\{W_0 + W_1\sin(\Omega t) + W_2\cos(\Omega t) + W_3\sin(2\Omega t) + W_4\cos(2\Omega t) + W_5\sin(3\Omega t) + W_6\cos(3\Omega t)\} + \overline{K}_{12}\{V_0 + V_1\sin(\ t) + V_2\cos(\Omega t) + V_3\sin(2\Omega t) + V_4\cos(2\Omega t) + V_5\sin(3\Omega t) + V_6\cos(3\Omega t)\}$$

$$-H_2\int_{-\infty}^{t} Y_2(t-\tau)\,d\{V_0 + V_1\sin(\Omega\tau) + V_2\cos(\Omega\tau) + V_3\sin(2\Omega\tau) + V_4\cos(2\Omega\tau) + V_5\sin(3\Omega\tau) + V_6\cos(3\Omega\tau)\} - \overline{H}_2\int_{-\infty}^{t} Y_2(t-\tau)\,d\{W_0 + W_1\sin(\Omega\tau) + W_2\cos(\Omega\tau) + W_3\sin(2\Omega\tau) + W_4\cos(2\Omega\tau) + W_5\sin(3\Omega\tau) + W_6\cos(3\Omega\tau)\} = 0 \qquad (3.9a)$$

and

$$\overline{K}_{15}\{B_0+B_1\sin(\Omega t)+B_2\cos(\Omega t)+B_3\sin(2\Omega t)+B_4\cos(2\Omega t)+$$

$$B_5\sin(3\Omega t)+B_6\cos(3\Omega t)+H_3\int_{-\infty}^{t}Y_2(t-\tau)\,d\{V_0+V_1\sin(\Omega\tau)+$$

$$V_2\cos(\Omega\tau)+V_3\sin(2\Omega\tau)+V_4\cos(2\Omega\tau)+V_5\sin(3\Omega\tau)+V_6\cos(3\Omega\tau)\}$$

$$+H_3\int_{-\infty}^{t}Y_2(t-\tau)\,d\{W_0+W_1\sin(\Omega\tau)+W_2\cos(\Omega\tau)+W_3\sin(2\Omega\tau)+$$

$$W_4\cos(2\Omega\tau)+W_5\sin(3\Omega\tau)+W_6\cos(3\Omega\tau)\}+M\Omega^2(W_1\sin(\Omega t)+$$

$$W_2\cos(\Omega t)+4W_3\sin(2\Omega t)+4W_4\cos(2\Omega t)+9W_5\sin(3\Omega t)+9W_6\cos(3\Omega t)$$

$$\overline{F}_0+\overline{F}_1\sin(\Omega t)=0 \qquad (3.9b)$$

where

$$B_0=C_0W_0+(1/2)(C_1W_1+C_2W_2+C_3W_3+C_4W_4+C_5W_5+C_6W_6)$$

$$B_1=C_1W_0+C_0W_1+(1/2)(-C_4W_1+C_3W_2+C_2W_3-C_6W_3-C_1W_4+C_5W_4+$$

$$C_4W_5-C_8W_5-C_3W_6+C_7W_6)$$

$$B_2=C_2W_0+C_0W_2+(1/2)(C_3W_1+C_4W_2+C_1W_3+C_5W_3+C_2W_4+C_6W_4+$$

$$C_3W_5+C_7W_5+C_4W_6+C_8W_6)$$

$$B_3=C_3W_0+C_0W_3+(1/2)(C_2W_1-C_6W_1+C_1W_2+C_5W_2-C_8W_3+C_7W_4+$$

$$C_2W_5-C_{10}W_5-C_1W_6+C_9W_6)$$

$$B_4 = C_4 W_0 + C_0 W_4 + (1/2)(-C_1 W_1 + C_5 W_1 + C_2 W_2 + C_6 W_2 + C_7 W_3 + C_8 W_4 + C_1 W_5 + C_9 W_5 + C_2 W_6 + C_{10} W_6)$$

$$B_5 = C_5 W_0 + C_0 W_5 + (1/2)(C_4 W_1 - C_8 W_1 + C_3 W_2 + C_7 W_2 + C_2 W_3 - C_{10} W_3 + C_1 W_4 + C_9 W_4 + C_{11} W_6 - C_{12} W_5)$$

$$B_6 = C_6 W_0 + C_0 W_6 + (1/2)(-C_3 W_1 + C_7 W_1 + C_4 W_2 + C_8 W_2 - C_1 W_3 + C_9 W_3 + C_2 W_4 + C_{10} W_4 + C_{11} W_5 + C_{12} W_6)$$

and

$$C_0 = W_0^2 + (1/2)(W_1^2 + W_2^2 + W_3^2 + W_4^2 + W_5^2 + W_6^2)$$

$$C_1 = 2W_0 W_1 - W_1 W_4 + W_2 W_3 - W_3 W_6 + W_4 W_5$$

$$C_2 = 2W_0 W_2 + W_1 W_3 + W_2 W_4 + W_3 W_5 + W_4 W_6$$

$$C_3 = 2W_0 W_3 + W_1 W_2 - W_1 W_6 + W_2 W_5$$

$$C_4 = (1/2)(W_2^2 - W_1^2) + 2W_0 W_4 + W_1 W_5 + W_2 W_6$$

$$C_5 = 2W_0 W_5 + W_1 W_4 + W_2 W_3$$

$$C_6 = 2W_0 W_6 - W_1 W_3 + W_2 W_4$$

$$C_7 = W_1 W_6 + W_2 W_5 + W_3 W_4$$

$$C_8 = (1/2)(W_4^2 - W_3^2) + W_2 W_6 - W_1 W_5$$

$$C_9 = W_3 W_6 + W_4 W_5$$

$$C_{10} = W_4 W_6 - W_3 W_5$$

$$C_{11} = W_5 W_6$$

$$C_{12} = (1/2)(W_6^2 - W_5^2)$$

The integrals in Eqs. 3.9 can be related to the complex moduli for the core material (see Appendix). For example

$$\int_{-\infty}^{t} Y_2(t-\tau)\,dT_2(\tau) = \int_{-\infty}^{t} Y_2(t-\tau)\,d\{V_0 + V_1 \sin(\Omega\tau) + V_2 \cos(\Omega\tau) +$$

$$V_3 \sin(2\Omega\tau) + V_4 \cos(2\Omega\tau) + V_5 \sin(3\Omega\tau) + V_6 \cos(3\Omega\tau)\} =$$

$$V_0 G_2'(0) + (V_1 G_2'(\Omega) - V_2 G_2''(\Omega))\sin(\Omega t) + (V_1 G_2''(\Omega) + V_2 G_2'(\Omega))\cos(\Omega t) +$$

$$(V_3 G_2'(2\Omega) - V_4 G_2''(2\Omega))\sin(2\Omega t) + (V_3 G_2''(2\Omega) + V_4 G_2'(2\Omega))\cos(2\Omega t) +$$

$$(V_5 G_2'(3\Omega) - V_6 G_2''(3\Omega))\sin(3\Omega t) + (V_5 G_2''(3\Omega) + V_6 G_2'(3\Omega))\cos(3\Omega t)$$

where $G_2'(\Omega)$ and $G_2''(\Omega)$ are the real and imaginary part, respectively, of the complex shear modulus of the core material evaluated at Ω. $G_2'(2\Omega)$, ..., $G_2''(3\Omega)$ are similarly defined. $G_2'(0)$ is the static elastic shear modulus of the core material.

The other integrals are treated in like manner and the coefficients of the various harmonics in Eqs. 3.9 are equated to zero. The resulting nonlinear, algebraic equations in W_i and V_i are, after defining $\bar{K}_T = \bar{K}_{11} + \bar{\bar{K}}_{12} - \bar{K}_{13}$:

$$\bar{K}_T W_0 + \bar{K}_{12} V_0 - H_2 G_2'(0) V_0 - \bar{H}_2 G_2'(0) W_0 = 0$$

$$\bar{K}_T W_1 + \bar{K}_{12} V_1 - H_2 G_2'(\Omega) V_1 - H_2 G_2''(\Omega) V_2 - \bar{H}_2 G_2'(\Omega) W_1 + \bar{H}_2 G_2''(\Omega) W_2 = 0$$

$$\bar{K}_T W_2 + \bar{K}_{12} V_2 - H_2 G_2''(\Omega) V_1 - H_2 G_2'(\Omega) V_2 - \bar{H}_2 G_2''(\Omega) W_1 - \bar{H}_2 G_2'(\Omega) W_2 = 0$$

$$\bar{K}_T W_3 + \bar{K}_{12} V_3 - H_2 G_2'(2\Omega) V_3 + H_2 G_2''(2\Omega) V_4 - \bar{H}_2 G_2'(2\Omega) W_3 + \bar{H}_2 G_2''(2\Omega) W_4 = 0$$

$$\bar{K}_T W_4 + \bar{K}_{12} V_4 - H_2 G_2''(\Omega) V_3 - H_2 G_2'(2\Omega) V_4 - \bar{H}_2 G_2''(2\Omega) W_3 - \bar{H}_2 G_2'(2\Omega) W_4 = 0$$

$$\bar{K}_T W_5 + \bar{K}_{12} V_5 - H_2 G_2'(3\Omega) V_5 + H_2 G_2''(3\Omega) V_6 - \bar{H}_2 G_2'(3\Omega) W_5 + \bar{H}_2 G_2''(3\Omega) W_6 = 0$$

$$\bar{K}_T W_6 + \bar{K}_{12} V_6 - H_2 G_2''(3\Omega) V_5 - H_2 G_2'(3\Omega) V_6 - \bar{H}_2 G_2''(3\Omega) W_5 - \bar{H}_2 G_2'(3\Omega) W_6 = 0$$

$$\bar{K}_{15} B_0 + H_3 G_2'(0) V_0 + \bar{H}_3 G_2'(0) W_0 + \bar{F}_0 = 0$$

$$\bar{K}_{15} B_1 + H_3 G_2'(\Omega) V_1 - H_3 G_2''(\Omega) V_2 + \bar{H}_3 G_2'(\Omega) W_1 - \bar{H}_3 G_2''(\Omega) W_2 + M\Omega^2 W_1 + \bar{F}_1 = 0$$

$$\bar{K}_{15} B_2 + H_3 G_2''(\Omega) V_1 + H_3 G_2'(\Omega) V_2 + \bar{H}_3 G_2''(\Omega) W_1 + \bar{H}_3 G_2'(\Omega) W_2 + M\Omega^2 W_2 = 0$$

$$\bar{K}_{15} B_3 + H_3 G_2'(2\Omega) V_3 - H_3 G_2''(2\Omega) V_4 + \bar{H}_3 G_2'(2\Omega) W_3 - \bar{H}_3 G_2''(2\Omega) + 4M\Omega^2 W_3 = 0$$

$$\bar{K}_{15} B_4 + H_3 G_2''(2\Omega) V_3 + H_3 G_2'(2\Omega) V_4 + \bar{H}_3 G_2''(2\Omega) W_3 + \bar{H}_3 G_2'(2\Omega) W_4 + 4M\Omega^2 W_4 = 0$$

$$\bar{K}_{15} B_5 + H_3 G_2'(3\Omega) V_5 - H_3 G_2''(3\Omega) V_6 + \bar{H}_3 G_2'(3\Omega) W_5 - \bar{H}_3 G_2''(3\Omega) W_6 + 9M\Omega^2 W_5 = 0$$

$$\bar{K}_{15} B_6 + H_3 G_2''(3\Omega) V_5 + H_3 G_2'(3\Omega) V_6 + \bar{H}_3 G_2''(3\Omega) W_5 + \bar{H}_3 G_2'(3\Omega) W_6 + 9M\Omega^2 W_6 = 0$$

The fourteen nonlinear algebraic equations were solved numerically by a method developed by Brown and Conte[34,35]. It is a gradient method with the program computing the gradient numerically rather than the user having to enter the partial derivatives explicitly. The program is on The University of Michigan Terminal System in the math library under the name NLSYS.

3.2 RESULTS OF NUMERICAL SOLUTION

Frequency response curves were obtained for two of the symmetric beams Kovac reported on and for an unsymmetric beam not previously investigated .

Results for a symmetric beam with face layers of .002" silicon-ferrite and a core of .0625" neoprene, forced with the static force and the harmonic force equal to .0425 lbs., indicate that superharmonic response is barely detectable and the predicted response was basically identical to results obtained assuming a single harmonic. Figure 3.1 shows the results for a beam with face layers of .008" steel and a core of .0625" neoprene and the bias force and the harmonic force equal to .085 lbs. For this case, superharmonic response is present but it does not have a significant effect on the frequency response curve.Included in Fig. 3.1 is the ratio of the magnitude of the 2Ω component of response to the magnitude of the Ω component as a function of forcing frequency. As indicated, this ratio is largest when forcing the beam near one-half its resonant frequency. Figure 3.2 shows similar curves for an unsymmetric beam of the type investigated experimentally later. Results show that for both the symmetric and unsymmetric beams, the superharmonic response is more pronounced if the bias force is larger than the harmonic force. Complex modulus data was taken from the curves supplied to Kovac by B.F. Goodrich.

The response curves for symmetric and unsymmetric beams have similar characteristics and the presence of a constant force does produce a superharmonic response. However, some other effect was responsible for the large increase in response amplitude observed when forcing the beam at one-half its resonant frequency.

Attention was then turned to the electromagnetic forcing mechanism used in the experiment. It was found that several undesirable effects associated with electromagnetic forcing can strongly influence the response of the beam and, in fact, obscure the true response. The next chapter discusses these effects, their influence on the beam and a method to minimize them.

3.3 EFFECT OF SYMMETRY ON DAMPING

Although not involved as one of the original reasons for this investigations, it is interesting to consider whether symmetric or unsymmetric beams are more effective in damping. A numerical study was done to determine if any general statements could be made regarding the effect of symmetry on damping.

The study was divided into thick face layer beams and thin face layer beams and used symmetric steel-neoprene-steel beams as references. The thick face layer reference had a total thickness of three times the core thickness and the thin face layer reference had a total thickness of one-and-a-quarter times the core thickness. The study was

done by considering the forced response of the beam using the assumed mode shapes, Eq. 3.2, in the linearized version of the governing equations, Eqs. 2.53. The sharpness of resonance, Q, was used as a measure of damping and was determined graphically from the forced response curves.

For thin face layers, making one outer layer of aluminum but keeping the thickness the same resulted in slightly less damping than the reference beam, while increasing the thickness of the aluminum layer so that the mass per unit length of the beam was the same as the reference resulted in more damping. However in this case the aluminum layer was one-third the thickness of the core and could not be considered thin. For thick face layers, making one layer of aluminum resulted in increased damping for both the equal thickness and equal mass cases. If instead of replacing one of the steel layers with aluminum, which is one-third as stiff as steel and weighs about one-third as much, it was replaced with phosphor-bronze, which is about one-half as stiff as steel but weighs slightly more, then the thin face layer beams showed less damping than the reference beam for both the equal thickness and equal mass cases. For thick face layers, the equal thickness and equal mass cases both showed more damping.

Using steel in both layers and making one layer one-tenth as thick as the other resulted in less damping for the thin face layer beam while the opposite was true for thick face layers.

It appears that for thin face layers symmetry results in more damping while for thick face layers the situation is reversed. However, generalizations should not be made and these examples serve to illustrate that statements concerning the effect of symmetry on damping cannot be made without qualification of the elastic and geometric properties of the outer layers and a thorough study should be made for any particular problem.

CHAPTER IV

FEEDBACK CONTROL SYSTEM

4.1 ELECTROMAGNETIC FORCING

In many instances it is desirable to force a structure without mechanical contact because the additional mass of the connecting mechanism can appreciably alter the characteristics of the structure being studied. One of the most common methods of noncontact forcing is by means of an electromagnetic coil, as shown in Fig. 4.1. Alternating current is passed through the coil and, assuming the structure material is ferromagnetic, the structure feels an alternating force. It is important to note that the structure senses a constant force plus a force alternating at twice the current frequency. Frequency doubling results because the ferromagnetic structure is attracted to both a north pole and a south pole of a magnet and, since with alternating current, the ends of the magnet near the structure are a north pole once per cycle and a south pole once per cycle, the structure is pulled twice per cycle of alternating current in the coil. In addition, because the structure is always being attracted, there is a nonzero mean force attracting the structure to the magnet. More formally, the force felt by the structure is proportional to the magnetic induction, B, squared. If the magnetic induction is $B_0 \sin(\Omega t)$, then the force is proportional to $(B_0^2/2)(1-\cos(2\Omega t))$. However, this is not strictly

the case with the setup of Fig. 4.1. Since most ferromagnetic core materials have a nonlinear relation between B and H, the magnetic intensity, and since H is directly proportional to the current in the windings, a harmonic current will not necessarily produce a harmonic B in the core and thus, the force will contain harmonics of the current frequency. The character of the harmonics is determined by the magnitude of the current and the B vs. H relations of the material. A typical B vs. H relation for a soft iron is shown in Fig. 4.2.

A second problem with this type of exciter is due to the strength of the magnetic field, and thus the force, being inversely proportional to the distance from the end of the coil. A qualitative indication of force variation with distance from the coil is shown in Fig. 4.3. This means that the structure is oscillating in a spatially nonuniform force field and this, coupled with the temporal variation which may contain harmonics due to the magnetic material nonlinearities, produces a force time history on the structure which can be different than a pure harmonic. Visual examination of the force time histories of recent investigators who have used this type of forcing device show this to be the case. Figure 4.4a shows the force time history of Kung[36] and Fig. 4.4b shows the time history of Bennett[37].

Clearly if the force contains harmonics due to the magnetic material nonlinearities, then the response of the

structure will contain harmonics. To see how the spatial variation in force can affect the response of the structure, consider a simple linear spring-mass-damper system driven by a harmonic force which has an amplitude that is linearly proportional to the mass displacement, x. Then the governing equation for the mass motion can be written as

$$m\ddot{x} + c\dot{x} + (k-F_1\cos(\Omega t))x = F_0\cos(\Omega t) \qquad (4.1)$$

This is a forced, damped Mathieu equation and, depending on the values of m, c, k, F_0, F_1 and Ω, can admit harmonic response at any one of several frequencies related to Ω. Thus a simple linear system with a slight variation from a purely harmonic force can respond in a complicated way. If the spring-mass-damper system were nonlinear, it would be difficult to determine what part of the harmonic content of the response is due to the system itself and what part is due to the deviation of the force from a pure harmonic.

There is a strong possibility that both the nonlinear magnetic material effect and the nonuniform spatial field influenced the outcome of Kovac's experiment. It is also possible that many of the harmonics witnessed by Bennett could be traced to the presence of unwanted distortions in his force time history. Spectral results, taken from repeating Kovac's experiment and using a fast Fourier transform on the force signal, indicated that when forcing a beam, which had a resonant frequency of 60 hz, with a supposed 25 hz harmonic force, 16 percent of the force was at 50 hz.

It appears that electromagnetic devices should be abandoned if harmonic forcing is desired. However, it seems worthwhile to make an effort to eliminate the serious drawbacks of electromagnetic devices and thus complement the various noncontacting displacement measuring instruments with an accurate noncontacting forcing mechanism. Due to lack of ideal magnetic, electrical and mechanical elements, a pure harmonic time history may not be possible in the laboratory but it may be possible to minimize the harmonics to a value felt to be negligible by the experimenter.

Discussion will now center on the development of such a mechanism which uses feedback to eliminate unwanted harmonics from the force time history. Such a device was developed by Plas and Janssen[38], two Belgian investigators in the design of machine tools. However, they controlled the B field rather than the force directly and it is not clear from their paper how the forcing frequency compared with the resonant frequencies of the cutting tool and the body being machined. This is important because the large displacements associated with resonance cause greater distortions in the force than at other frequencies.

If the structure to be investigated is a nonlinear beam, then the experimental setup, without feedback, can be summarized in block diagram fashion as in Fig. 4.5. A function generator supplies a harmonic voltage, considered the input, to the power amplifier which in turn supplies harmonic current to the coil. The coil current, governed by the

resistive, inductive, capacitive effects in the coil circuit, produces a nonharmonic B which forces the beam to oscillate, in accordance with its own dynamics, in the nonuniform field. In addition to the nonlinear B vs. H effect, hysteresis and eddy current losses in the magnetic material affect the relation between the current and B. In this representation, the force, rather than the beam displacement, is considered the output and is not, in general, harmonic. Basically this is the same setup used by Bennett, Kung, Kovac, Yan and many other experimenters.

4.2 BASIC CONCEPTS OF FEEDBACK CONTROL

At this point some of the basic concepts of feedback control will be introduced and some of the problems associated with it discussed. Conceptually, the idea of using feedback to control the output of a system is quite simple. For example, suppose a system tends to distort the amplitude of a sinusoid, as shown in Fig. 4.6, and it is desired to have the output follow the input sinusoid. Then some or all of the output signal can be used to modify the input to the system so that the output more nearly resembles a sine wave. The term feedback comes from the fact that the output is fed back to modify the original input to the system and this modified input is used to drive the system. In the present case, the system tends to distort the input sinusoid by making positive peaks of the output smaller in magnitude than the negative peaks. What is needed on the input side is a signal whose positive peaks are larger than the

negative peaks so when the system distorts this signal, the output positive and negative peaks are of equal value, as shown in Fig. 4.7. By the nature of the distorted output, subtracting some of the system output from the input sinusoid tends to subtract less from the positive peaks than from the negative peaks and this difference signal, although having less overall amplitude, has positive peaks which are larger than the negative peaks, as illustrated in Fig. 4.8. This difference signal, commonly called the error signal, is exactly of the form needed for input if the output is to be sinusoidal and is thus used as input to the system. The point where the output is subtracted from the input is referred to as the summing junction. These ideas are shown schematically in Fig. 4.9.

However, straightforward and simple this might seem, there are several problems of importance when implementing such a scheme. Some of the problems are general problems of feedback control and some are associated with the electromagnetic forcing system. As noted above, subtracting some of the output from the original input reduces the input amplitude to the system and thus reduces the output. As the output approaches the input, the error signal becomes smaller and the output becomes less. This can be remedied by amplifying the error signal, or as it is commonly called, increasing the gain, so that the actual input to the system is larger. This idea is shown in Fig. 4.10.

Another problem with feedback involves the time response of the system being controlled. This refers to the behavior of the system when subject to a step input. Ideally, the system output should be a step occurring at exactly the same time as the input step. In general, however, the output response is not a step and it occurs a short time later due to dissipation in the system. Interpreted differently, if in addition to distorting the amplitude of a sinusoid, the system causes the output to lag the input, then part of the difference between the input and output is simply a result of them being out of phase, as shown in Fig. 4.11. If the amplitude distortion of the sine wave is slight but there is appreciable phase distortion, then the majority of the error is due to the phase distortion. The feedback system must compensate for the phase distortion as well as the amplitude distortion and this may be the most difficult part. Ideally, when a feedback system is working properly, there is no phase difference between the input and output. In the electromagnetic forcing system of Fig. 4.5, the prime sources of poor time response are due to the resistive and inductive effect in the magnetic coil circuit, hysteresis in the magnetic material and eddy current loss in the core.

A third problem encountered in feedback systems is stability. If the output of a system is out of phase with the input by 180^0, then addition of feedback will cause the system to become unstable. This is because the subtraction at the summing junction becomes an addition and the input to the system grows without bound. For phase shifts other

than 180^0, addition of feedback and an amplifier can also cause instabilities. In most instances this factor limits the amount of amplification that is possible.

A fourth concern, more closely associated with the practical aspects of feedback, is the problem of unwanted noise. To see how noise can affect a feedback system, referring to Fig. 4.12, suppose noise enters the feedback path somewhere between the point where the output is measured and the summing junction. The feedback signal being compared with the input signal is the actual output signal plus the noise. The summing junction generating the error signal interprets the noise as part of the distortion caused by the system and so a signal is sent forward through the system to compensate for it. The noise goes through the system and actually gets into the output and now the output is less representative of the input signal than it was without feedback. Two common forms of noise are 60 and 120hz ripple from supply line voltage and random noise generated in electronic equipment.

Another problem with noise relates to stability. The system may not appreciably change the phase of signals at frequencies within the range of the input but it may shift by 180 degrees frequencies which are contained in the noise. If the noise is generated in the feedback signal, the subtraction at the summing junction is a 180^0 phase shift and when the noise passes through the system it senses another 180^0 phase shift, the net result being a 360^0

shift of the signal when it appears on the output. When this is fed back as part of the output, it directly adds to the original source of noise, making the situation worse.

Two problems peculiar to the present electromagnetic system are the problem of frequency doubling and the problem of measuring the force accurately. With feedback, at the summing junction a signal of frequency Ω is being compared with a signal of fundamental frequency 2Ω. To remedy this problem, the alternating magnetic field was superimposed upon a static magnetic field. The static field magnetically polarizes the structure and when the alternating field is impressed on the beam, the force alternates predominantly with frequency Ω, provided the maximum value of the alternating field is less than the static field. If $B = B_0 + B_1 \sin(\Omega t)$, $B_1 \leq B_0$, the force then becomes proportional to

$$B_0^2 \{ (1 + \tfrac{1}{2}(B_1/B_0)^2) + 2(B_1/B_0)(\sin(\Omega t) - \tfrac{1}{4}(B_1/B_0)^2 \cos(2\Omega t)) \} \quad (4.2)$$

Recall, however, that due to magnetic material nonlinearities, H of the form $H_0 + H_1 \sin(\Omega t)$ will not necessarily produce B of the form $B_0 + B_1 \sin(\Omega t)$. With this method there is a static force plus an alternating force and both can be varied independently as long as the static force is greater than the alternating force. Note that if $B_0 = B_1$ there is about a 25% component of force at 2Ω and if $B_0 = 4B_1$ the 2Ω component is about 6%. So with this method of eliminating frequency doubling, the force will contain a

harmonic even without the effects of the nonlinear material or the nonuniform spatial field. However, this unwanted component can be eliminated with the feedback used to eliminate the other unwanted effects.

The problem of measuring the force on the structure is an important one since it is the force which is to be controlled. The magnet is producing the force on the structure and so reflects the force on the structure. If the magnet were floating free in space, then by Newton's Third Law, the force on it would be equal and opposite to the force it exerts on the structure. If the magnet were a known point mass, then knowing its acceleration, the force on it would be known. This situation can be closely approximated by suspending the magnet on fine wires, such that its natural pendulum frequency is much lower than the forcing frequencies, and measuring its acceleration with an accelerometer.

The other approach is to use a fixed magnet and measure the force on the structure by measuring the force on the magnet at its mounting points. This is approximated by making the natural frequency of the magnet on its mounts much higher than the forcing frequencies and using the strain in the mounts as a measure of force or making the mounts out of a piezoelectric material. A variation of this approach, used in this investigation and described in detail later, uses a semi-rigid mount and the displacement of the magnet is used as a measure of the force.

4.3 DESIGN OF FEEDBACK UNIT

Rather than do a detailed theoretical analysis of the nonlinear control problem, which would involve modeling the magnetic field and the interaction of the magnetic field with the beam dynamics, the approach taken to design a feedback system was to add simple electrical or mechanical devices to the existing experimental setup of Bennett and Kovac and evaluate their effects. The setup is described in more detail in their work but basically it consists of forcing the beam specimens with the middle leg of an E shaped magnet which was suspended by fine wires from a modified lathe bed. The lathe bed, as shown in Fig. 4.13, served both as a point of suspension for the magnet and as a support fixture for the beams. Although the suspended magnet was eliminated after the first unsuccessful attempt to incorporate feedback, the lathe bed continued to serve as a support fixture for the beams. Extensive electrical and mechanical changes were made to the forcing system before any decrease in force distortion was realized. These changes, their advantages and shortcomings are discussed and then a description and evaluation of the most successful design is presented.

The backbone of the control system effort was an LM-20 analog computer which had a working voltage of ± 100 volts. The working voltage was an important factor because the output signals from the force measuring transducers were on the order of a millivolt (mv) and had to be amplified

considerably to be useful. In the first attempt to incorporate feedback, an additional set of windings was added to the middle leg of the E shaped magnet, to produce the polarizing field, and the output of the accelerometer was subtracted from the sinusoidal input. The acceleration of the magnet was measured with an Endevco Model 15 piezoelectric accelerometer which had a voltage sensitivity of 6.85 mv/g. The magnet and accelerometer weighed 1.1 lb. which resulted in a force sensitivity of 6.23 mv/lb. The accelerometer was electrically isolated from the magnet by using a plexiglas mount. The natural frequency of the magnet and accelerometer combination was 5 hz and the resonant frequency of the beam specimen being used was about 50 hz. The alternating current for the electromagnet was provided by a 75 watt McIntosh audio amplifier and the direct current to polarize the beam was provided by a Hewlett-Packard Model 6427B D.C.Power Supply.The sinusoidal input was provided by a Hewlett-Packard Model 3264 Function Generator. A summing amplifier on the analog was used as a summing junction. Since the main concern at this point was with the forcing device, no measurements were made of the beam response.

With forces on the beam in the range of .1 lb., the voltage from the accelerometer was about .5 mv. This signal had to be compared with a voltage from the function generator of about 2 to 4 volts. Because of the ± 100 volt working voltage of the analog,it was best to be manipulating

voltages in the ±10 to ±90 volt range. The output of the function generator could be amplified with no problem but settling for even 20 volts from the accelerometer meant that its output had to be amplified 40,000 times. Fortunately, this particular model accelerometer could be used directly with an oscilloscope and so one vertical deflection amplifier of a Tektronic 502A Dual Beam Oscilloscope was used to amplify the accelerometer signal by connecting the accelerometer to one trace and tapping the output of the vertical amplifier.

The accelerometer had an operating range from .1 g to 1000 g and thus was operating on the low end of its spectrum. This, coupled with the broadband noise associated with the output of the accelerometer, caused the signal to noise ratio from the accelerometer to be about 10:1, smaller than desired. For this reason the output from the oscilloscope amplifier was filtered with a low-pass R-C filter to eliminate some of the noise. Figure 4.14 shows a schematic of this system.

Even with filtering, the signal to noise ratio was not as large as desired. In addition, in the frequency range 20-50 hz, the accelerometer frequency response was not flat. These two factors limited the success of this system. With any amount of feedback the broadband noise from the accelerometer caused the windings to actually vibrate (transformer hum) and this was reflected in additional noise on the accelerometer output. In addition,

with large amounts of feedback, the magnet began to swing at 5 hz and made physical contact with the beam.

Since this particular accelerometer was not suitable for measuring the low acceleration levels and low frequencies being used in the experiment, a search was made for other accelerometers which might be more suited for this application. Bell & Howell and Honeywell had piezoresistive accelerometers suitable for low acceleration ranges but their natural frequencies were too close to the frequencies being used in the experiment. Endevco claimed to have one in the offing but it was not available at that time.

At this time it was decided to try the fixed magnet approach. Incorporated into this idea was a scheme to reduce the spatial nonuniformity of the magnetic field. Lines of flux, as a magnetic field is commonly referred to, travel in uniform, parallel paths as long as they are inside a ferromagnetic material. When the field enters into a nonferromagnetic media, such as air, the lines of flux tend to spread out and become unevenly distributed due to lack of a well defined ferromagnetic path. This spreading of the field, as it leaves one media and enters another, is referred to as fringing and accounted for part of the spatial nonuniformity of the field. As shown in Fig. 4.15, as the field leaves the beam end of the middle leg of the magnet, some of the field goes to the beam and returns through the outer legs of the E. Other lines go directly to the outer legs and still others go back to the

base of the middle leg. How much goes where depends on the gap between the beam and the middle leg, the gap between the legs and the length of the legs. Part of the force distortion is due to fringing and if this could be minimized, the control system would not have to compensate for as much force distortion. If the magnetic coil was fixed to a steel bar which in turn was attached to the steel end pieces holding the beam, then the lines of flux would have a well defined path from the magnet, through the beam specimen, into the end pieces and back through the steel bar to the magnet. In addition, for a given number of windings, the force produced would be much greater with this scheme since almost all the flux lines pass through the beam. In order to have a reasonably large electronic force signal, one other idea was incorporated into the fixed magnet system. Referring to Fig. 4.16, the magnetic coil was mounted on a vertical strut, $1\frac{1}{2}$" from the point where the strut attached to the bar connecting the steel end pieces. The strut was extended upward another $2\frac{1}{2}$" and the displacement of the tip of the strut was used as a measure of the force the magnet was exerting on the beam. Extending the cantilever beyond the magnetic coil and measuring the displacement of the tip gave larger displacement signals than if measurements were taken where the coil was mounted. The displacement was measured with a Bentley-Nevada Proximeter Model 316 which accurately measures displacements of 10^{-5} inches. If the

natural frequencies of the strut are much greater than the forcing frequencies, the displacement of the strut will give a satisfactory representation of the force and can be calibrated statically. This can be seen by considering that for forcing frequencies less than the first natural frequency of the strut, the response of the strut can closely approximated by a one-degree-of-freedom system and for such a system, the displacement varies by only 4% from zero frequency (static) to .2 of resonant frequency, for a given force level. Fig. 4.17 shows this magnet configuration.

A Bentley-Nevada proximeter is a noncontacting inductive device which can be used to measure the displacement of any electrically conducting object.A high frequency alternating current in a coil in the probe generates a magnetic field which produces eddy currents in the object being measured. The eddy currents in turn produce a magnetic field which interacts with the original field, the interaction changing the total inductance of the coil circuit. The air gap affects this mutual inductance and can be determined by measuring changes in electrical quantities in the coil circuit. A typical output voltage vs. air gap distance for a Model 316 is shown in Fig. 4.18. Choosing actual physical dimensions for the strut became a trade-off between keeping the natural frequency of the strut high and keeping the deflections large enough to give a high signal to noise ratio from the proximeter. The

bar connecting the two end pieces clamping the beam specimens was made of one inch square steel stock and the strut was made of one fourth inch by two inch steel. The magnet was a three eighths inch diameter bolt would with two sets of windings of 125 turns each of #26 enameled copper wire. The first resonant frequency of the strut was 400 hz. This force measuring system provided an output between 50 and 100 mv/lb, depending on the sensitivity setting of the proximeter, and the displacements of the strut were so small that the nonlinearity of the proximeter was not a problem. To further improve the force signal to noise ratio, a π filter was used to eliminate much of the proximeter power supply ripple which was affecting the output of the proximeter. To insure against interference between the proximeter and the magnetized strut, a small piece of copper was cemented to the strut where the displacements were being measured. The proximeter was mounted on a piece of plexiglass so that ground loops or currents caused by the magnetic field would not affect proximeter operation. The passive R-C low-pass filter was used in the feedback path to filter out the high frequency carrier signal of the proximeter and the resonant frequency of the strut. A General Radio Model 1309-A Oscillator was substituted for the Hewlett-Packard function generator.

This system, shown in Fig. 4.19, was virtually ineffective because the force on the beam was substantially out of phase with the signal from the oscillator and to overcome the

phase difference, large amounts of gain were necessary and the system became unstable in a low (2-5 hz) frequency mode. The phase between the input sinusoid and the output force with no feedback applied, referred to as open loop phase response is shown in Fig. 4.20. When looking at the phase response, recall that the system at hand is a nonlinear system and the characteristics of the system depend on the amplitude of the input. In addition, since the open loop output is not a pure sinusoid, phase angle does not mean the same as when comparing two harmonic signals and in fact may be misleading. However, since the output is predominantly one frequency, the phase angle is a good indicator of the system characteristics and was used effectively throughout the design of the feedback system. The phase measurements were made with an Ad Yu Phase Meter Type 406L, an instrument which measures the phase angle between zero crossings of two periodic signals.

The fact that the force signal lagged the input was a combination of electrical lags in the forward and feedback circuits, hysteresis and eddy losses in the magnet and an effect due to the beam being part of the magnetic circuit. The magnet coil circuit behaved as a resistor and an inductor in series. In such a circuit, the current, which causes the force, lags the applied voltage, in this case the output of the McIntosh. The low-pass R-C filter produced a lag in the feedback force signal. However, most

of the lag was due to the beam being part of the magnetic circuit. It is important to understand this lag because it was a serious disadvantage to making the beam part of the magnetic circuit. The static field of course, had no temporal variation but it had a spatial variation, being strongest near the pole of the magnet. The time varying field caused the beam to move back and forth in the non-uniform static field as well as in its own nonuniformity. The static field, which has to be as strong as the alternating field to keep the beam polarized, produced a force variation due to the beam moving back and forth within it and so the total alternating force felt by the beam was due in part to the temporally alternating field and in part due to a force induced by the beam moving within nonuniform fields. Since the alternating force due to the nonuniform fields was in phase with the beam displacement and the force due to the alternating current had a phase governed by the R-L characteristics of the magnet, hysteresis and eddy current losses, the phase of the total alternating force relative to the sinusoidal input from the oscillator was a combination of the two effects. The beam displacement increasingly lags the total alternating force as the forcing frequency increases until it lags 90^0 at beam resonance and continues to lag, increasing to 180^0 at frequencies beyond resonance. Hence, the total force on the beam increasingly lagged the input sinusoid as the forcing frequency increased. Making the beam part of the circuit

created a magnetic circuit whose reluctance - resistance to establishing a magnetic field - varied periodically according to beam dynamics because the air gap, which was the prime source of reluctance, depended on beam displacement. The open loop phase response in such a situation was detrimental to applying feedback. In addition, having the beam part of the magnetic circuit introduced lags due to hysteresis and eddy current effects of the additional steel in the circuit.

There was nothing that could be done to eliminate the lag related to the beam-displacement-dependent force just discussed, but some of the electrical lags could be minimized and leads could be produced with additional elements to compensate for lags. Two methods of lag compensation were tried. One simply consisted of putting a capacitor in series with the magnetic coil. The coil circuit then became a series R-L-C circuit. In such a circuit, the current leads the applied voltage at frequencies lower than the resonant frequency of the circuit. The lead angle is given by:

$$\tan^{-1} \frac{\left(\frac{1}{2\pi Cf}\right) - 2\pi Lf}{R}$$

where f is the frequency of the applied voltage. The ratio of output current to applied voltage is:

$$\frac{1}{\sqrt{R^2 + (2\pi Lf - \frac{1}{2\pi Cf})^2}}$$

Unfortunately, it is seen that any appreciable lead is obtained at the expense of current amplitude.

A second method of lag compensation is to use a differentiator in the forward loop. A differentiator amplifies high frequencies more than low frequencies but gives all frequencies a phase shift of $+\pi/2$. The derivative of a harmonic signal can be added in some proportion to the signal itself and the result is a signal which leads the original signal from 0 to $\pi/2$ degrees, depending on the amount of differentiation used. Putting a differentiator in the forward loop, just before the McIntosh amplifier, caused the input to the McIntosh to lead the output of the General Radio Oscillator and this lead, coupled with the lead in the R-L-C coil circuit, compensated for lags produced by the other effects so at the summing junction the oscillator output and the force signal could be made to be in phase with each other. Because a true representation of the output force was desired at the summing junction, the differentiator was put in the forward loop. Putting it in the feedback loop would have accomplished the same lag compensation but it would tend to amplify the higher harmonics of the force and an inaccurate representation of the output force would be compared to the reference sinusoid at the summing junction.

Initially, this system did not work. With any appreciable amount of feedback and gain, the system was unstable. However, the instability was of high frequency, the frequency being the same as the strut natural frequency. The instability was due to the differentiator and a ripple in the direct current power supply of the analog. The ripple, which had a fundamental frequency of 120 hz, was reflected in the output of the analog operational amplifiers as small pulses which were amplified by the McIntosh and excited the strut at its natural frequency. The strut proximeter sensed this vibration and fed the signal into the system. Despite the low-pass filter, enough of the signal remained in the system so that when this high frequency signal was differentiated, its amplitude increased enough to further excite the strut at its natural frequency and the oscillations grew without bound.

Several modifications were made in order to eliminate some of the problems. The LM-20 analog was replaced with an LM-10 which had much less noise. The number of windings on the magnet was doubled to compensate for the loss of power caused by the capacitor and the strut was stiffened to increase the natural frequency, felt to be low. The passive filter and oscilloscope amplifier were replaced with a Dana Model 3520 DC amplifier with an active low-pass filter built in. It was necessary to insert a blocking capacitor in the feedback just before the Dana Amplifier to block the constant voltage associated with the static

air gap of the proximeter used to measure the strut displacement. The constant voltage ranged from -6 to -11 volts, depending on the static air gap, and had to be eliminated or it would overload the input to the Dana which was there to amplify the 50-100 mv/lb signal from the strut. This was not a problem with the oscilloscope amplifier since a blocking capacitor was built into the oscilloscope. A Krohn-Hite band-pass filter, Model 330N, was inserted in the forward loop just before the McIntosh to help suppress any noise which might get into the system. The configuration which is summarized in Fig. 4.21, was successful in reducing the second harmonic in the force from 10% to 3% but only over a limited range of frequencies. Any attempt to further reduce the harmonics in the force resulted in a loss of stability in the strut frequency mode. For frequencies above 35 hz, the system could not sufficiently compensate for the lags and still have the same power output as at the lower frequencies. The differentiator could compensate for lag but it would amplify any noise in the pass-band of the Krohn-Hite which had to be sufficiently wide to avoid further phase distortion. Adjusting the capacitance would compensate for lag without amplifying the noise but at a loss of output power. At any given forcing frequency, it was a question of tuning the system to get a balance of power, phase compensation and minimal noise amplification.

Since most of the phasing problems could be traced to

the beam being part of the magnetic circuit, at the expense of fringing, the magnetic circuit was eliminated. Since the method of measuring force with the cantilever strut arrangement was successful, this idea was retained and the magnetic circuit eliminated by making the strut out of aluminum. With this modification, the strut frequency was 466 hz.

In the process of measuring the phase effect of this new configuration, an additional source of lag was discovered.The alternating current and direct current windings shared the same core and so were inductively coupled. The inductive coupling of the two windings and the internal impedance characteristics of the direct current power supply, which is essentially a short circuit for alternating current, combined to produce an inductive load for the McIntosh which was more complicated than a simple R-L circuit. To reduce the effect, a 35 millihenry choke was put in series with the direct current power supply to isolate it from the core. The setup with these ideas incorporated is shown in Fig. 4.22. Also shown in Fig. 4.22 are the amplitude and phase relations between input and output, assuming harmonic input for the various linear elements,as well as the characteristics of the nonlinear elements. Figure 4.23a and b show the harmonic content of a .05lb force at 20 and 50 hz, respectively, with and without feedback, using this system. Note that the 2nd harmonic of the force is greater when the forcing frequency is near beam resonance

due to increased beam displacement in the nonuniform field and thus the feedback system has more to compensate for. The force distortion was a function of the magnitude of the force and the forcing frequency. For frequencies below one-half the beam resonant frequency, the force distortion was relatively small while at one-half the resonant frequency, the distortion was higher. For further increases in frequency, the distortion decreased only to increase again as the frequency approached beam resonance. The distortion level generally increased with increasing force but this was not always the case. The spectral results are taken from a Hewlett-Packard 3580A Spectrum Analyzer. The system represents an improvement over the magnetic circuit system because it operated over a wider range of forcing frequencies. However, any increase in gain to get better performance resulted in loss of stability. The system went unstable with a low frequency instability, the frequency of the instability depending on the lower cut-off of the band-pass filter. The instability frequency was evident on the spectral plots and is indicated on Fig. 4.23. It was felt that the low frequency phase distortion of the band-pass filter in the forward loop was causing the instability. It was moved to the feedback loop, as shown by the dotted lines in Fig. 4.22, with no effect. The band-pass filter was eliminated and a low-pass Ithaco Filter, Model 4213, with direct current coupling was used in the feedback loop. The instability continued but at .9 hz and

it was felt that the McIntosh, which is transformer coupled on the output and has poor phase response below 5 hz, was responsible for the instability. To rectify this, the McIntosh had to be replaced with an amplifier with similar output capabilities but with direct current coupling. None was readily available so an amplifier was built using an RCA HC2500 solid state operational amp which had high output current capabilities. The circuit diagram and input-output capabilities of the amplifier are shown in Fig. 4.24.

With the new amplifier capable of transmitting direct current, the separate direct power supply and windings could be eliminated and the constant bias current and the alternating current could be applied with the same circuit and windings. Instead of using a pure sinusoid as input, the sinsuoid could be biased so the input was of the form $V_0 + V_1 \sin(\Omega t)$. In addition, since the constant field and the alternating field could be generated using the same circuit elements in the forward loop, it would be possible to incorporate a square rooting device before the RCA amplifier to counter the squaring effect of the magnet. However, a bias on the input would reduce the amount of alternating voltage that could be applied before the maximum input capability of the amplifier was reached. This also raised the question of whether to feed back a voltage proportional to the constant output force. Heretofore, the input to the summing junction was $V_1 \sin(\Omega t)$ and the

feedback signal was periodic with the constant component of the force being blocked by the capacitor which was there to block the constant voltage associated with the static air gap of the proximeter. With the input to the summing junction $V_0 + V_1 \sin(\Omega t)$, and it made sense to have the feedback signal be a constant plus a periodic portion. However, before these ideas were tried, it was important to determine what effect just replacing the McIntosh had on the performance.

With the RCA amplifier, feedback reduced the second harmonic in the force more than the previous system but the system was limited by an instability not witnessed before. Figure 4.25 shows the 30 hz force spectrum with and without feedback. The peak at 466 hz (with no feedback) is the strut natural frequency. The spectrum with feedback shows a broadband noise centered at 275 hz. This noise led to an instability when the gain was further increased. The first thoughts were that this was an effect due to the addition of the RCA amplifier. However, a close inspection of the force spectrum (similar to Fig. 4.23) using the McIntosh but extending to 500 hz, showed a tendency for increasing amplitude around 275 hz when feedback was employed. The amplitude never reached the magnitude witnessed using the RCA amplifier because the system went unstable in the low frequency mode before the gain was high enough to significantly amplify the 275 hz noise. The broadness of the spectrum was puzzling because a structural

frequency would have shown as a sharp peak and there was no indication of excessive electrical noise in this frequency range as evidenced by the flatness of the spectra in this region with no feedback.

It was a serious error not to look for the source of the broadband noise at that time. It was later discovered that the phase response of the Ithaco filter was responsible for the instability. The phase shift of the system plus the phase shift of the Ithaco summed to be 180^0 at 275 hz and resulted in positive feedback of the random noise at that frequency. Changing the cut-off frequency of the Ithaco merely changed the frequency of the instability. However, at that time the philosophy was that the instability would not be a problem if the open loop system had better phase response and the square rooting device could be incorporated, both of the ideas aimed at reducing the amount of amplitude and phase distortion the feedback system had to compensate for thus requiring less gain to reduce the 2nd harmonic to a reasonable level.

To improve the phase distortion, an inner feedback loop was added around the RCA amplifier to reduce the phase difference between the voltage into the amplifier and the current out, due to the inductive effect of the coil, making the RCA amplifier more like a voltage controlled current source. Voltage from the series resistor in the coil circuit was fed back to a summing amplifier just before the RCA amplifier. For low values of force, about .01 lb,

the phase distortion could be reduced to 1^0 up to 80 hz but for larger forces, it was not possible to feed back the same amount of voltage, from the resistor, and use the same gain without causing an instability in this inner loop and thus the 1^0 could not be realized at all force levels.

A square rooting circuit, using a 37 segment diode multiplier was inserted in the system, just after the summing junction. Diode multipliers are a specialization of diode function generators which can be used to produce a nonlinear relation between two voltages. They approximate the nonlinear relation with a piecewise linear relation by using a series of diodes and variable resistors. The resistors are adjusted so that over a certain range of the input voltage only certain diodes conduct and the slope of the output vs. input is determined by other resistor values. As the input voltage changes, other diodes stop or start conducting, changing the input-output relation. In this manner, a sequence of linear segments is developed, each with a different slope and each valid only over a certain range on input voltage. Since the diode square rooting circuit approximated the curve $y = \sqrt{x}$ with straight line segments, it was important to adjust the input to the circuit so that all 37 straight line segments were being used, thus making a better approximation to the square root function.

Much effort was given to feeding back a voltage proportional to the bias force. Basically all that had to be done was to replace the blocking capacitor, in the feedback, with a circuit to nullify the voltage due to the static air gap of the proximeter. Then any voltage out of the nullifying circuit would be directly proportional to the total force, both the constant part and the alternating portion. A nullifying circuit was built using a 30 K ohm potentiometer and a battery. Unfortunately the proximeter and nullifying circuit combination was plagued with a serious drifting problem. This meant that the voltage out of the nullifying circuit representing the constant force continually changed value. The drift had the appearance of a capacitance effect in some element or elements. All cable lengths were shortened to minimize any capacitance effects associated with coaxial cables. The system was grounded carefully and the proximeter power supply was replaced with batteries to eliminate effects of change in line voltage. With all these changes, the drift was reduced to about 20 mv/hr, still a substantial amount considering that if 5.0 mv represents .1 lb, in one minute this .1 lb force representation is 5.3 mv. However the 20 mv/hr drift is quite small compared to the static voltage of -6 to -11 volts, the output of the proximeter.

The idea of feeding back a constant voltage was abandon and so the system appeared as shown in Fig. 4.26. Because of the square rooting circuit, the force had less

2Ω component even without feedback. It had been hoped that if the feedback reduced the 2nd harmonic by, say, 7 db without square rooting and the square rooting reduced the 2nd harmonic by 7 db, then the square rooting and feedback would reduce the 2nd harmonic by 14 db. Such was not the case for this nonlinear system. The feedback was mostly compensating for the squaring effect because it was only about one-half as effective when the square rooting circuit was added.

The 275 hz instability still existed and at this time it was found to be due to the Ithaco filter, a four-pole Butterworth. Ironically, the Ithaco had been put in the feedback loop to attenuate the strut resonant frequency. It did attenuate that frequency but it was due mostly to cancellation by 180^0 phase shift, partly due to the filter, rather than by amplitude attenuation.

It was felt that the system was producing a reasonably clean harmonic force and the effect of feedback was evident. It was decided to use this system to investigate nonlinear beam response. Chapter 5 reports the results of using this system to force three-layer beams.

CHAPTER V

EXPERIMENTAL RESULTS USING THE FORCING SYSTEM

This chapter discusses the results of using the forcing system, described in Chapter 4, to study the nonlinear vibration of three-layer beams, giving particular attention to the superharmonic response, the spatial mode shape and the performance of the forcing system.

5.1 BEAM SPECIMENS AND THE CLAMPING MECHANISM

The experiment was done with unsymmetric beams, the lack of symmetry dictated by the fact that one layer had to be ferromagnetic, for forcing, but the other had to be non-ferromagnetic to avoid erroneous readings from the beam displacement measuring proximeter. Since Kovac reported on a variety of specimens and witnessed the same general response with all of them and Chapter 3 revealed the same general response for symmetric and unsymmetric beams, it was felt necessary to test only one beam extensively and study the response.

The beam tested was constructed of phosphor bronze, neoprene and steel. The phosphor bronze was .010 inch thick and alloyed to be of spring hardness, a rating for bronze alloys. The neoprene was .062 inch thick and the steel was .010 inch thick. The layers were bonded together with Loc-Tite IS-12[39], a single stage adhesive. The beams were one inch wide by thirteen inches long including the one and a half inch brass fillers on each end in place of the

neoprene core for those segments of the beam actually in the support and so, the actual length of the beam between the clamped supports was ten inches. The steel end pieces, which in the second attempt to incorporate feedback were part of the magnetic circuit, provided the support condition and were six inch by six inch by four and a half inch blocks bolted to the lathe bed. Within the end pieces were a set of steel jaws which actually provided the clamping mechanism. Two one inch by three inch steel bars were bolted across the top to give the support fixture additional rigidity. Details concerning the flexibility are given in Bennett's[37] work.

5.2 BEAM AND FORCE MEASUREMENTS

The displacement of the beam was measured with a Bentley-Nevada Model 308 proximeter. The proximeter was attached to what used to be the tool mount on the lathe bed and could be moved along the length of the beam with the tool movement mechanism. Since the relation between the proximeter output voltage and the beam displacement is nonlinear, a diode function generator was built to compensate for the nonlinearity and resulted in a relation that was quite close to linear over a one fourth inch of beam displacement. However, the voltage-displacement characteristics of the proximeter depend on the material being measured, being dependent on the conductivity, and the sensitivity setting of the proximeter. With this particular setup, the sensitivity was adjusted so that the output was quite linear over the beam displacement range without using the

diode circuit, thus simplifying the experimental setup. Fig. 5.1 shows the calibration curve for the proximeter.

The forcing system was calibrated using a pulley and known weights, as shown in Fig. 5.2. With this scheme, calibration could be done with the beam specimen in place. This was important because taking the specimen in and out of the support fixture was time consuming and it was important to calibrate the forcing mechanism before and after each run to know the exact value of force used. Day to day changes in calibration were enough so that it was a good idea to calibrate the force system routinely.

5.3 EXPERIMENTAL RESULTS

Experimental and theoretical frequency response curves for two different forcing conditions are shown in Figs. 5.3 and 5.4. The value of the static force was chosen to be larger than the alternating force to have a more pronounced superharmonic response. Also plotted is the ratio of the 2Ω component of response to the Ω component, with and without feedback. The amount of feedback and gain used was a value so that the force system was stable during the time it took to compute spectral results at each frequency point, a time of at least five minutes. The spectral results were taken with the Hewlett-Packard 3580A Spectral Analyzer and the rms beam displacement was determined by measuring the output of the proximeter with a Ballentine True RMS Voltmeter, Model 323 L-01. In Figs. 5.3 and 5.4, the frequency is normalized by dividing the forcing frequency by the

resonant frequency of infinitesimal vibrations about the statically deflected position induced by the bias force. The bias force stiffens the beam due to the in-plane forces and causes the resonant frequency about the deflected position to be greater than the resonant frequency about the no-load position.

Figure 5.5 shows the spatial mode shape when forcing the beam at resonant frequency and at one-half the resonant frequency. The results were taken from the case with F_0= .18 lb., F_1=.073 lb. but the same general shape was observed for other values of force and other frequencies.

Figure 5.6 shows several characteristics of the forcing system when forcing the beam at F_0=.15 lb., F_1=.05 lb. Included in the figure is the ratio of the 2Ω component of force to the Ω component of force, with and without feedback. Shown also is the phase relation at the summing junction between the input signal and the feedback signal, i.e., the output of the Ithaco low-pass filter, with and without feedback. Included for reference are the phase distortion of the low-pass filter and the inductive lag in the coil circuit, without any inner loop feedback. The phase data for the filter and the coil are strictly for a harmonic signal into the element and a harmonic signal out while the other data was taken using the square rooting element, the inner inductive feedback loop and includes the nonlinear effect of the magnet on the force signal.

5.4 DISCUSSION

Agreement between theoretical and experimental curves for both the rms displacement and the ratio of harmonics is quite good. Feedback in the forcing system affects the beam response, particularly when forcing the beam near one half the resonant frequency. An important point is that even without feedback, the 2Ω component of displacement seemed to correlate within reason to what the theory predicted. This is felt to be due to the 2Ω component of force being quite low, even without feedback. One would expect that the theory would predict more superharmonic response than actually observed because the amount of superharmonic depends on the same factor that causes the frequency response curve to incline to the right, namely, the rigidity of the axial restraint. The theory, of course, uses a perfect axial restraint while in practice, there is always a tendency for the clamps to permit motion in the axial direction, either through slippage or flexibility. With feedback, the superharmonic response of beam is less than predicted by theory indicating that with feedback, the true response of the beam is evident. However, it is interesting to consider the following rough calculations. When forcing the beam near resonance, a .05 lb. force causes approximately .019 inch, rms, of displacement. When forcing the beam at one-half resonance, if the force contains about four percent of a component at twice the forcing frequency, which is the beam resonant frequency, one would expect four percent x .019 inch,

rms, of displacement to be at twice the forcing frequency, considering just linear beam response. This results in .00076 inch, rms, of displacement at twice the forcing frequency. However, the spectral results indicate that the ratio of 2Ω response to Ω response is a maximum of .18 when forcing the beam near one-half the resonant frequency and using the .0025 inch, rms, displacement at that frequency means that the 2Ω component of the displacement has an amplitude of .00045 inch, rms, less than expected considering just linear beam response to a force consisting of the two harmonics. What is missing is all consideration of phase. The phase of the linear beam response to the 2Ω component of force is different than the phase of the superharmonic 2Ω component and it is possible that both effects interact in such a way, with proper cancelation due to phasing, that it only appears that the superharmonic response of the beam is being measured. The phases can be determined theoretically but to determine phase experimentally requires spectral analysis which preserves information about phase. This raises the question of being able to tolerate <u>any</u> harmonics in the force when studying nonlinear vibrations.

The approximate mode shape was a good representation of the actual mode shape, for all frequencies, although the actual shape was flatter at the center of the beam, being flattest at resonance. The flatness is expected because the in-plane forces are tending to keep the beam straight and the effect becomes more pronounced with large transverse

displacements. Since the theory of Chapter 2 shows no basic difference between symmetric and unsymmetric beams, except for the coupling of axial and transverse motion, it is felt that the mode shape and frequency response characteristics observed for this unsymmetric beam would be observed for a symmetric beam under similar conditions.

Figure 5.6, which shows the characteristics of the forcing system, indicates that feedback was effective in reducing the force distortion but, because of the 275 hz instability, was limited in performance. Chapter 6 will present recommendations for possible improvements in the system but it is important to note that the phase distortion and the amount of 2Ω harmonic in the force is still dependent on beam response even though eliminating the magnetic circuit eliminated much of the dependence. This dependence indicates that somehow the beam still effects the magnetic field strength. At one point it was felt that the geometry of the support fixture and the steel bar connecting the end pieces, and holding the aluminum force strut, still provided a path. Making the connecting bar out of aluminum and the bolt holding the strut out of brass had no effect and so this investigator can only conjecture that the steel lathe bed, the steel end pieces, the steel axial restraints and, of course, the steel in the beam specimen, still carry some of the magnetic field.

For these force levels, the inner feedback loop reduced the inductive phase distortion by approximately one-

half and so the reduced inductive effect plus the effect of the low-pass filter contribute to part of the total phase distortion but the rest comes from the eddy current losses, hysteresis and an apparent phase distortion because a harmonic signal is being compared to a nonharmonic signal. This apparent phase distortion would be different if the phase between maximum values was being measured rather than the phase between zero crossings.

It was dissappointing not to have realized a more effective feedback system. However, the original motivation of this investigation was to determine the cause of the unexpected behavior observed by Kovac. After it was discovered that the forcing system caused much of the behavior, it was felt it would be simple to eliminate the unwanted effects. This was not the case, for the problem is quite complicated. However, the work report on here is important because it will alert experimenters to the serious effects magnetic forcing systems can have on the outcome of the experiment and the work provides a reference and direction for future efforts.

CHAPTER VI

CONCLUSION

6.1 SUMMARY

This work was initiated to investigate the superharmonic response observed experimentally by a previous investigator while studying the nonlinear vibrations of symmetric, three-layer, axially restrained sandwich beams. The beams were constructed with stiff, elastic outer layers and soft viscoelastic cores and were forced with a contactless electromagnetic shaker. Unexpected behavior was observed in both the temporal response and the spatial mode shape when forcing the beam at one-half its resonant frequency. Since the electromagnet exerted a constant plus an alternating force on the beam, a certain amount of superharmonic response could be expected. However, this being the case, the commonly used method of modeling the constitutive behavior of the viscoelastic core with complex moduli evaluated at the forcing frequency, was not valid.

In an attempt to explain the observed behavior and to extend previous work to include dissimilar outer layers, a beam theory was developed, using the principle of virtual work, which included the individual bending resistance of the outer layers and multiple frequency response of the core. The beam theory was considered as a special case of plate theory and, after enforcing interface conditions, two governing equations resulted. In arriving at the two equations, it was found that for unsymmetric beams, a first

order coupling exists between the in-plane displacements and the out-of-plane displacements while for symmetric beams, the coupling is of second order. Also it was found that the thin face sheet assumption is more restrictive for unsymmetric beams than for symmetric beams. Applying Galerkin's method and harmonic balance led to 14 nonlinear, algebraic equations which were solved numerically to predict the response of the beams to a constant plus a harmonic force. Although superharmonic response was predicted, it was nowhere near the amount observed. Also, it was found that symmetry has an effect on damping effectiveness but it depends on the thickness of the outer layers compared to the core.

It was found that certain effects associated with the electromagnetic forcing device seriously altered the response of the beam and obscured the true behavior. The nonlinear relation between B and H, for ferromagnetic materials, and the variation in force with distance from the poles of the magnet affected the force the beam actually sensed. In addition, an interference between the magnetic field and the inductive probe used to measure the beam displacement had resulted in erroneous measurements of beam response.

The unwanted effects of the forcing mechanism can be reduced by using principles of feedback control. However, the contactless electromagnetic forcing device is a complicated electrical-mechanical-magnetic system and application of control principles, although straightforward in theory,

is not simple in practice. Electrical components which are suitable for passive observation and measurement often have characteristics which are detrimental for application to a control system. Several feedback systems were tried before the unwanted effects were reduced. The first attempt involved the use of a freely suspended magnet, the acceleration of the magnet being used as a measure of force. However, the acceleration levels were too low to produce an accurate force signal from the accelerometers available and so a second scheme involved a fixed magnet to get a more useful force signal. In addition, with this system, the beam was made part of the magnetic circuit in order to minimize the fringing effects. This system was impossible to control because the force was coupled directly to the beam motion, a condition which was the exact opposite of what was desired. In the third configuration the magnetic circuit was eliminated but the fixed magnet was retained. The system still depended somewhat on beam dynamics but it did reduce the unwanted effects over a range of frequencies. The system was beset by instabilities related to the phase distortion characteristics of the various electrical components in the system. The final configuration used a nonlinear element in the forward loop, a square-rooting circuit, and an inner feedback loop to reduce the inductive effects. The system was used to study nonlinear vibration of a three-layer unsymmetric beam.

Experimental results indicated that the fundamental mode shape for a three-layer unsymmetric beam is similar to a half-sine wave even when forced into the range of geometric nonlinearities. The results indicated that superharmonic response is evident when forcing the beam at one-half the resonant frequency and experimental data agrees well with the theoretical predictions.

6.2 FUTURE WORK

There are several areas which merit further effort both with the three-layer beams and with continued development of the feedback system.

The study concerning the effect of symmetry on damping indicated that future work could be directed at optimizing the elastic and/or geometric properties of the constraining layers to get maximum damping from a given core material. In practice, the designer is generally limited in the choice of materials and may have a weight, thickness or frequency constraint and it would be worth pursuing the question of given certain constraints and materials, how might the materials be used to be most effective in damping. In addition, the assumed linear displacement field led to questionable results concerning the shear force distribution. This same condition exists in theories for homogeneous, elastic beams but, because shear has little effect on the deformation, the problem is not serious. However, for these composite beams with soft cores, shear is an important consideration and it would be interesting to consider a more

sophisticated assumed displacement field.

With the continued development of the feedback system, there is considerable room for improvement. A very narrow band-reject filter, tuned to reject the strut natural frequency, should be inserted in the feedback path in place of the Ithaco low-pass filter. A band-reject filter would have more favorable phase distortion characteristics than the low-pass filter, however, with any phase distortion at all, there is always the question of stability. It would be desirable to eliminate, or at least minimize, the nonlinear B vs. H relation of the magnetic core. Consideration should be given to eliminating the ferromagnetic core altogether to eliminate the B vs. H effect as well as the inductive effect and use glass or a ceramic to support the windings. The other approach would be to use another inner feedback loop to control the relation between B and the input to the RCA amplifier. B could be measured with a small search coil or a Hall effect probe.

Elimination of all ferromagnetic material from the support fixture is felt to be important. Since for a given path length, air has at least 1000 times more reluctance than steel, it is best to eliminate any steel which might serve as a magnetic path even if this steel appears to be far removed from the magnet.

APPENDIX

For harmonic shearing strain, $\gamma(t)$, at frequency Ω, the constitutive law for a linear viscoelastic material can be written as

$$S(t) = (G_2'(\Omega) + jG_2''(\Omega))\gamma(t) \tag{1}$$

where $S(t)$ is the shear stress, $\gamma(t) = \gamma_o e^{j\Omega t}$, γ_o is a constant, $j = \sqrt{-1}$ and $G_2'(\Omega)$ and $G_2''(\Omega)$ the real and imaginary parts, respectively, of the complex shearing modulus. The hereditary integral representation and the complex modulus representation are equivalent for this case of harmonic shearing strain, that is

$$(G_2'(\Omega) + jG_2''(\Omega))\gamma(t) = \int_{-\infty}^{t} Y_2(t-\tau)d\gamma(\tau) \tag{2}$$

substituting for $\gamma(t)$ yields

$$(G_2'(\Omega)+jG_2''(\Omega))\gamma_o e^{j\Omega t} = \int_{-\infty}^{t} Y_2(t-\tau)\gamma_o j\Omega e^{j\Omega\tau}d\tau \tag{3}$$

Changing variables so that $\xi = t-\tau$, one gets

$$(G_2'(\Omega)+jG_2''(\Omega))\gamma_o e^{j\Omega t} = \int_{\infty}^{o} Y_2(\xi)\gamma_o j\Omega e^{j\Omega(t-\xi)}(-d\xi) \tag{4}$$

The right hand side can be rearranged to give

$$(G_2'(\Omega)+jG_2''(\Omega))\gamma_o e^{j\Omega t} = \{j\Omega \int_{o}^{\infty} Y_2(\xi)e^{-j\Omega\xi}d\xi\}\gamma_o e^{j\Omega t} \tag{5}$$

Expanding and equating real and imaginary parts, one gets

$$G_2'(\Omega) = \Omega \int_0^\infty Y_2(\xi) \sin(\Omega\xi) d\xi$$

and

$$G_2''(\Omega) = \Omega \int_0^\infty Y_2(\xi) \cos(\Omega\xi) d\xi$$

Thus the relaxation function is related to the complex modulus through a one-sided Fourier transform.

REFERENCES

1. Habip, L.M., "A Survey of Modern Developments in the Analysis of Sandwich Structures," Applied Mechanics Reviews, Vol. 18, No. 2, Feb. 1965, pp. 93-98.

2. Yu, Y.-Y., "A New Theory of Elastic Sandwich Plates, One-Dimensional Case," Journal of Applied Mechanics, Trans. ASME, Series E, Vol. 81, pp. 415-421.

3. _____, "Flexural Vibrations of Elastic Sandwich Plates," Journal of Aerospace Sciences, Vol. 27, No. 4, April 1960, pp. 272-282.

4. _____, "Simplified Vibration Analysis of Elastic Sandwich Plates," Journal of Aerospace Sciences, Vol. 27, No. 12, Dec. 1960, pp. 894-900.

5. Kerwin, E.M., "Damping of Flexural Waves by a Constrained Viscoelastic Layer," Journal of Acoustical Sciences, Vol. 31, No. 7, July 1959, pp. 952-962.

6. DiTaranto, R.A., "Theory of Vibratory Bending for Elastic and Viscoelastic Layered Finite-Length Beams," Journal of Applied Mechanics, Vol. 32, No.4, Dec.1965, pp. 881-886.

7. _____ and W. Blasingame, "Composite Damping of Vibrating Sandwich Beams," Journal of Engineering for Industry, Vol. 89, No. 4, Nov. 1967, pp. 633-638.

8. Jones, I.W., V.L. Salerno and A. Savacchio, "An Analytical and Experimental Evaluation of the Damping Capacity of Sandwich Beams with Viscoelastic Cores," Journal of Engineering for Industry, Vol. 89, No. 3, Aug. 1967, pp. 438-444.

9. Yin, T.P., T.J. Kelly and J.E. Barry, "A Quantitative Evaluation of Constrained-Layer Damping," Journal of Engineering for Industry, Vol. 89, No. 4, Nov. 1967, pp. 773-784.

10. Mead, D.J and S. Markus, "The Forced Vibration of a Three-Layer, Damped Sandwich Beam with Arbitrary Boundary Conditions," Journal of Sound and Vibration, Vol. 10, No. 2, Sept. 1969, pp. 163-175.

11. _____, "Loss Factors and Resonant Frequencies of Encastre' Damped Sandwich Beams," Journal of Sound and Vibration, Vol. 12, No. 1, May 1970, pp. 99-112.

REFERENCES (continued)

12. Mead, D.J. and R.A. DiTaranto, "Resonance Criteria of a Damped Three-Layer Beam," Journal of Engineering for Industry, Vol. 94, No. 1, Feb. 1972, pp. 175-180.

13. Grootenhuis, P., "The Control of Vibrations With Viscoelastic Materials," Journal of Sound and Vibration, Vol. 11, No. 4, April 1970, pp. 421-433.

14. Agbasiere, J.A. and P. Grootenhuis, "Flexural Vibration of Symmetrical Multi-Layer Beams With Viscoelastic Damping," Journal of Mechanical Engineering Science, Vol. 10, No. 3, June 1968, pp. 269-281.

15. Nakra, B.C. and P. Grootenhuis, "Structural Damping Using a Four-Layer Sandwich," Journal of Engineering for Industry, Vol. 94, No. 1, Feb. 72, pp. 81-86.

16. Folie, G.M., "Transverse Bending of Sandwich Plates," Revue Roumaine Des Sciences Techniques Série De Mechanique Appliquée, Tome 17, No. 1, 1972, pp. 19-36.

17. Yan, M.-J. and E.H. Dowell, "Governing Equations for Vibrating Constrained-Layer Damping Sandwich Plates and Beams," Journal of Applied Mechanics, Vol. 39, No. 4, Dec. 1972, pp. 1041-1046.

18. _____, "High-Damping Measurements and a Preliminary Evaluation of an Equation for Constrained Layer Damping," American Institute of Aeronautics and Astronautics Journal, Vol. 11, No. 3, March 1973, pp. 388-390.

19. Krajcinovic, D., "Sandwich Beam Analysis," Journal of Applied Mechanics, Vol. 39, No. 3, Sept. 1972, pp. 773-778.

20. _____, "Vibrations of Laminated Beams," American Institute of Aeronautics and Astronautics Journal, Vol. 10, No. 10, Oct. 1972, pp. 1265-1266.

21. Chan, H.C. and Y.K. Cheung, "Static and Dynamic Analysis of Multi-Layered Sandwich Plates," International Journal of Mechanical Sciences, Vol. 14, No. 6, June 1972, pp. 399-406.

22. Reissner, E., "Finite Deflections of Sandwich Plates," Journal of Aeronautical Sciences, Vol. 15, No. 7, July 1948, pp. 435-440.

REFERENCES (continued)

23. Chu, H.-N., "Influence of Transverse Shear on Nonlinear Vibrations of Sandwich Beams With Honeycomb Cores," Journal of Aerospace Sciences, Vol. 28, No.5, May 1961, pp. 405-410.

24. Yu, Y.-Y., "Comment of Influence of Transverse Shear on Nonlinear Vibrations of Sandwich Beams With Honeycomb Cores," Journal of Aerospace Sciences, Vol. 29, No. 7, July 1962, pp. 886-888.

25. _____, "Nonlinear Flexural Vibrations of Sandwich Plates," Journal of the Acoustical Society of America," Vol. 34, No. 9, Sept. 1962, pp. 1176-1183.

26. Wempner, G.A. and J.L. Baylor, "General Theory of Sandwich Plates With Dissimilar Facings," International Journal of Solids and Structures, Vol. 1, No. 2, 1965, pp. 157-177.

27. Habip, L.M., "Moderately Large Deflections of Asymmetrical Layered Elastic Plates," International Journal of Solids and Structures, Vol. 3, No. 2, 1967, pp. 207-215.

28. Kovac, E.J., Jr., W.J. Anderson and R.A. Scott, "Forced Nonlinear Vibrations of a Damped Sandwich Beam," Journal of Sound Vibration, Vol. 17, No. 1, July 1971, pp. 25-39.

29. Kovac, E.J., Jr., "Forced Nonlinear, Damped Vibration of a Symmetric Three-Layer Composite Beam," Ph.D. Dissertation, University of Michigan, 1970.

30. Stoker, J.J., Nonlinear Vibrations in Mechanical and Electrical Systems, Interscience Publishers Inc. New York, 1950, p. 112.

31. Meirovitch, L., Elements of Vibration Analysis,McGraw-Hill, N.Y., N.Y., to be published.

32. Novozhilov, V.V., Foundations of the Nonlinear Theory of Elasticity, Graylock Press, Rochester, N.Y, 1953.

33. Herrmann, George, "Influence of Large Amplitudes on Flexural Motions of Elastic Plates," NACA TN 3578.

34. Brown, Kenneth M. and S.D. Conte, "The Solution of Simultaneous Nonlinear Equations," Proceedings of the 22nd National Conference of The ACM, pp. 111-114.

REFERENCES (concluded)

35. Byrne and Hall, ed., Numerical Solution of Systems of Algebraic Equations, Academic Press, New York, 1973.

36. Kung, G.C. and Y.-H. Pao, "Nonlinear Flexural Vibrations of a Clamped Circular Plate," Journal of Applied Mechanics, Vol. 39, No. 4, Dec. 1972, pp. 1050-1054.

37. Bennett, J.A., "A Multiple Degree of Freedom Approach to Nonlinear Beam Vibrations," Ph.D. Dissertation, University of Michigan, Ann Arbor, Michigan, 1969.

38. Plas, J. and L. Janssen, "A Transistorized Contactless Electromagnetic Exciter," International Journal of Machine Tool Design and Research, Vol. 12, No. 1, March 1972, pp. 1-16.

39. Loctite Corporation, 705 N. Mountain Road, Newington, Connecticut 06111.

FIGURES

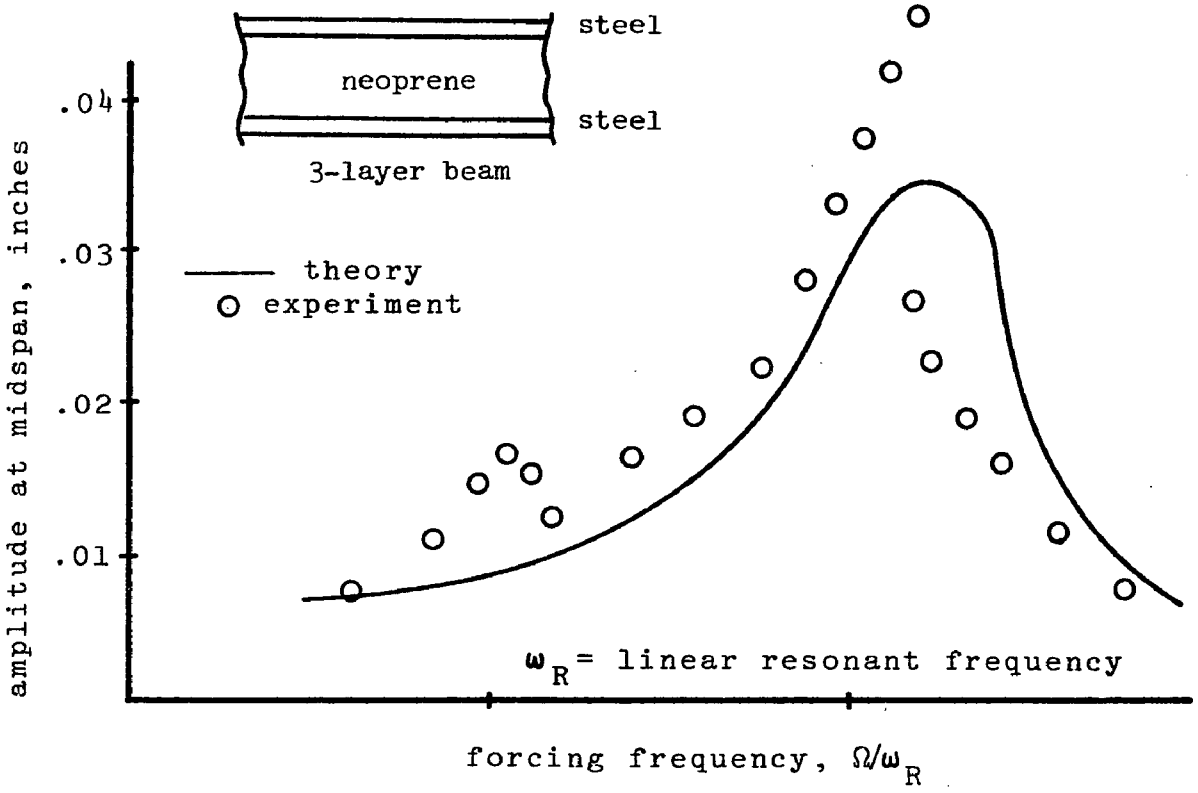


Figure 1.1. Kovac's frequency response.

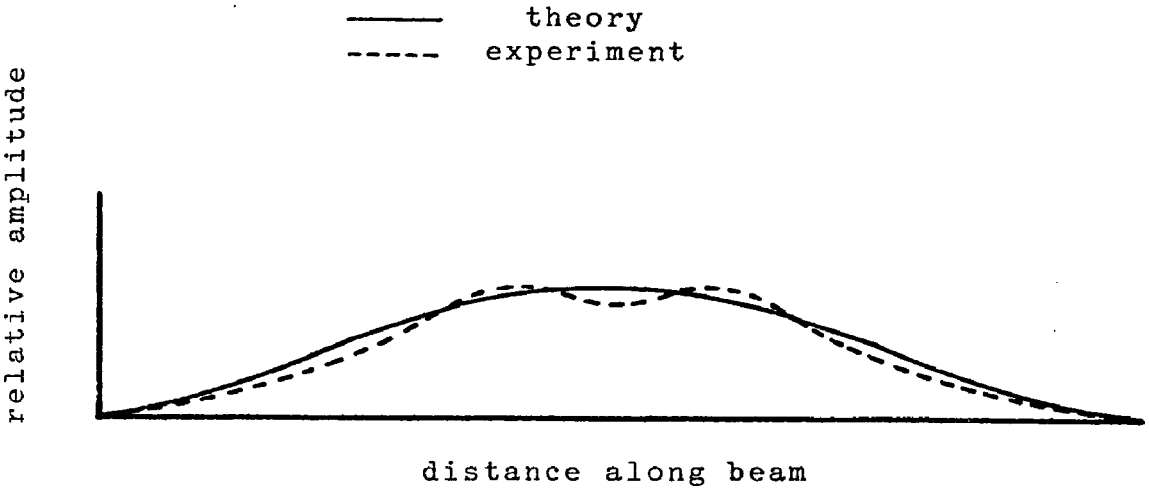


Figure 1.2. Kovac's mode shapes.

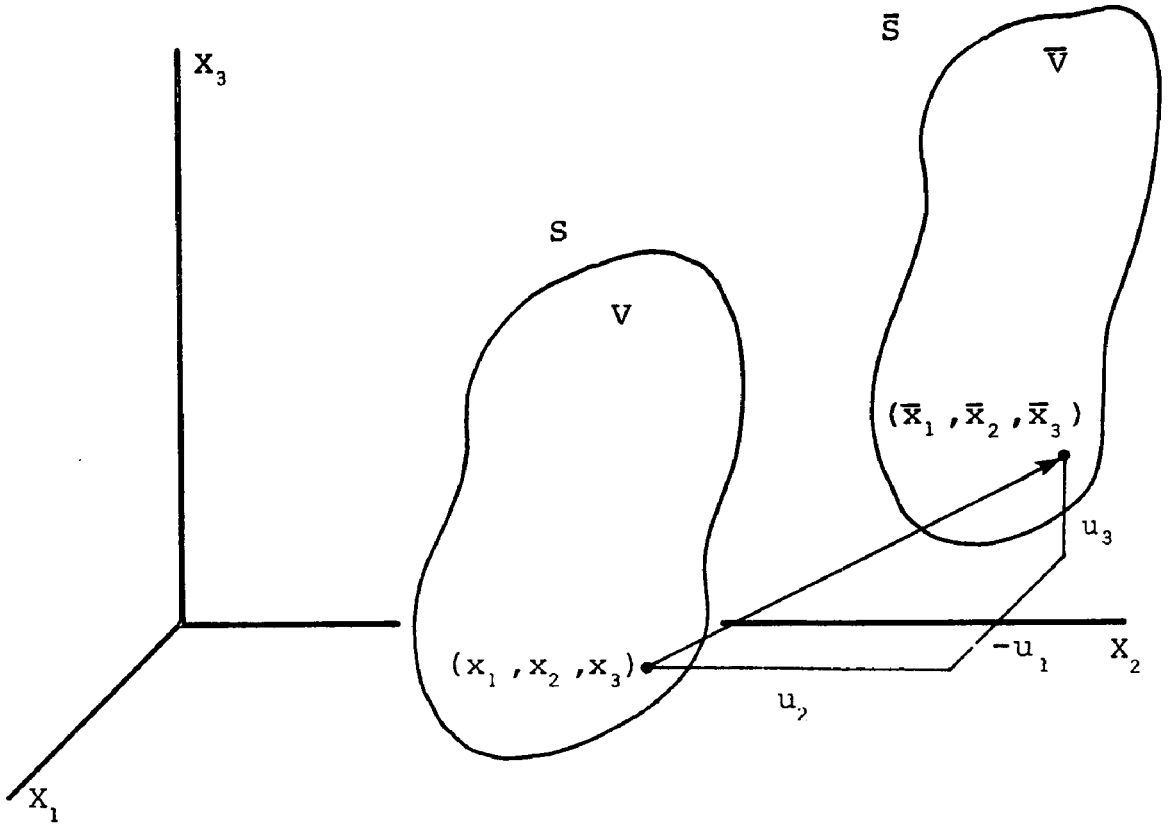


Figure 2.1. Deformation of a body.

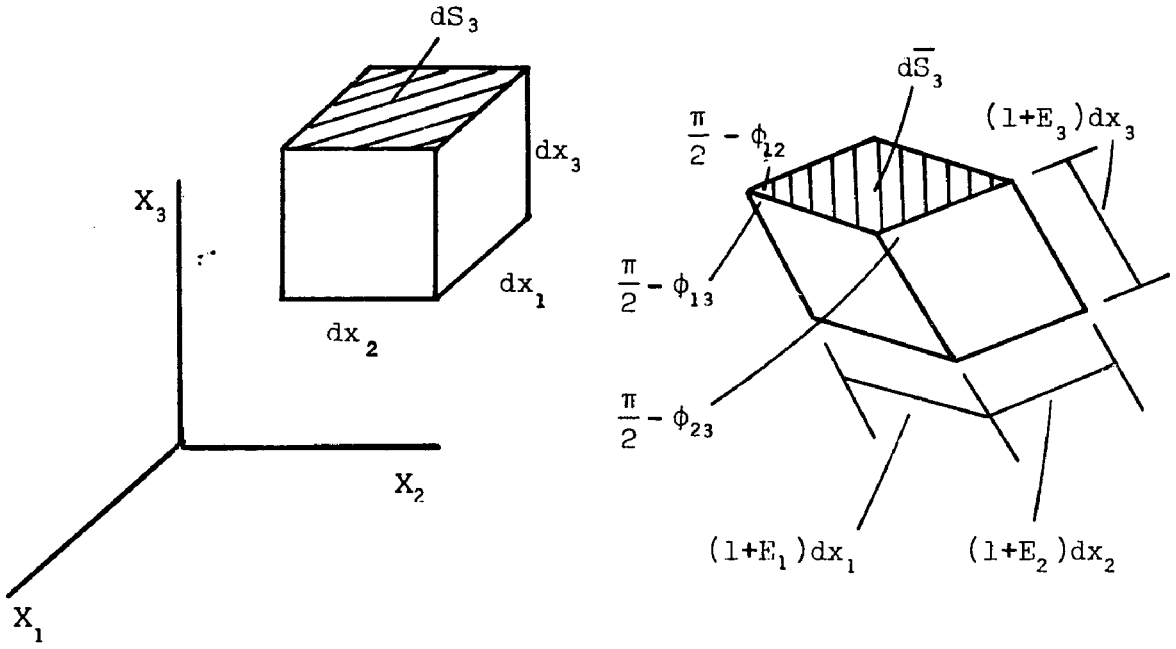


Figure 2.2. Deformation of an infinitesimal cube.

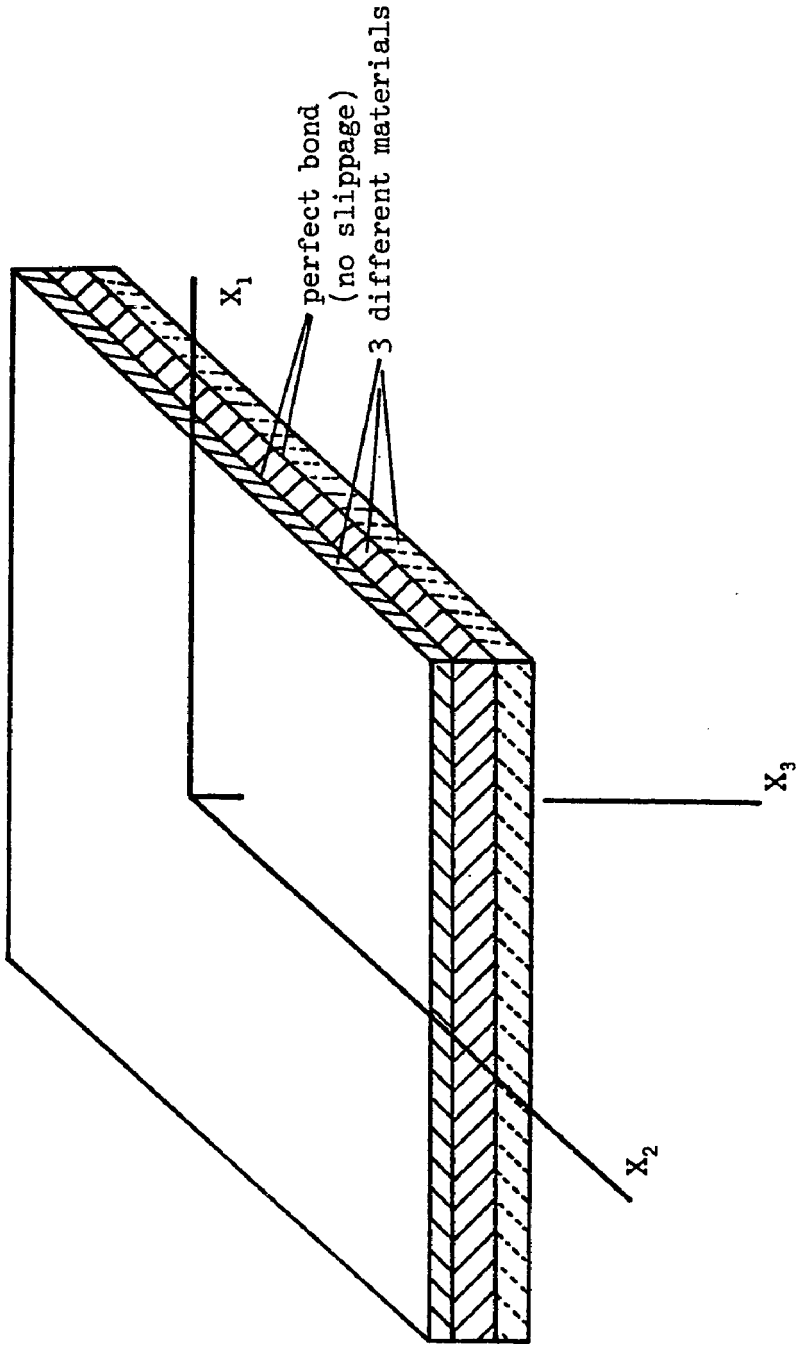
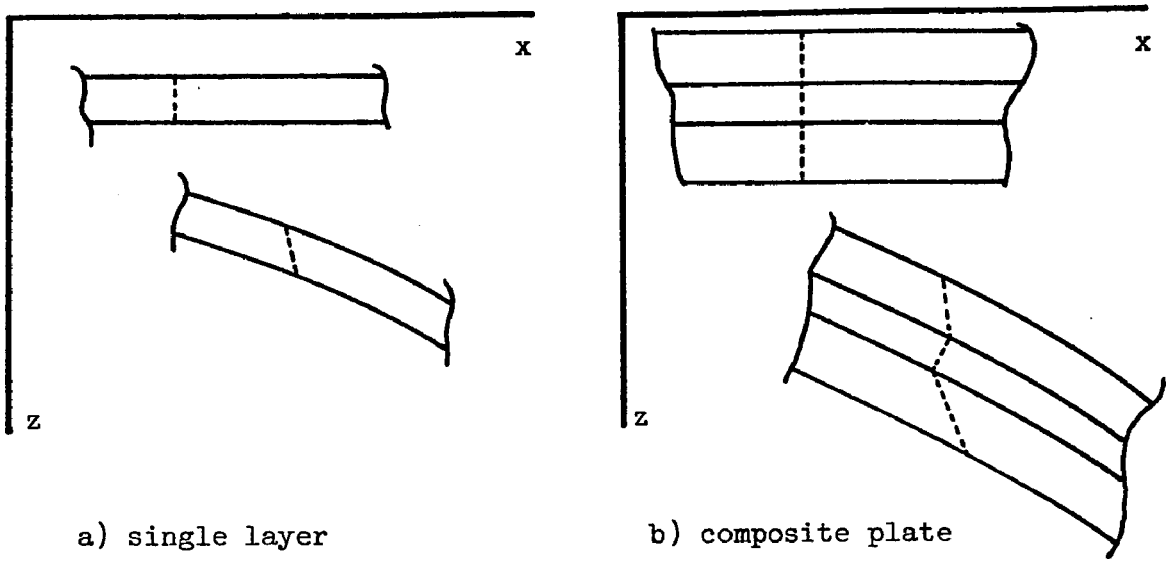


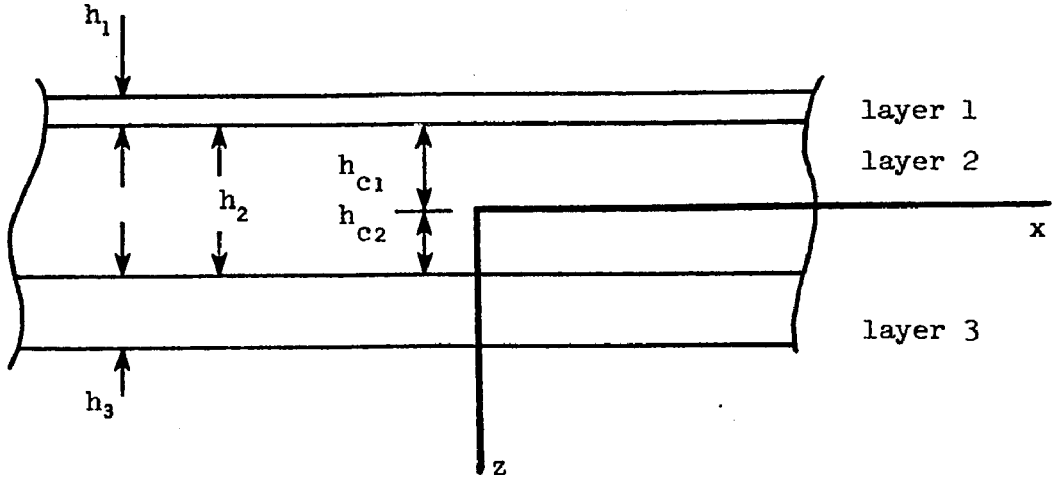
Figure 2.3. Three-layer plate configuration.



a) single layer

b) composite plate

Figure 2.4. Assumed displacement field.



$$z_0 = -(h_{c1}+h_1) \qquad z_1 = h_{c2}$$

$$z_2 = -h_2 \qquad z_3 = h_{c2}+h_3$$

Figure 2.5. Beam geometry.

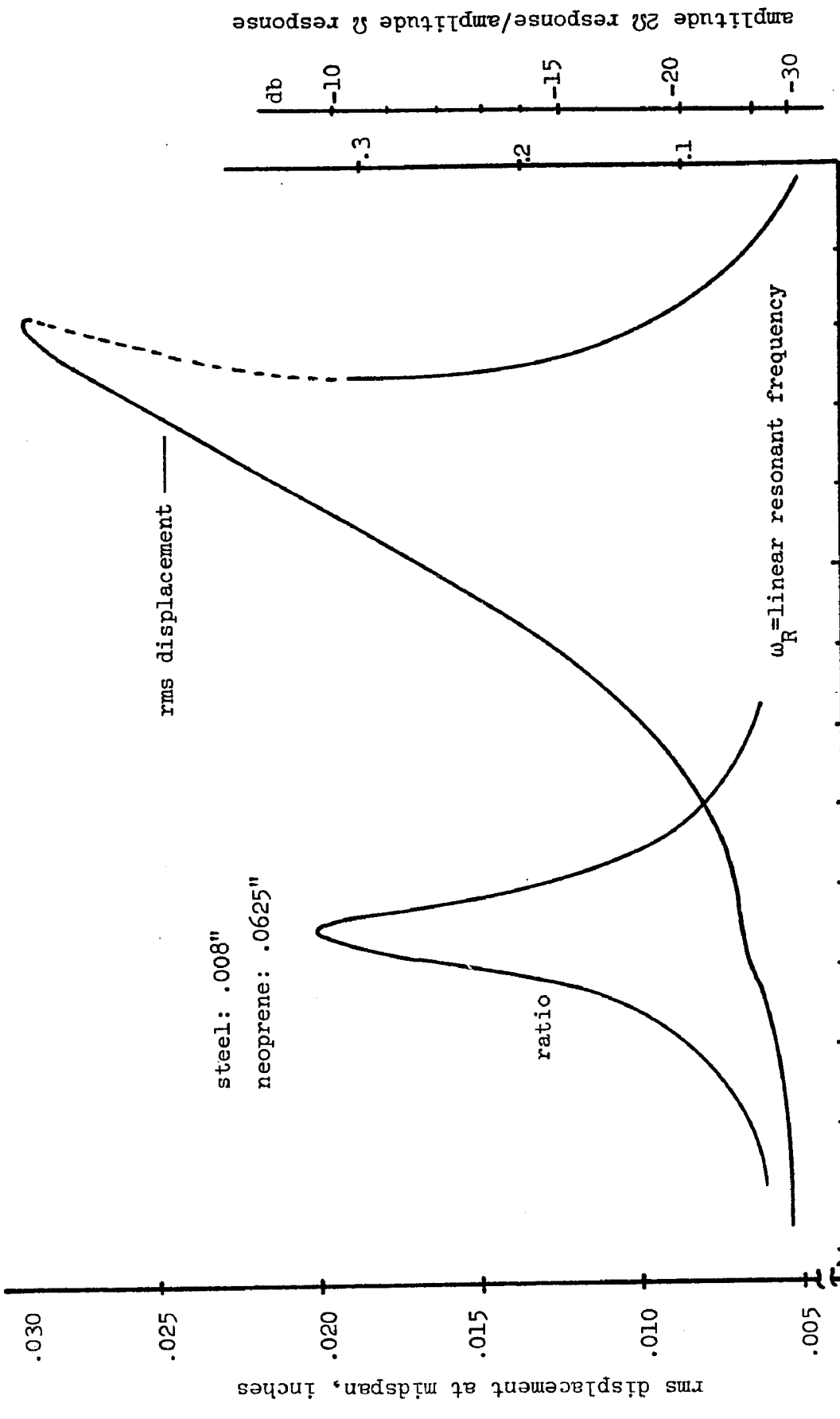


Figure 3.1. Response of symmetric 3-layer beam.

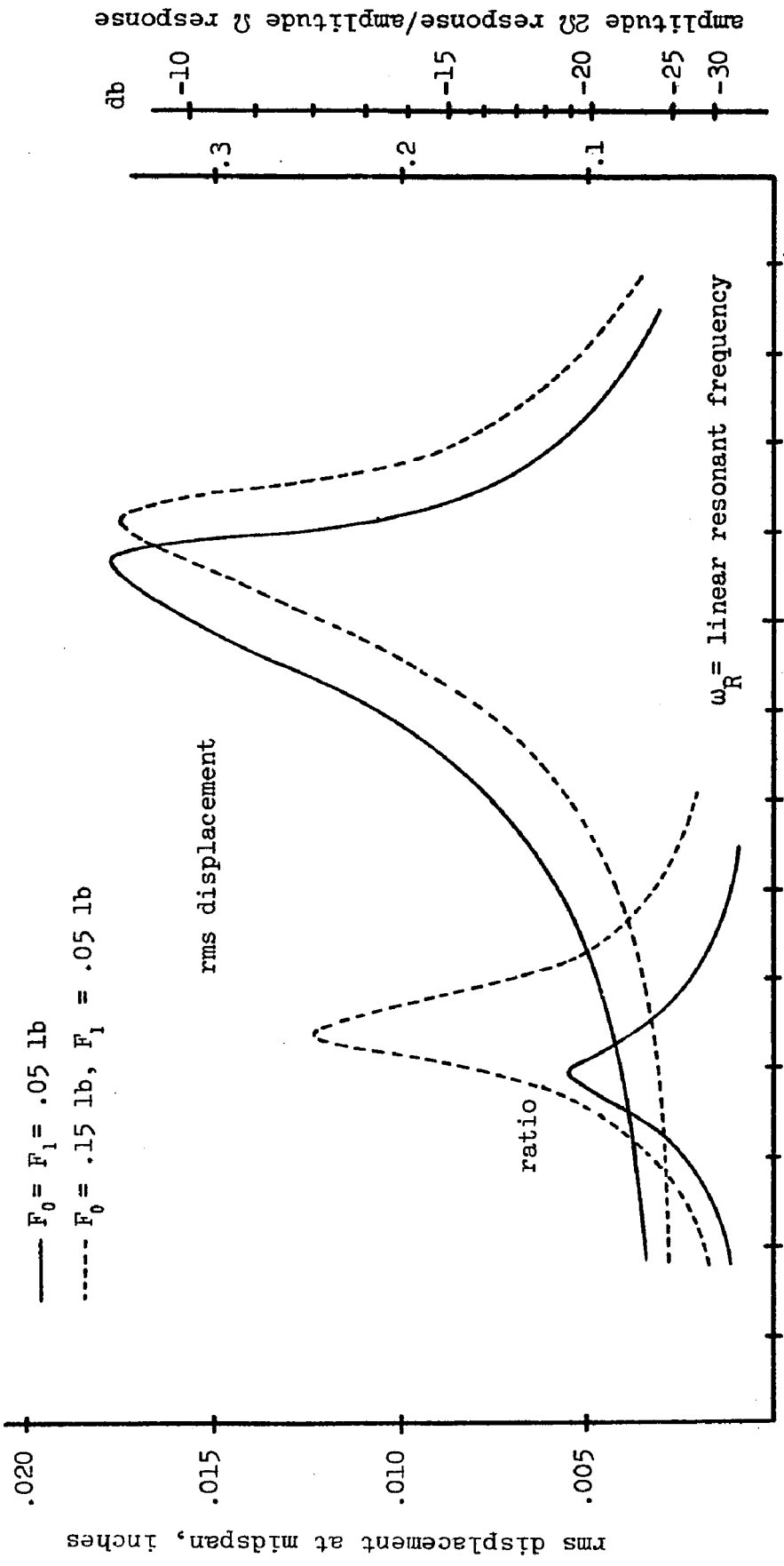


Figure 3.2. Response of unsymmetric 3-layer beam - 2 values of bias force.

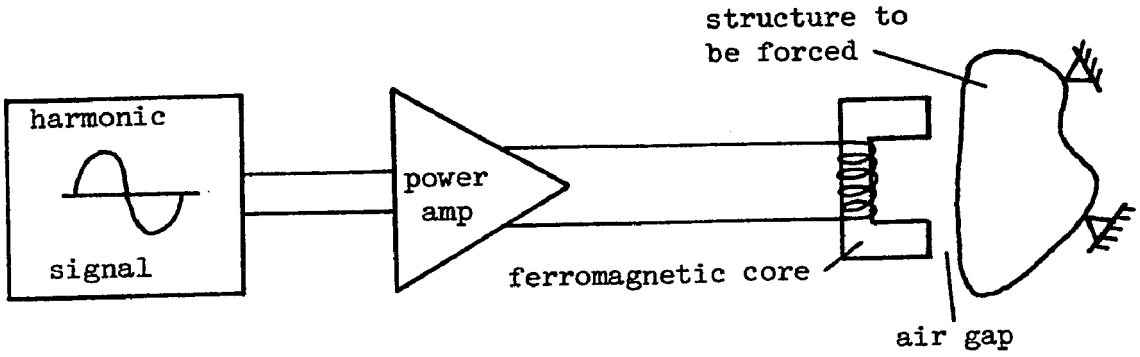


Figure 4.1. Standard set up.

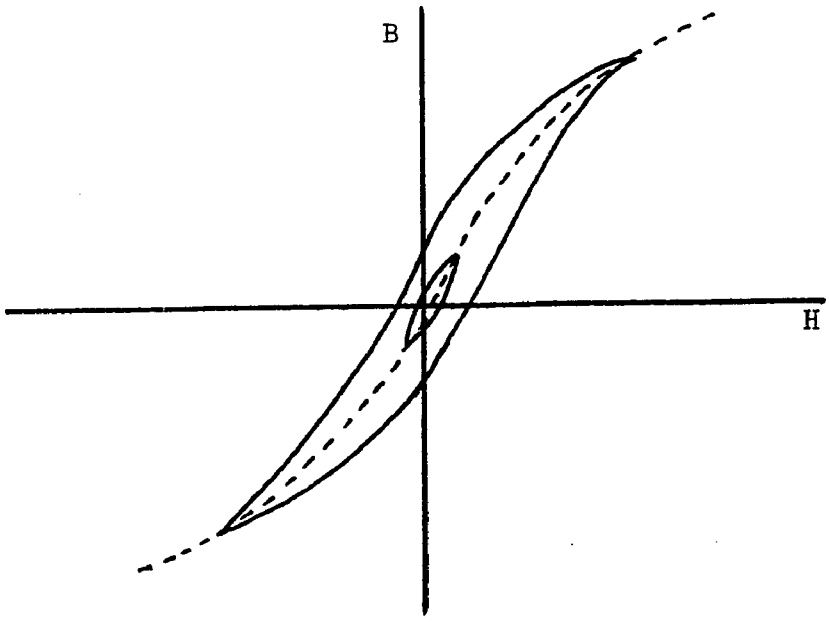


Figure 4.2. Typical B vs. H relation.

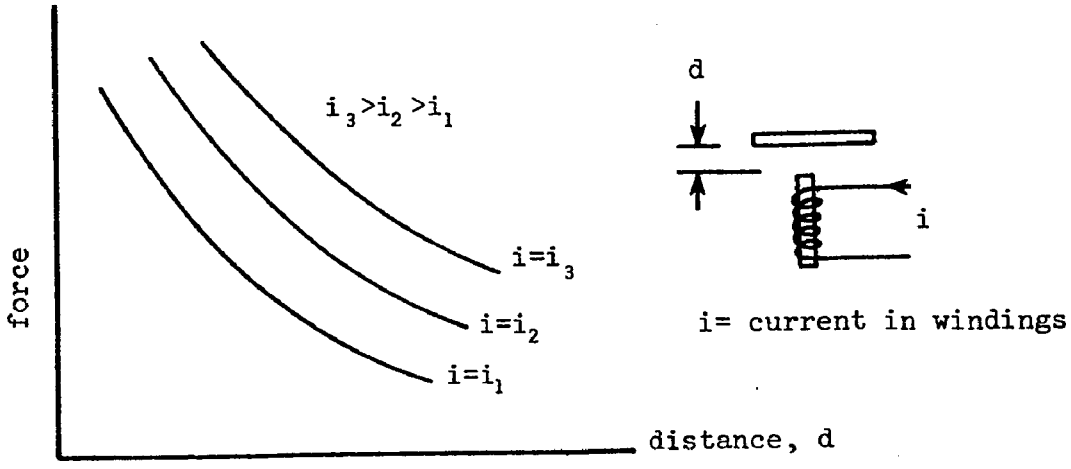
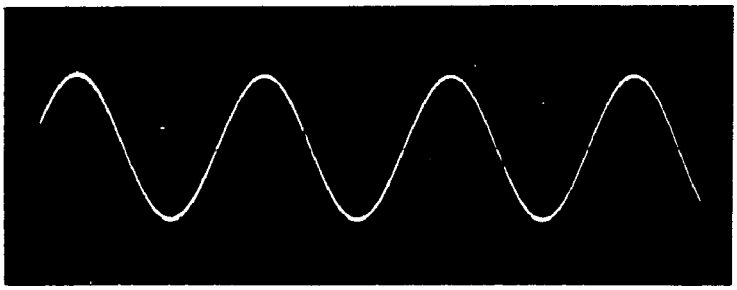


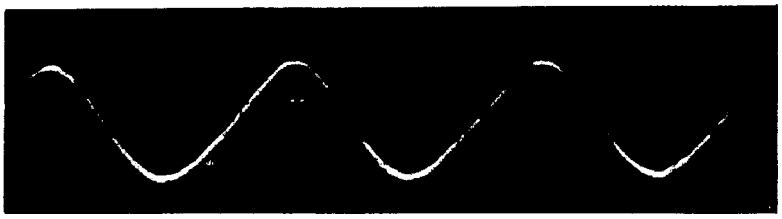
Figure 4.3. Variation of force with distance.



a) Kung's



true sinusoid



b) Bennett's

Figure 4.4. Force time histories of recent investigators.

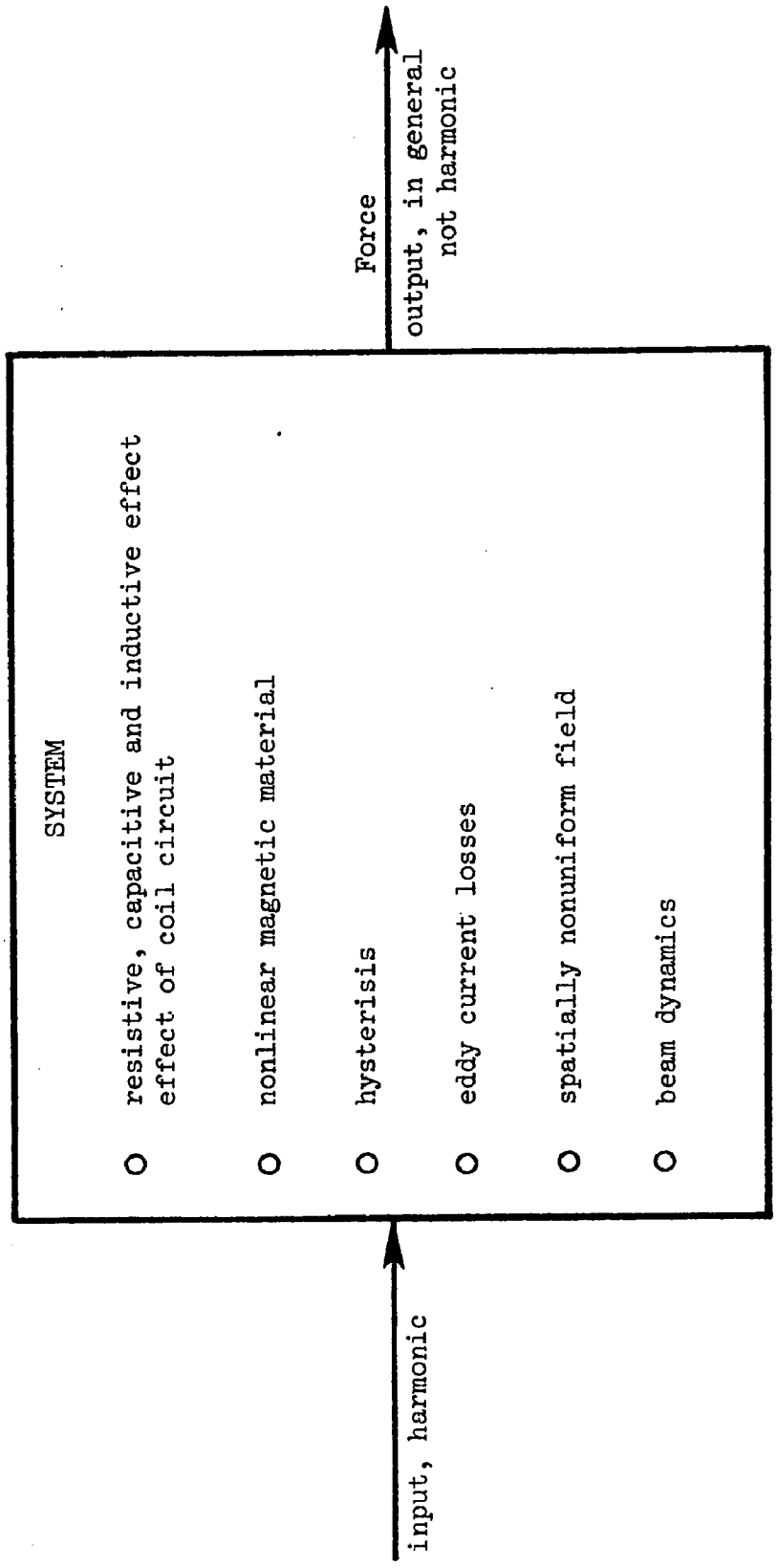


Figure 4.5. Problem summary.

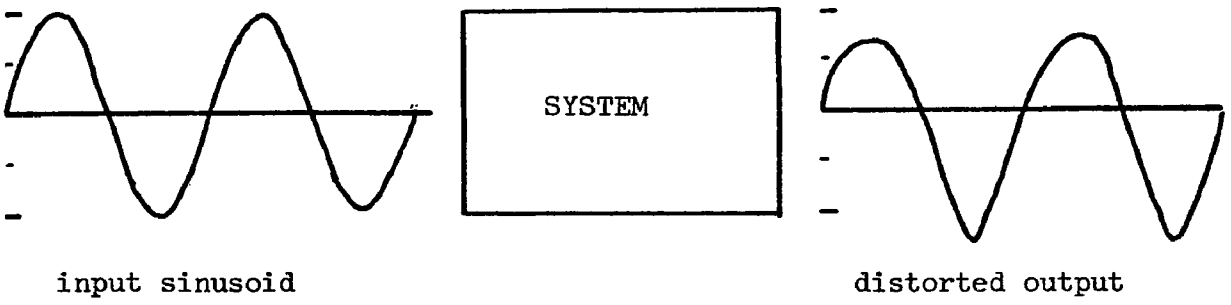


Figure 4.6. Distortion caused by system.

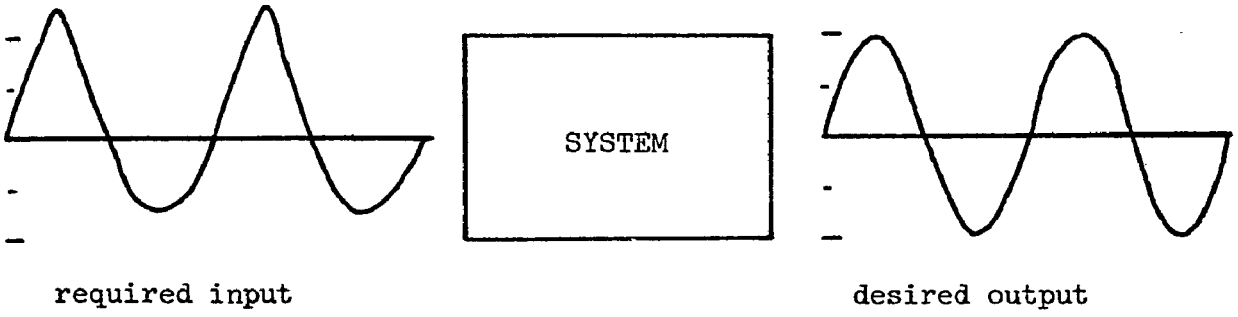


Figure 4.7. Input needed for desired output.

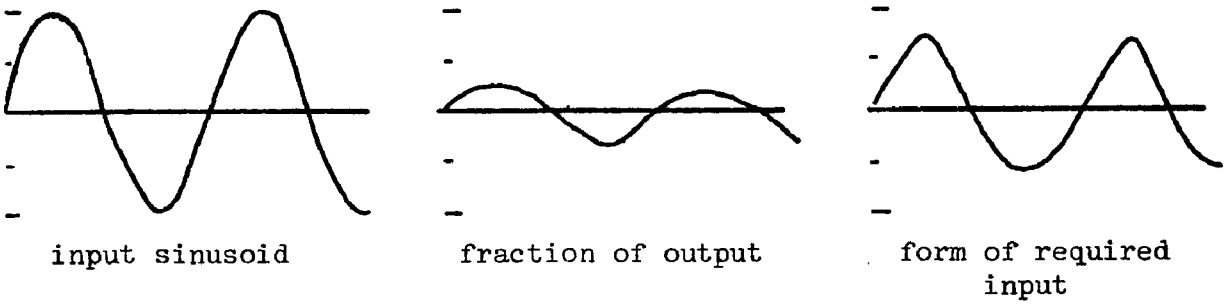


Figure 4.8. Use of output to get required input.

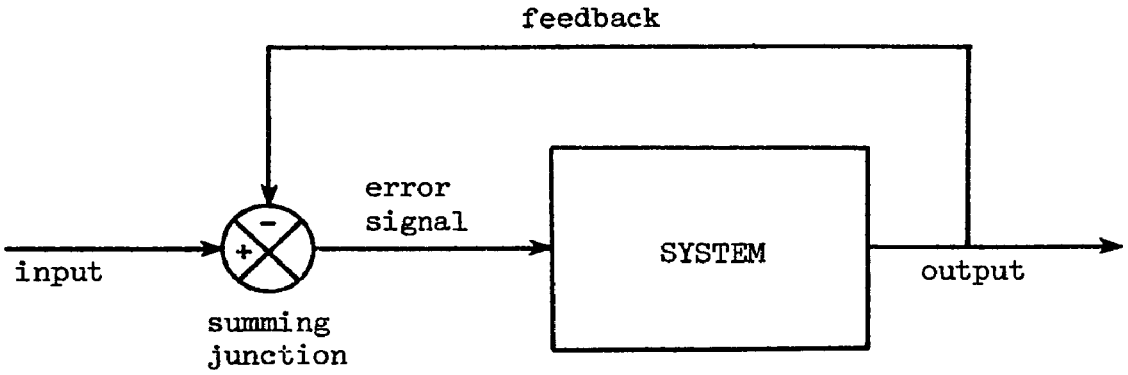


Figure 4.9. Simple feedback system.

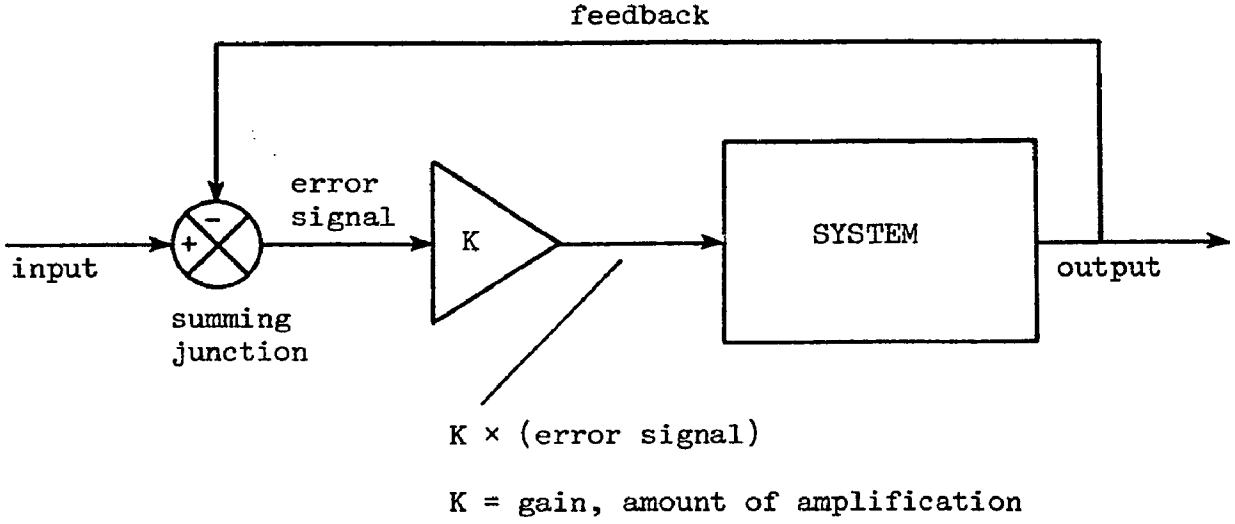


Figure 4.10. Amplifier in a feedback system.

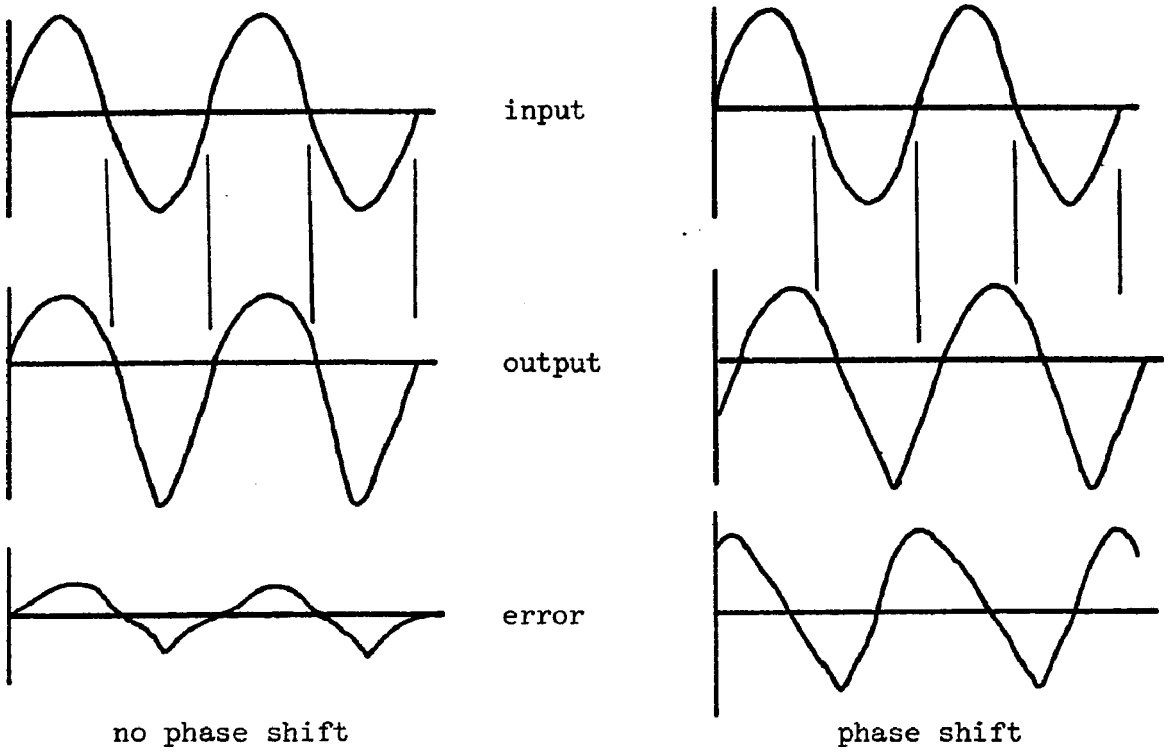


Figure 4.11. Effect of phase distortion on error.

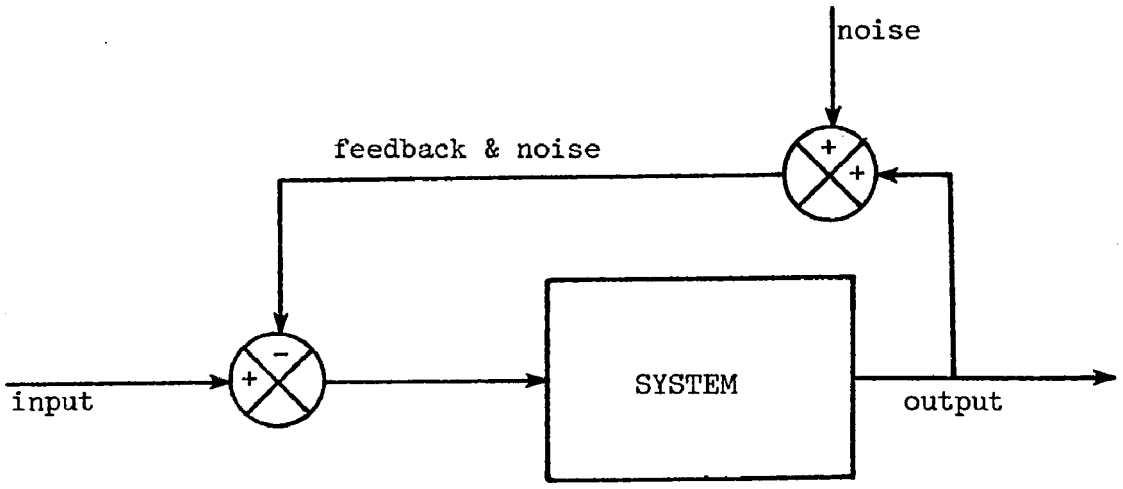


Figure 4.12. Noise entering feedback loop.

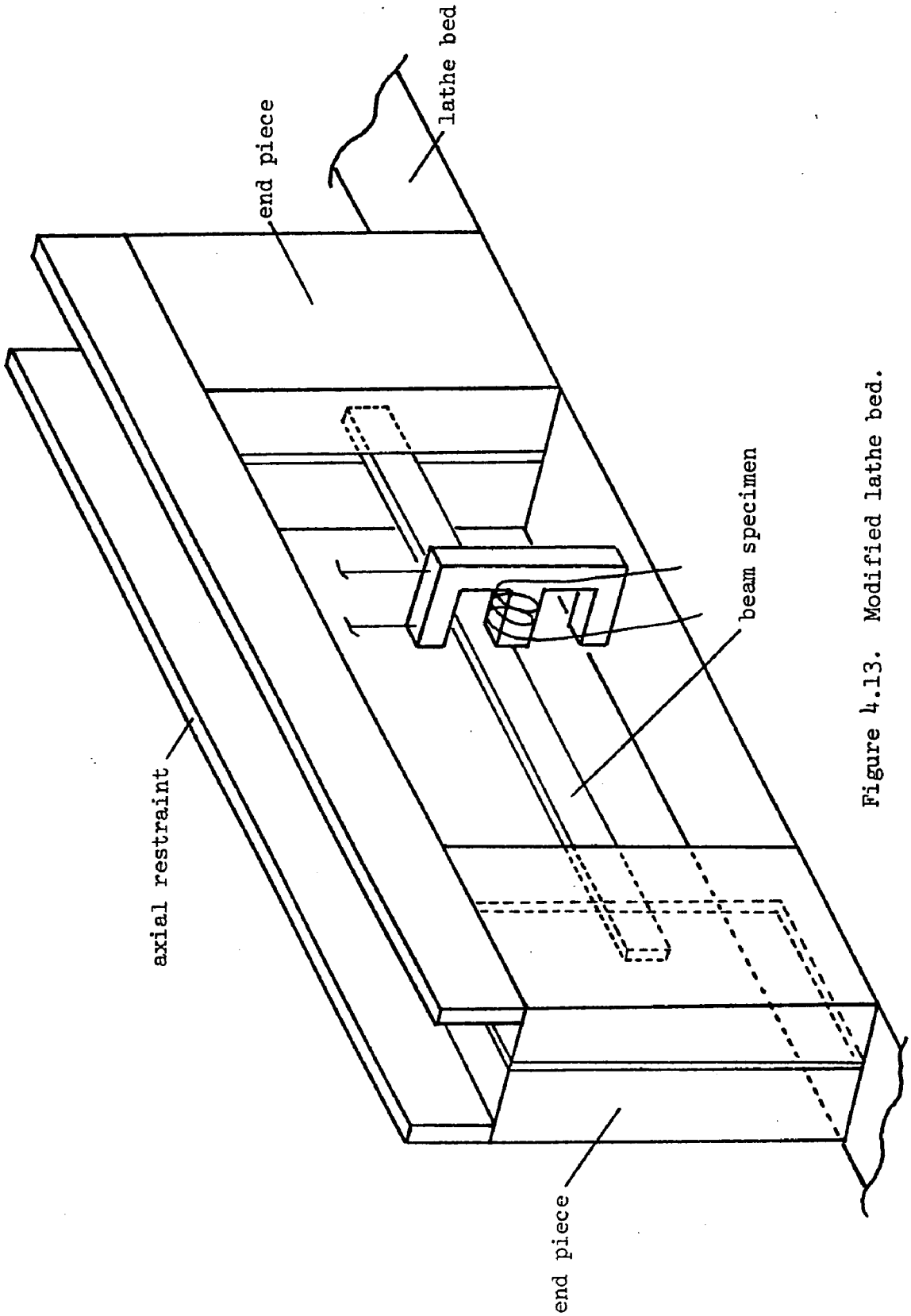


Figure 4.13. Modified lathe bed.

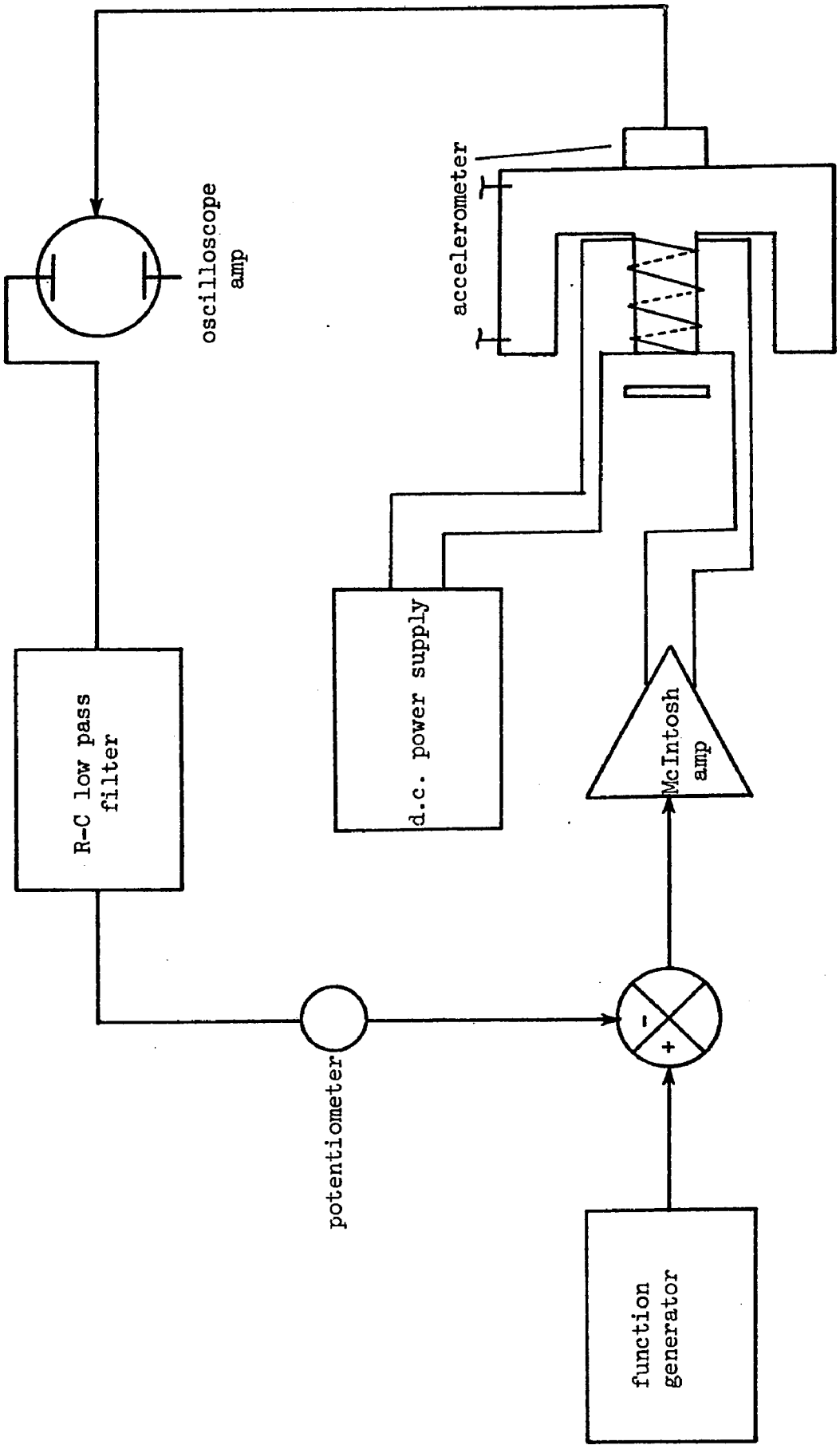


Figure 4.14. Feedback system using free floating magnet.

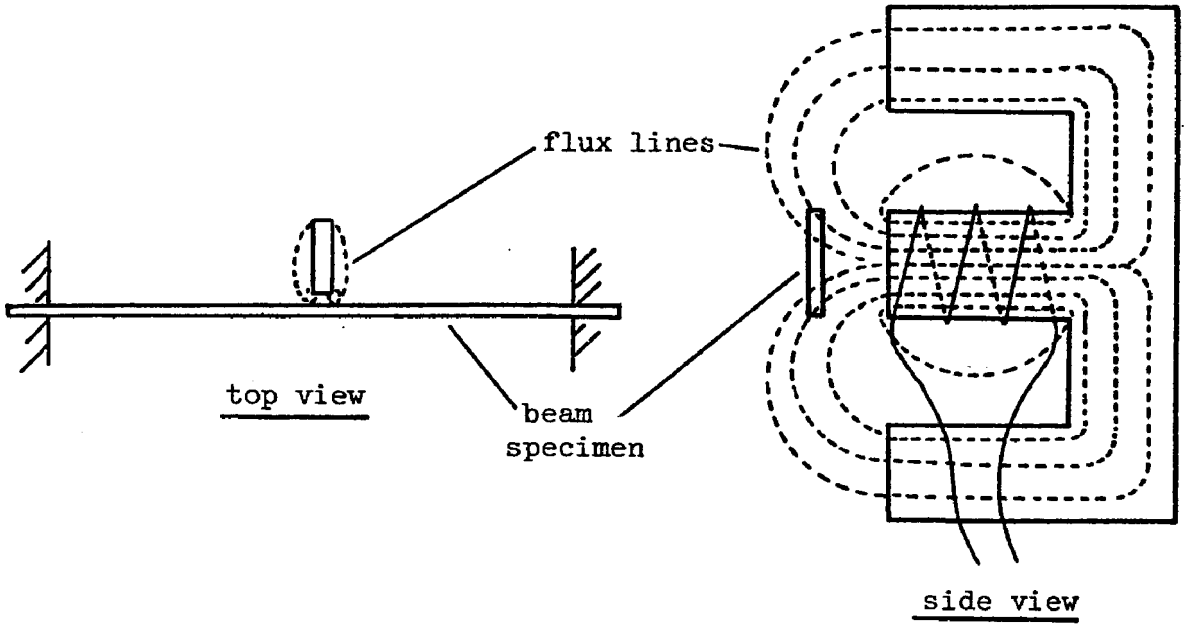


Figure 4.15. Fringing of 'E' magnet.

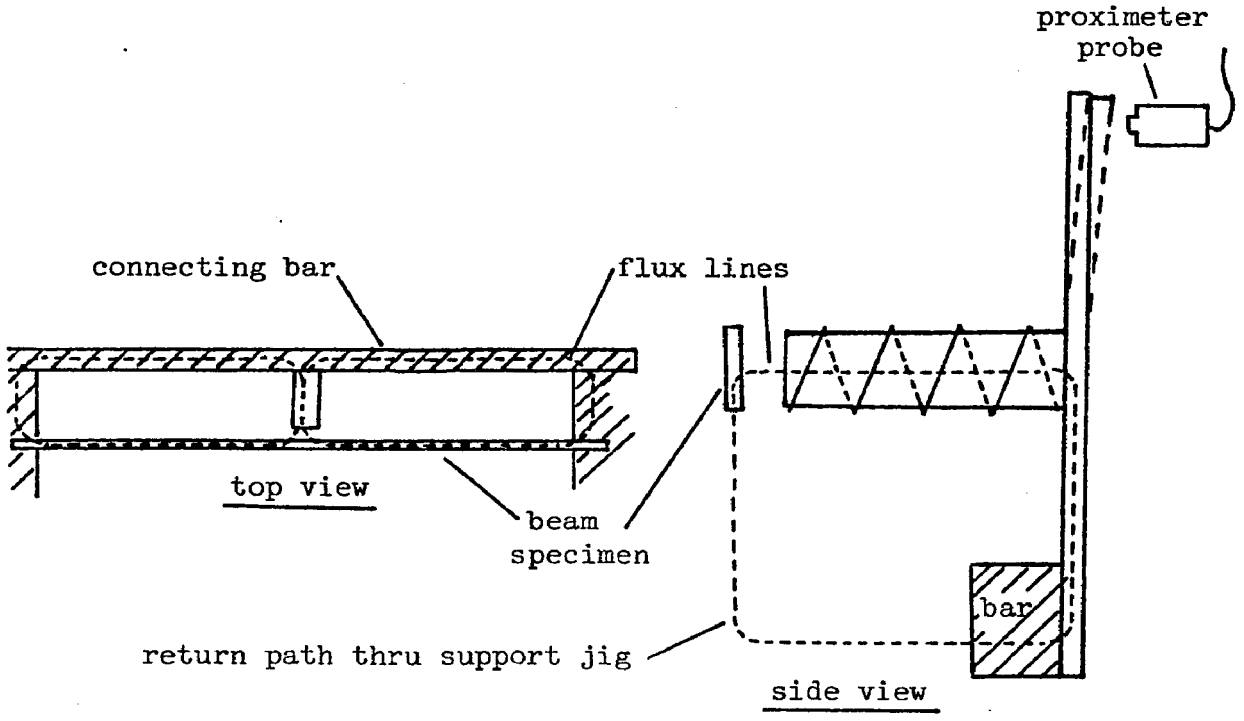


Figure 4.16. Fringing with beam in magnetic circuit.

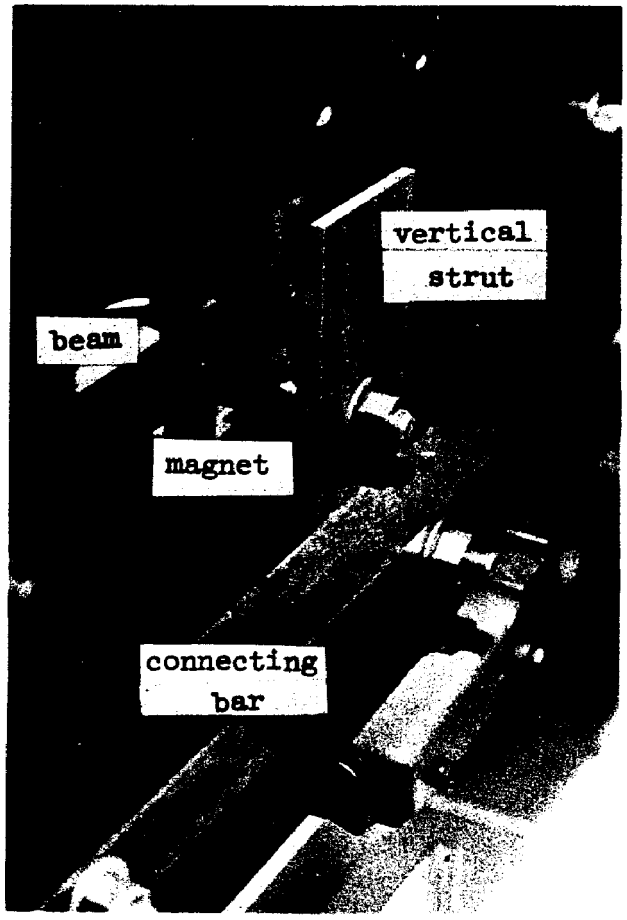


Figure 4.17. Fixed magnet and magnetic circuit

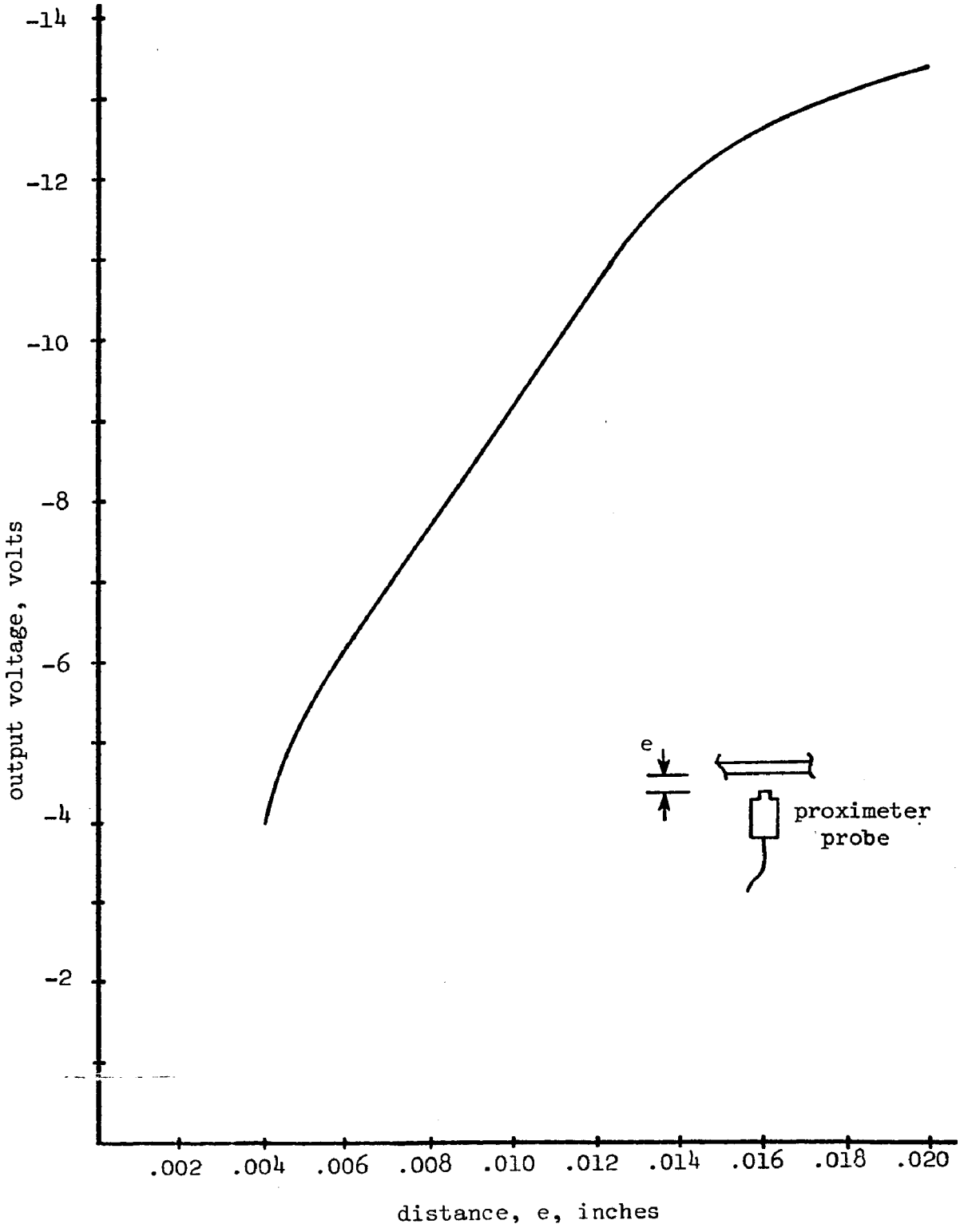


Figure 4.18. Bentley-Nevada Model 316 proximeter calibration

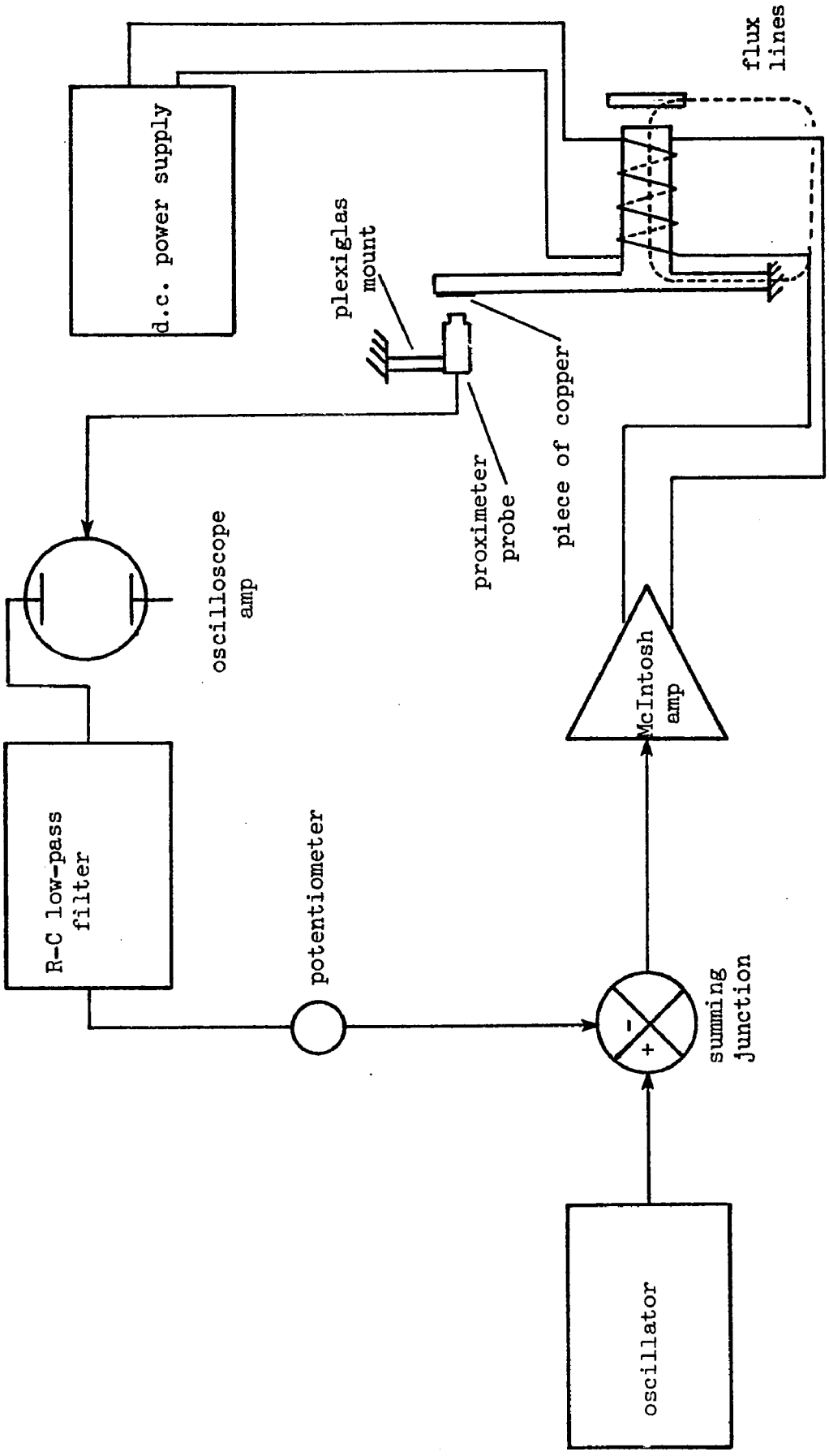


Figure 4.19. Feedback system using fixed magnet and magnetic circuit.

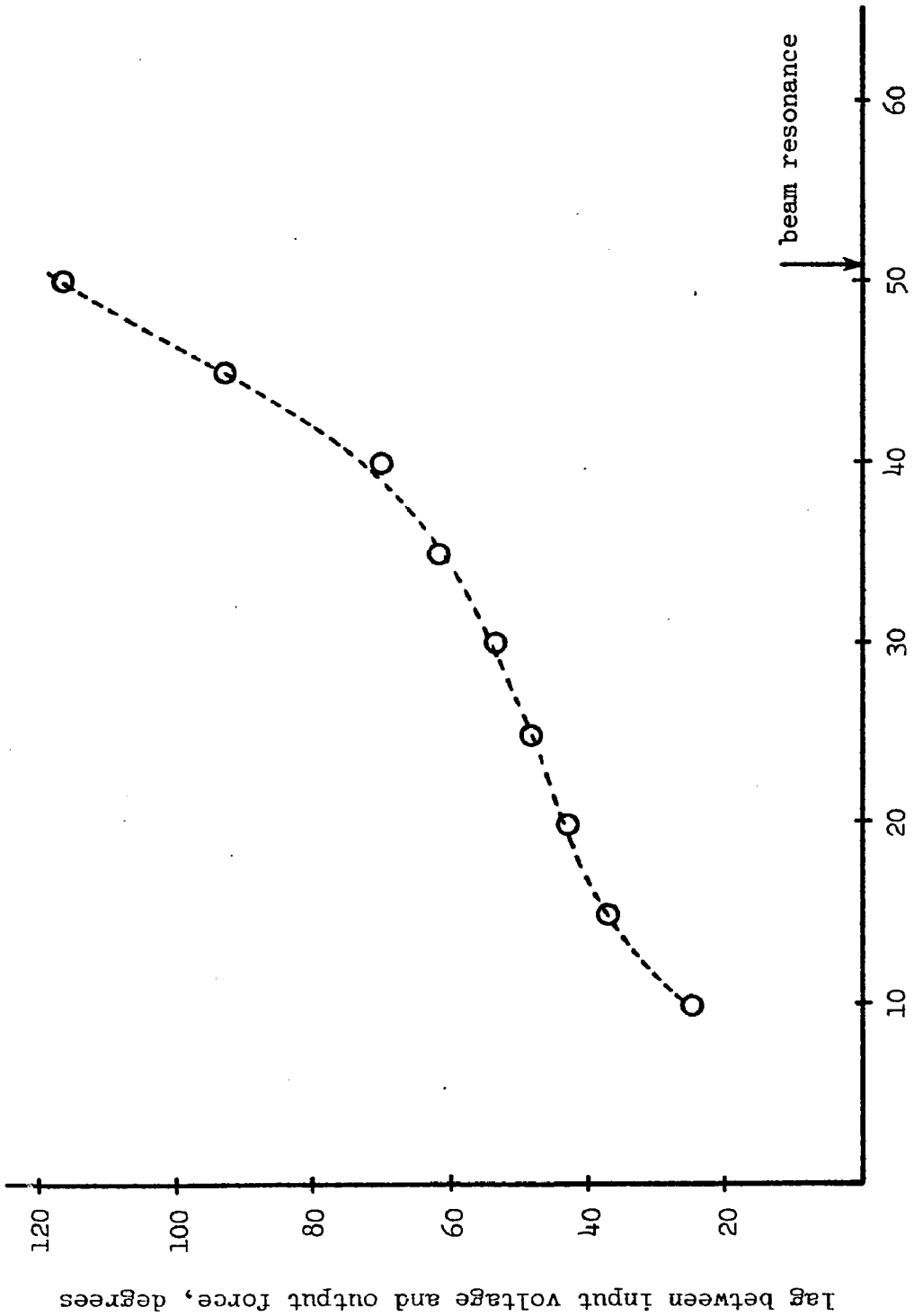


Figure 4.20. Open loop phase response of magnetic circuit system.

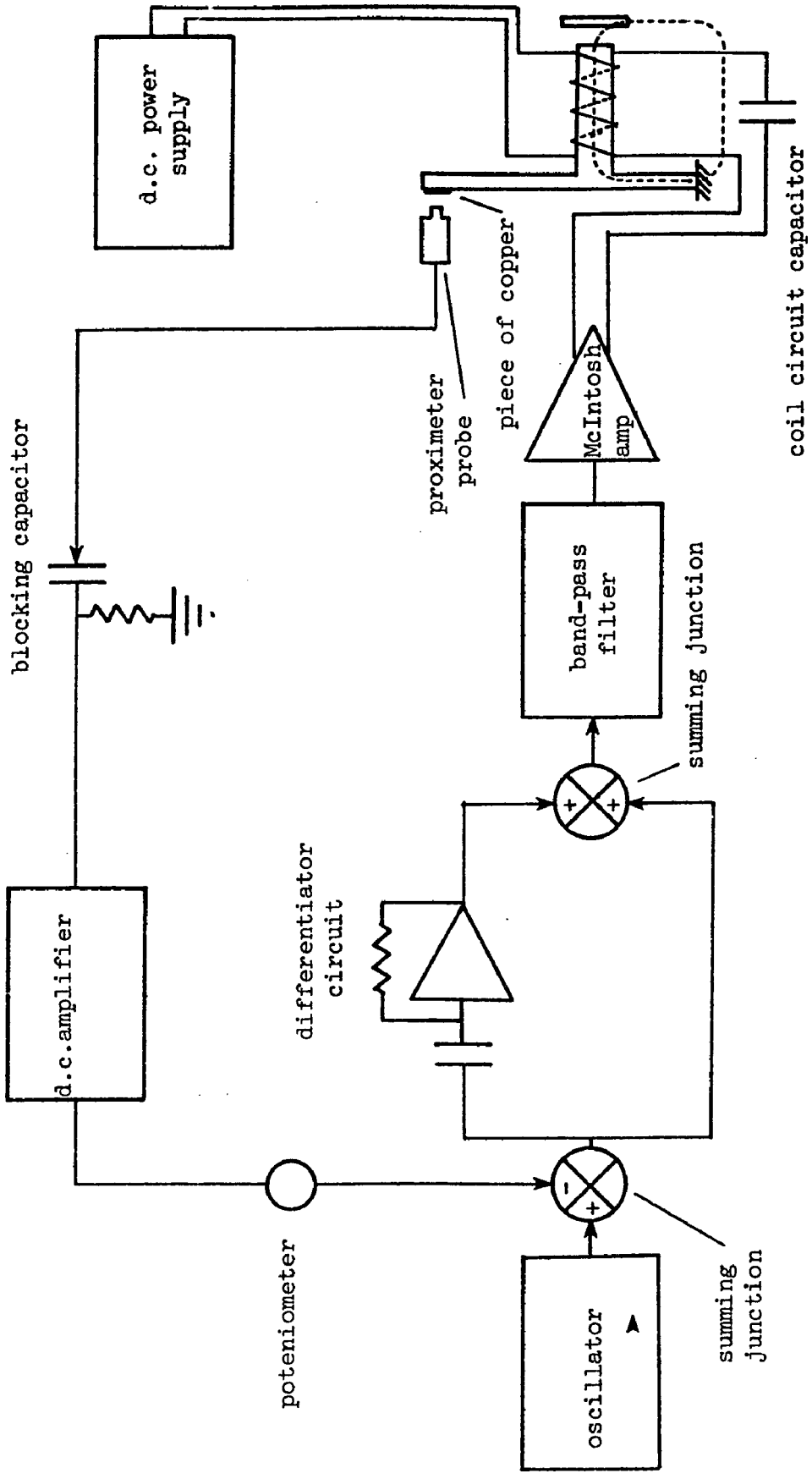


Figure 4.21. Differentiator in magnetic circuit system.

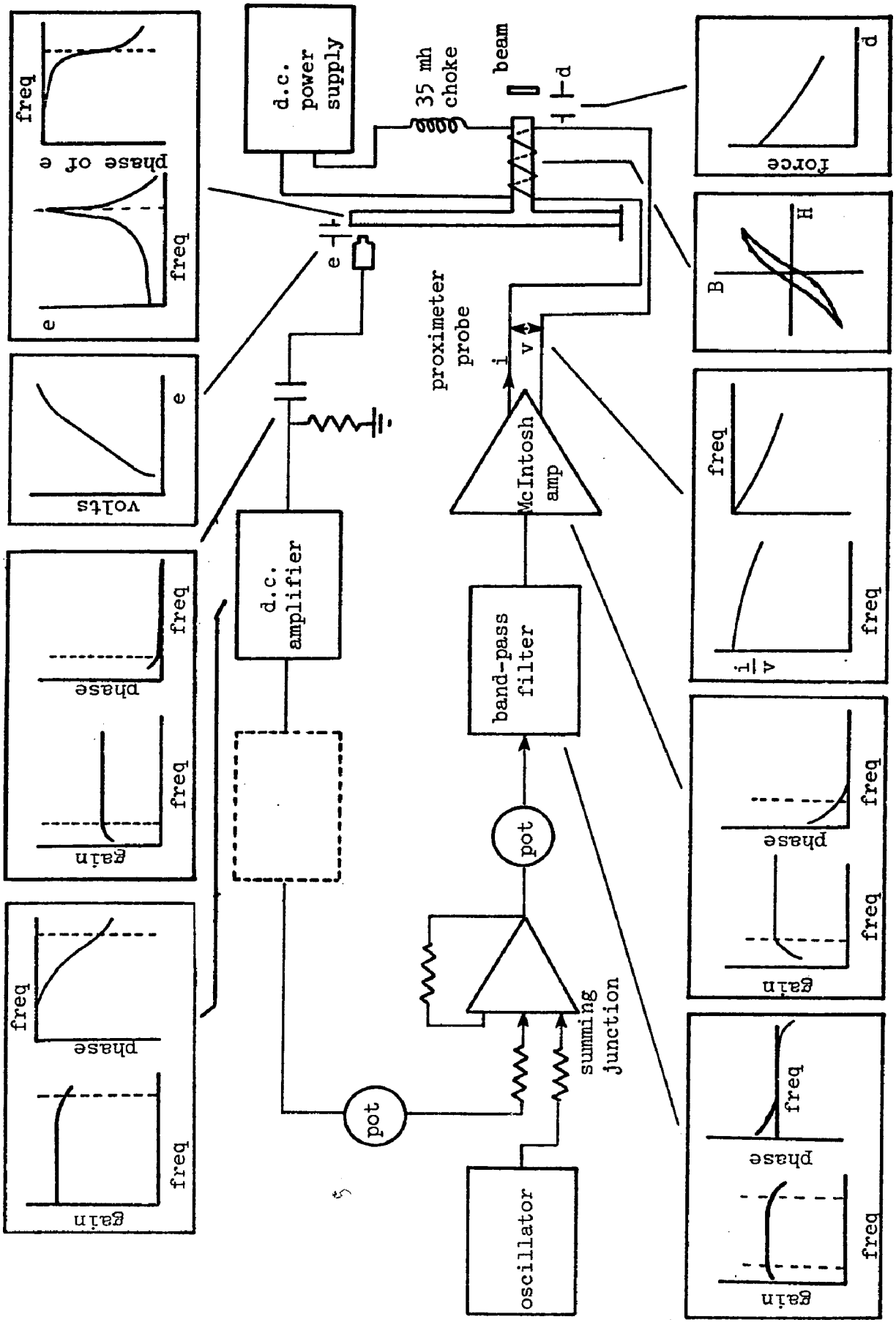


Figure 4.22. System and element characteristics - elimination of magnetic circuit.

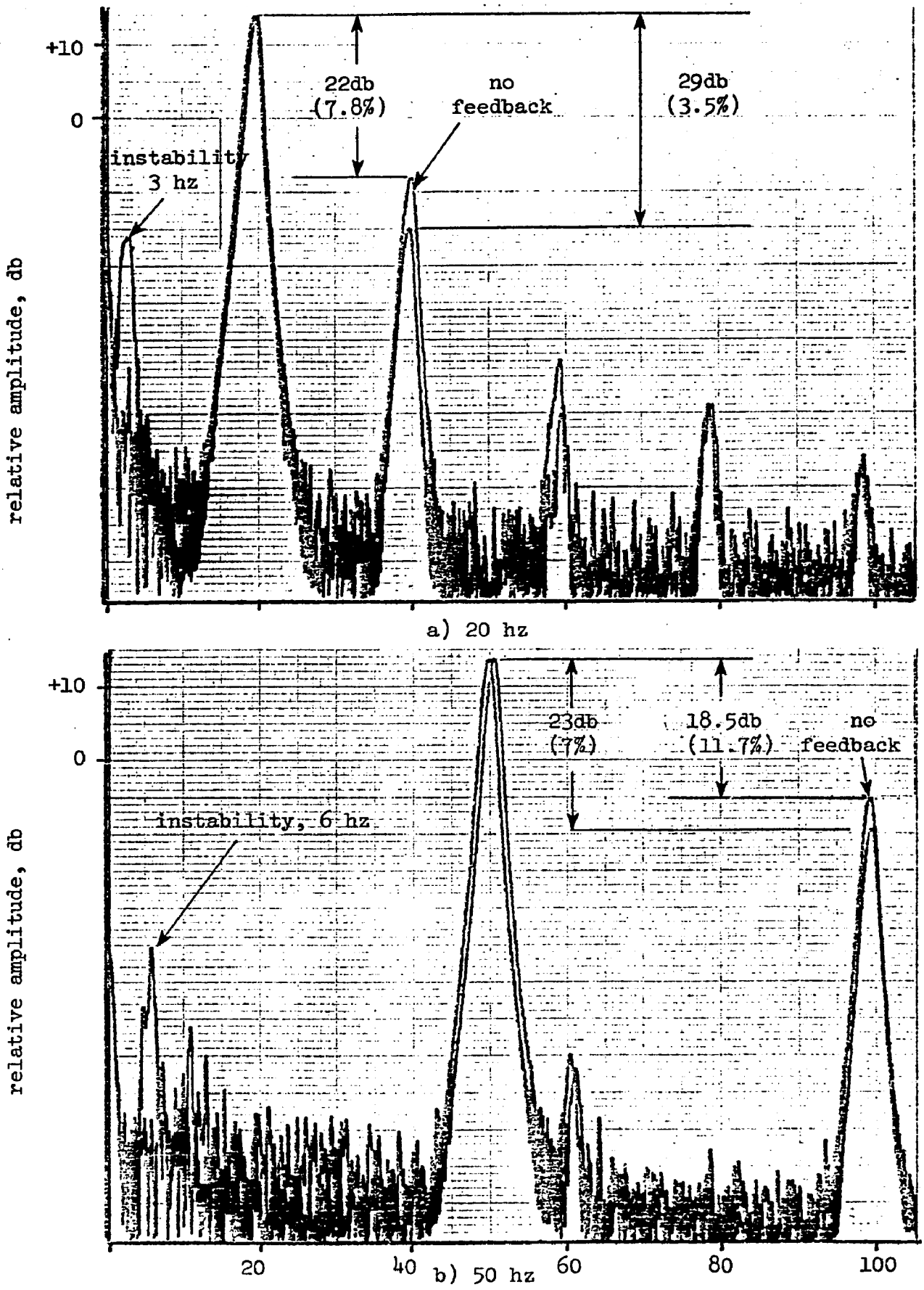


Figure 4.23. Force spectrum

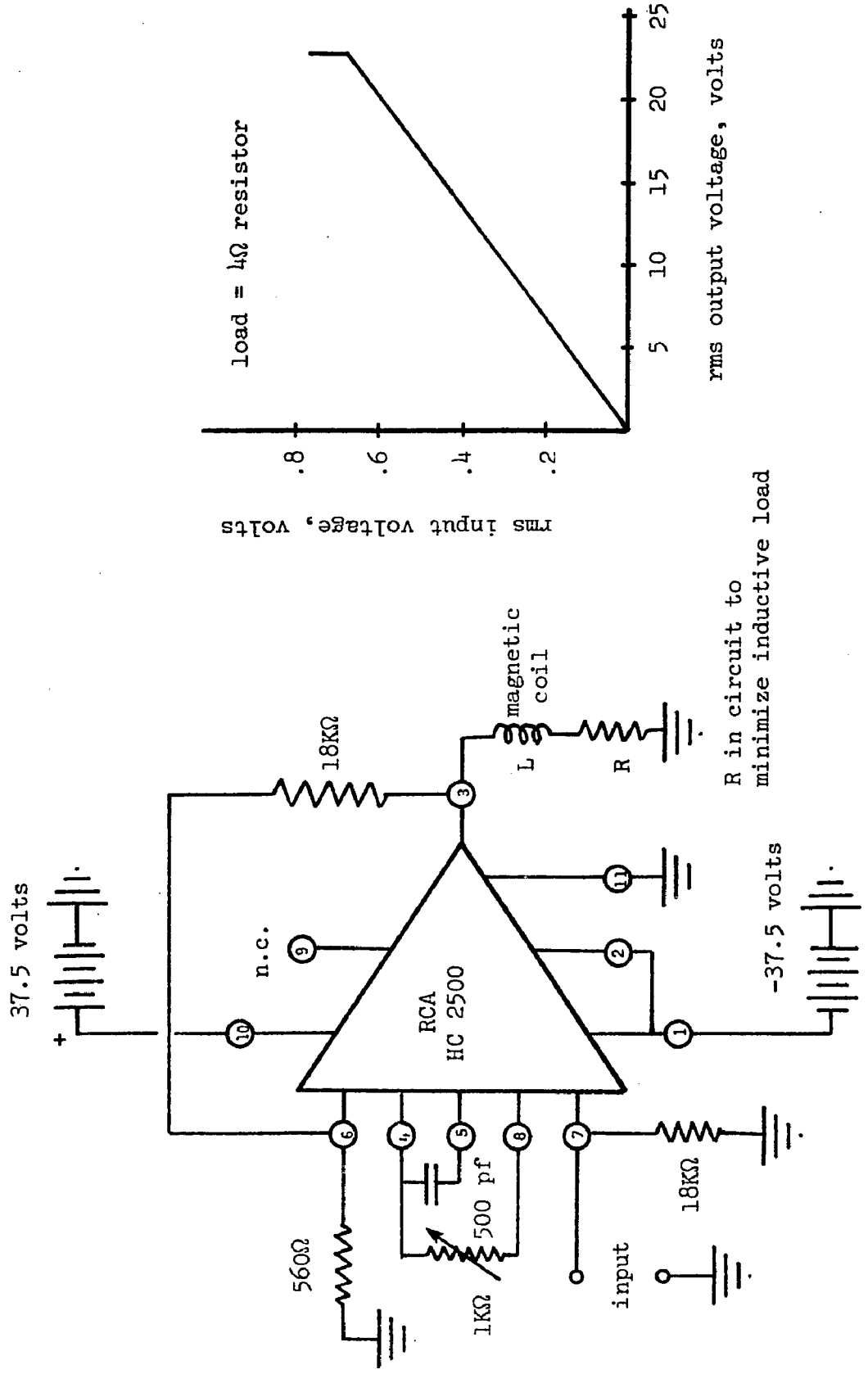


Figure 4.24. Amplifier circuit diagram and input-output characteristics.

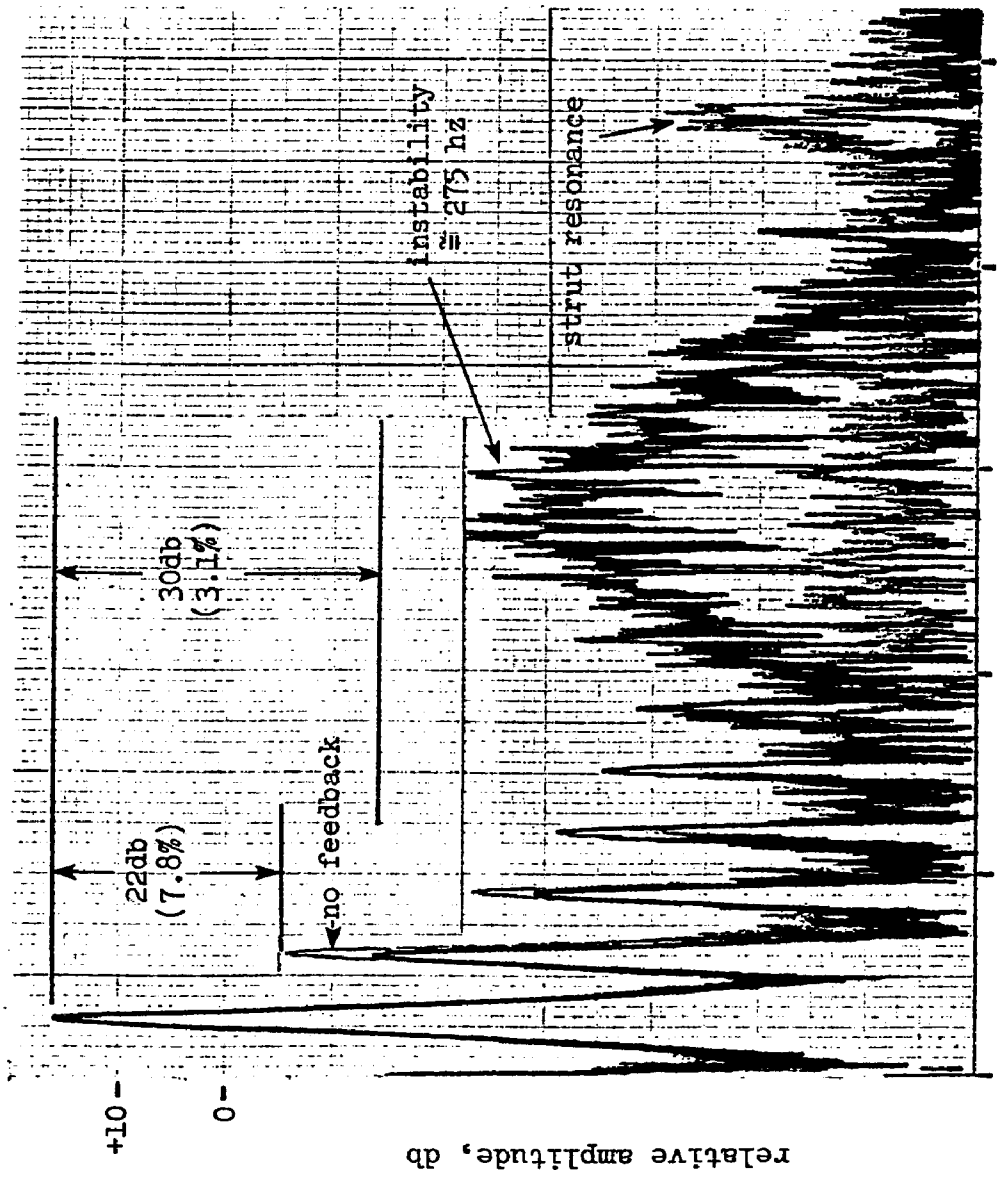


Figure 4.25. 30 hz forcing spectrum.

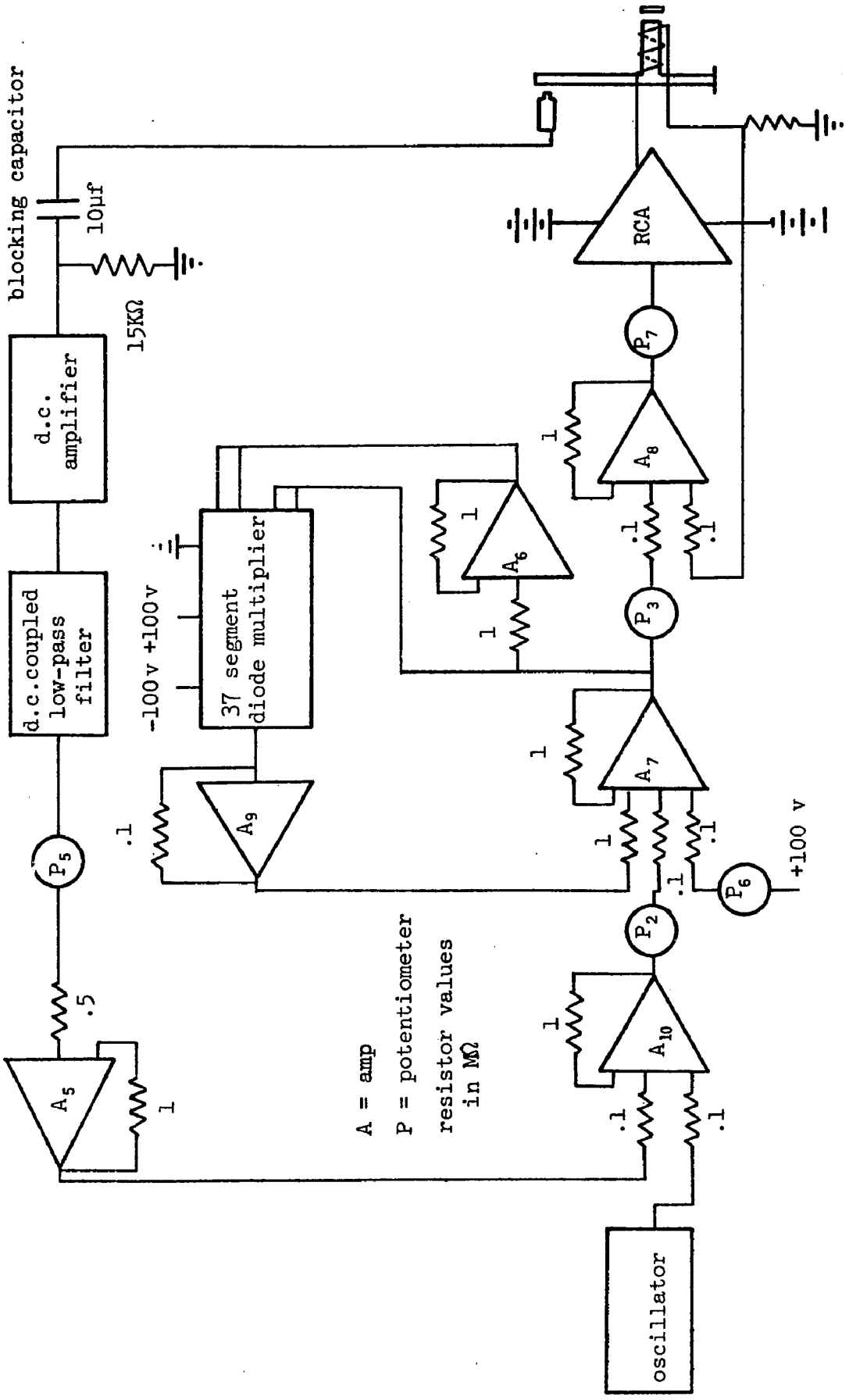


Figure 4.26. Final configuration of feedback system.

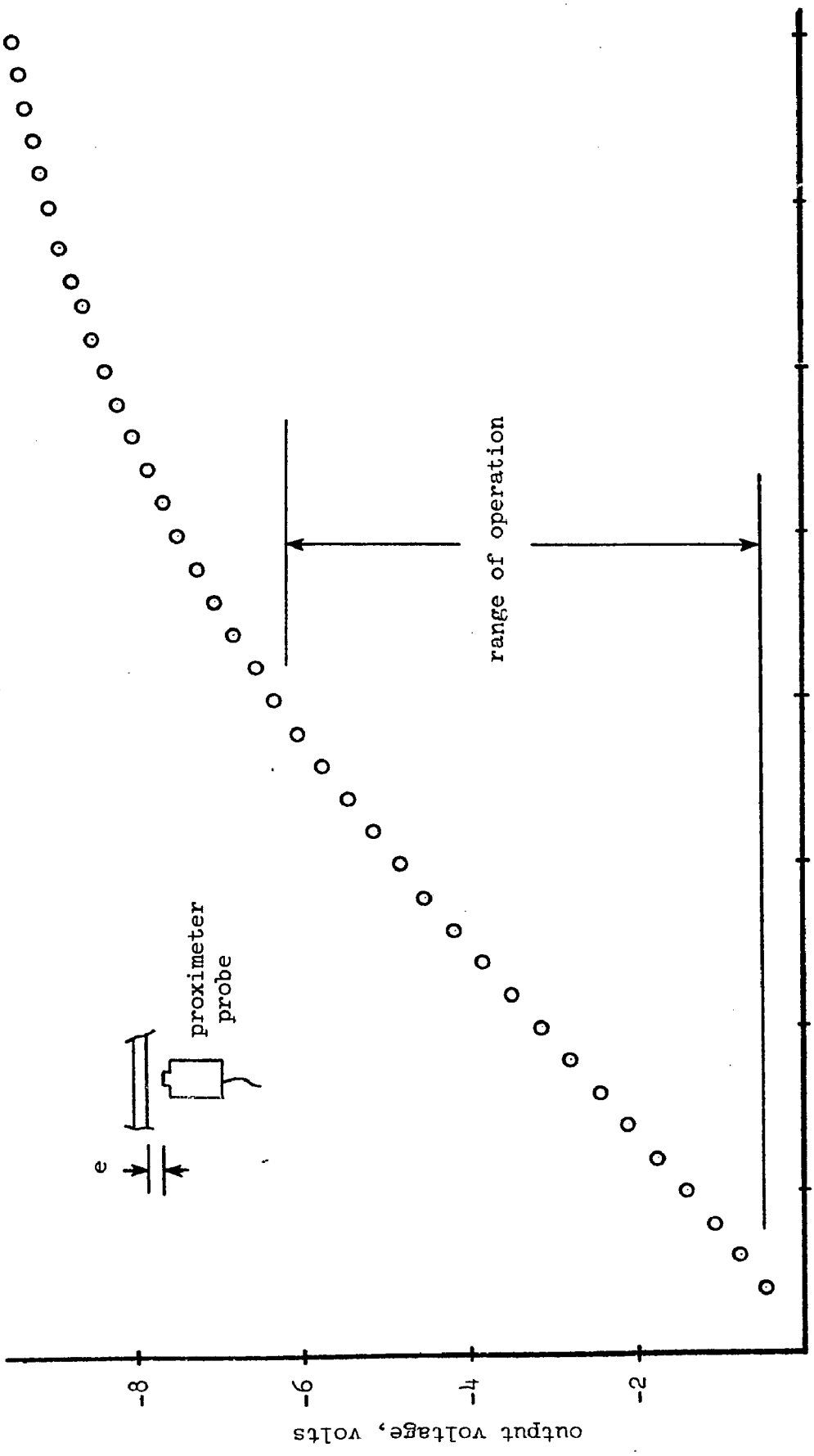


Figure 5.1. Beam displacement proximeter calibration, Model 308 Bentley-Nevada.

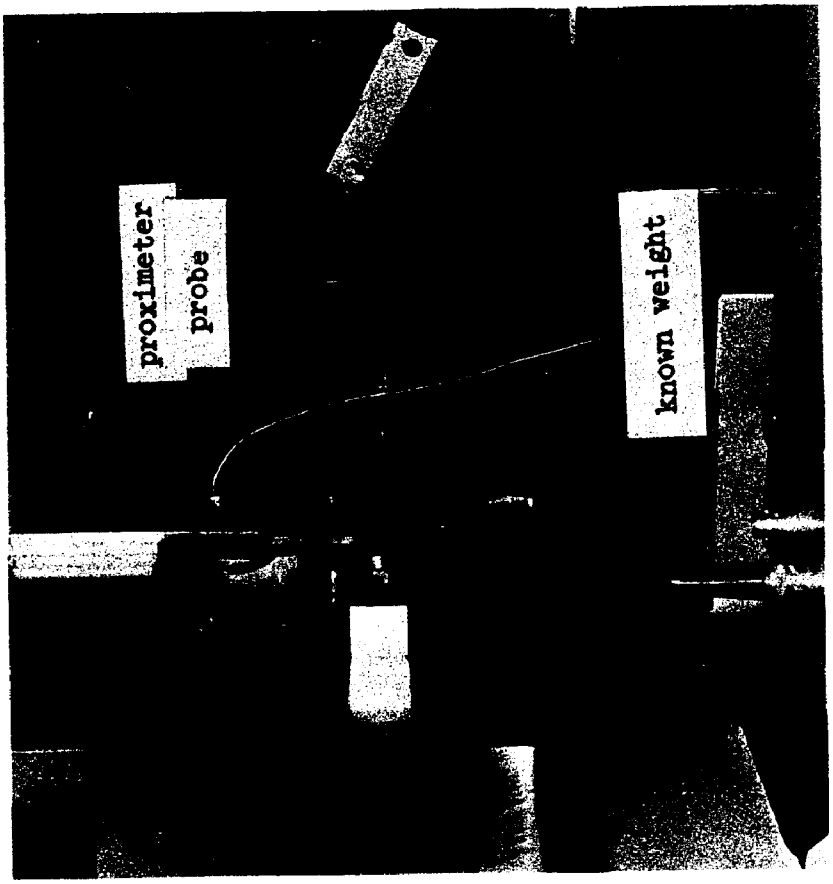


Figure 5.2. Force calibration procedure

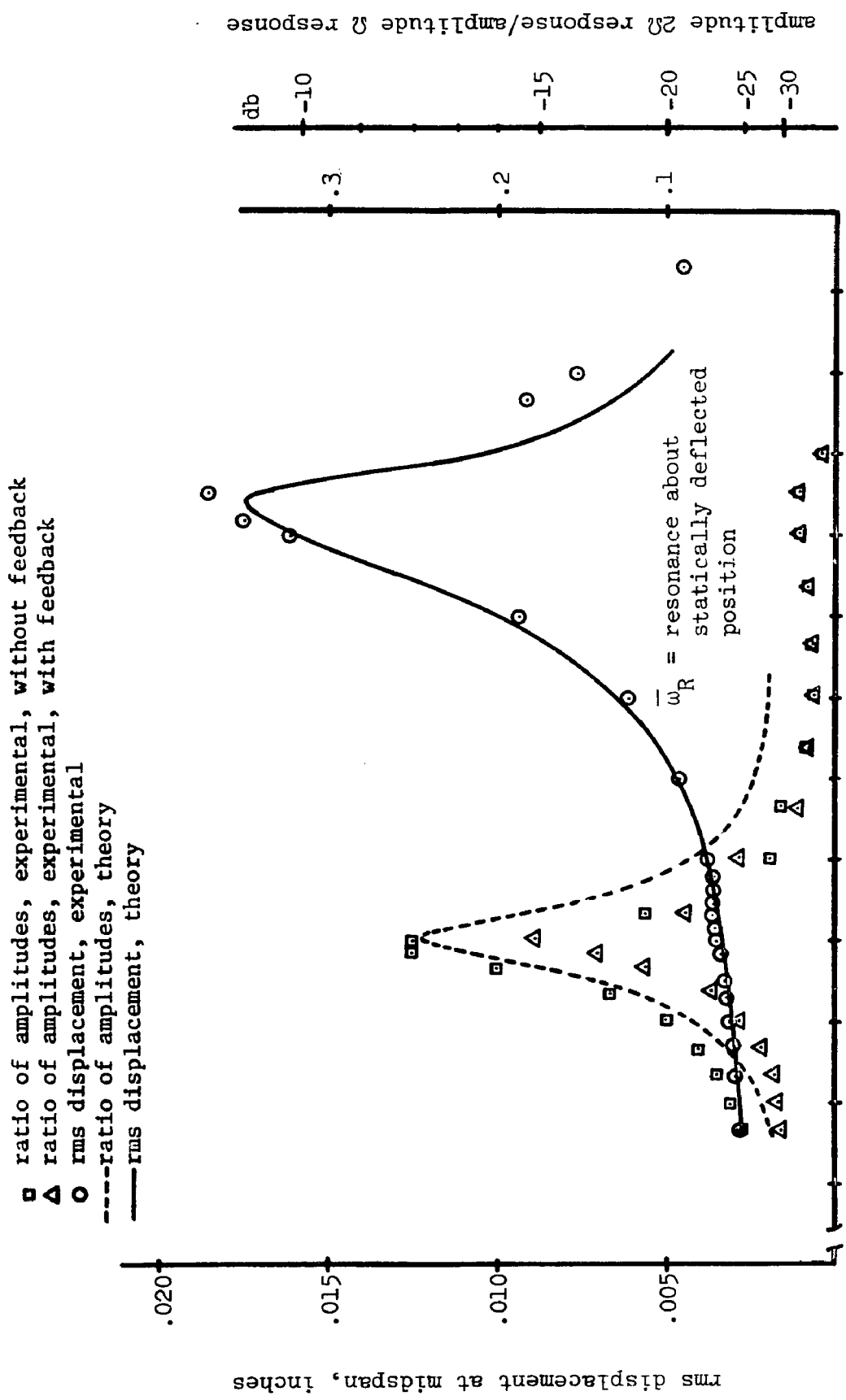


Figure 5.3. Response of unsymmetric beam, F_0 = .15 lb., F_1 = .05 lb.

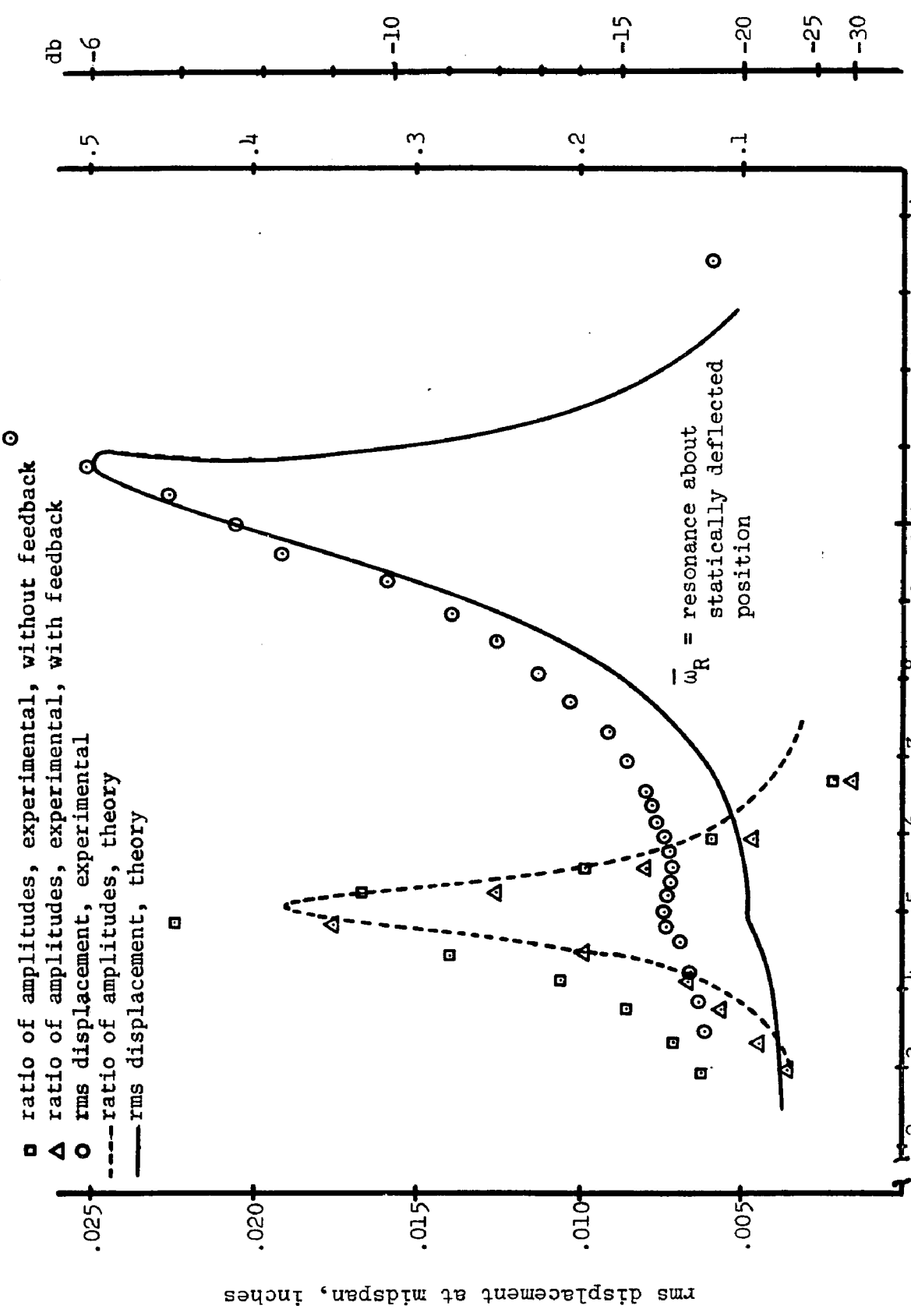


Figure 5.4. Response of unsymmetric beam, F_0 = .18 lb., F_1 = .073 lb.

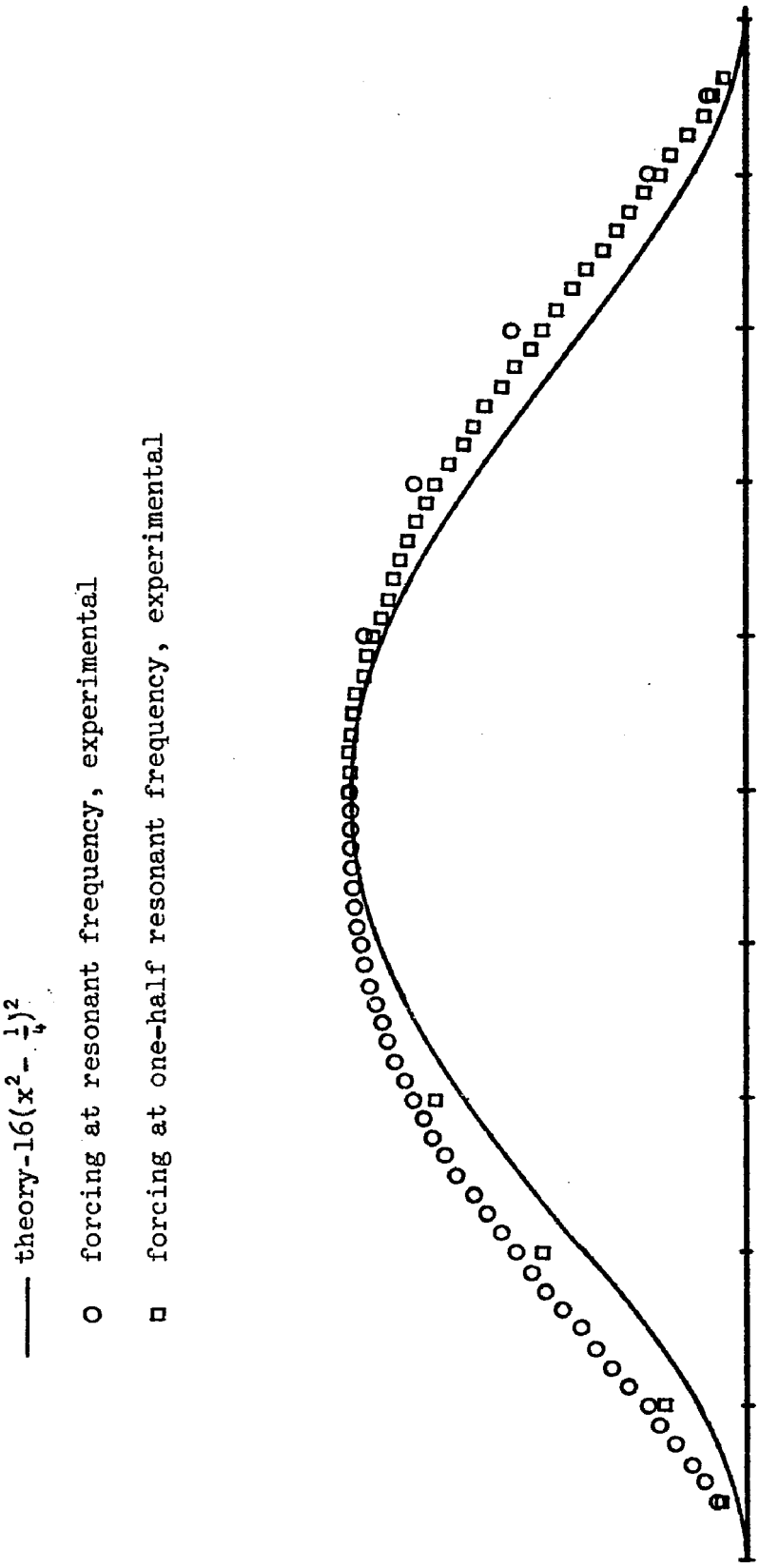


Figure 5.5. Mode shapes for unsymmetric beam.

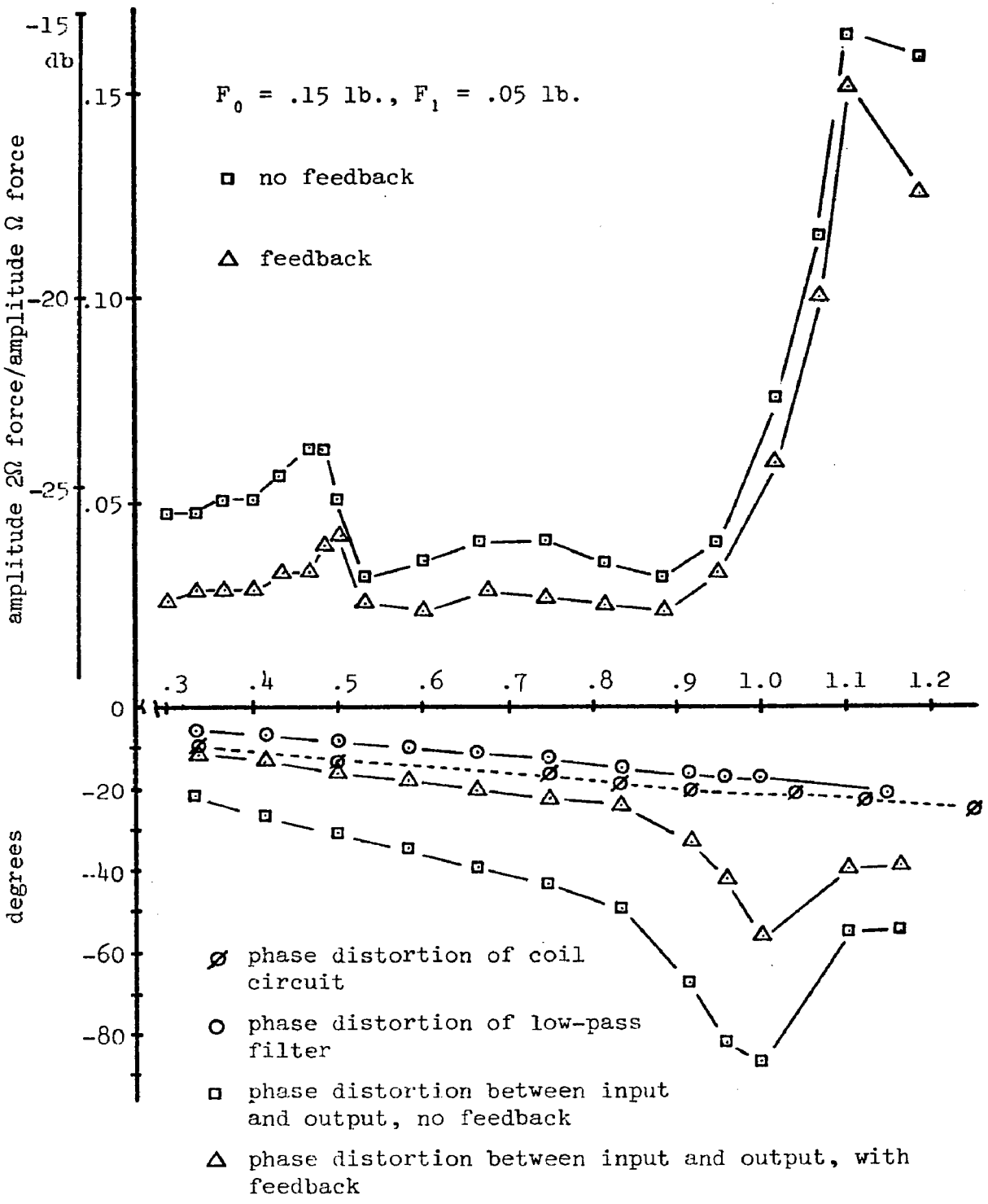


Figure 5.6. Characteristics of feedback system.